

# Institute of Molecular Physics Polish Academy of Sciences

DISSERTATION

## Magnetic properties of Fe-based ultrathin films – first principles calculations

Joanna Katarzyna Marciniak

Supervisor: dr hab. Mirosław Werwiński

Co-supervisor: dr Justyna Rychły-Gruszecka



Poznań 2024

---

## Acknowledgements

Thank you to everyone who contributed to this dissertation, especially:

to my husband for his time spent on discussions, supporting me in difficult moments,  
help with correcting this guide and every small helpful gesture,

to my parents for keeping me curious about the world surrounding me, and

to my supervisors for their time and effort in supporting me with my research.

Without all this support, I would not have reached this point.

I also acknowledge the financial support of the National Science Centre Poland under the decision DEC-2018/30/E/ST3/00267 and resources provided by the Poznan Supercomputing and Networking Center (PSNC) and Institute of Polish Academy of Sciences.

---

## Abstract

One of the key aspects of technological development is the increasing miniaturization of electronic circuits and their components. In the case of data storage devices, the main challenge in this miniaturization is the magnetic recording trilemma. It describes the competition between the density of stored information, the thermal stability of the memory cell and the possibility of recording. Several different approaches to this problem are proposed. One way to reduce the magnetic field required for recording may be to use the tilt of the magnetic easy axis of the material relative to the magnetic field used for recording. This approach – applied to  $L1_0$  FePt and  $L1_0$  FeNi layers – is one of the main issues discussed in the presented doctoral dissertation.

In this dissertation, I investigated the properties of the above-mentioned ultrathin magnetic films with  $L1_0$  structure, as well as another Fe-based material:  $\text{Fe}_{0.7}\text{Co}_{0.3}$ . The research focused on determining the effect of film's modification on their basic magnetic properties: the direction of the easy magnetization axis, the magnetocrystalline anisotropy energy, and the spin and orbital magnetic moments. The considered modifications were the film's thickness change in the  $L1_0$  structures and octahedral interstitial doping with B, C, and N atoms in the  $\text{Fe}_{0.7}\text{Co}_{0.3}$  alloy. I performed the electronic structure calculations. I used density functional theory – mainly in the implementation of the full-potential local-orbital (FPLO) computational code and using the exchange-correlation potential in the form proposed by Perdew, Burke, and Ernzerhof.

The basic differences between layers of different thickness and dopant type were observed in the values of magnetocrystalline anisotropy energy and orbital magnetic moments. The orientation of the film's surface also affects the direction of the easy magnetization axis. In the (010)  $L1_0$  FePt and  $L1_0$  FeNi systems, I observed a preference for the tetragonal [001] direction of the  $L1_0$  phase, located in the plane of the ultrathin layer. The use of the (111) surface allowed obtaining a tilted magnetization direction, and changing the thickness of the (111) surface layer allowed for setting a specific tilt value. The observed properties may prove useful in designing computer memories using the tilt of the magnetization axis with respect to the magnetic switching field.

---

## Streszczenie

Jednym z kluczowych aspektów rozwoju technologii jest coraz większa miniaturyzacja obwodów elektronicznych i ich elementów. Głównym problemem tej miniaturyzacji w przypadku urządzeń do przechowywania danych jest trylemat zapisu magnetycznego. Opisuje on konflikt pomiędzy gęstością przechowywanych informacji, stabilnością termiczną komórki pamięci i możliwością zapisu. W przypadku magnetycznych dysków twardych, proponowanych jest kilka różnych podejść do rozwiązania problemu. Jednym ze sposobów zmniejszenia pola magnetycznego wymaganego do zapisu może być wykorzystanie pochylenia magnetycznej osi łatwej materiału względem pola magnetycznego wykorzystywanego do zapisu. Takie podejście – zastosowane do warstw  $L1_0$  FePt i  $L1_0$  FeNi – jest jednym z głównych wątków poruszonych w przedstawionej rozprawie doktorskiej.

W ramach niniejszej dysertacji zbadalam właściwości wymienionych ultracienkich warstw magnetycznych o strukturze  $L1_0$ , jak i kolejnego materiału na bazie Fe:  $Fe_{0.7}Co_{0.3}$ . Badania skupiały się na określeniu wpływu modyfikacji warstw na ich podstawowe właściwości magnetyczne: kierunek osi łatwej magnetyzacji, energię anizotropii magnetokrystalicznej oraz spinowe i orbitalne momenty magnetyczne. Rozważanymi modyfikacjami były zmiana grubości warstwy w strukturach  $L1_0$  i domieszkowanie atomami B, C i N w oktaedrycznych pozycjach międzywęzłowych w stopie  $Fe_{0.7}Co_{0.3}$ . Przeprowadzone przeze mnie badania miały formę obliczeń struktury elektronowej. Wykorzystałam teorię funkcjonału gęstości – głównie w implementacji zawartej w kodzie obliczeniowym full-potential local-orbital (FPLO) i z zastosowaniem potencjału korelacyjno-wymennego w ujęciu Perdew, Burke’a i Ernzerhofa.

Podstawowe różnice pomiędzy warstwami o różnej grubości i rodzaju domieszki zostały zaobserwowane w wartościach energii anizotropii magnetokrystalicznej oraz orbitalnych momentów magnetycznych. Rodzaj powierzchni warstwy również wpływa na kierunek osi łatwej magnetyzacji. W układach  $(010)$   $L1_0$  FePt i  $L1_0$  FeNi zaobserwowałam preferencję dla kierunku teragonalnego  $[001]$  fazy  $L1_0$ , umiejscowionego w płaszczyźnie ultracienkiej warstwy. Natomiast wykorzystanie powierzchni  $(111)$  pozwoliło na otrzymanie pochylonego kierunku namagnesowania, a zmiana grubości warstwy o powierzchni  $(111)$  dała możliwość ustalania konkretnej wartości pochylenia. Obserwowane właściwości mogą okazać się przydatne w projektowaniu pamięci komputerowych wykorzystujących pochylenie osi magnetyzacji względem magnetycznego pola przetłaczającego.

## Contents

<b>1</b>	<b>Aim and motivation</b>	<b>4</b>
<b>2</b>	<b>Researched materials</b>	<b>6</b>
<b>3</b>	<b>Methods</b>	<b>7</b>
3.1	Brief overview on computational methods . . . . .	7
3.2	Density functional theory and its application . . . . .	8
3.3	Practical aspects of the calculations . . . . .	10
<b>4</b>	<b>Research description</b>	<b>12</b>
4.1	DFT calculation of intrinsic properties of magnetically hard phase $L1_0$ FePt	12
4.2	$L1_0$ FePt thin films with tilted and in-plane magnetic anisotropy: A first-principles study . . . . .	13
4.3	Magnetic anisotropy of $L1_0$ FeNi (001), (010), and (111) ultrathin films: A first-principles study . . . . .	15
4.4	First-principles study of the magnetic anisotropy of ultrathin B-, C-, and N-doped FeCo films . . . . .	16
<b>5</b>	<b>Summary</b>	<b>17</b>
<b>6</b>	<b>Copies of the articles</b>	<b>18</b>
6.1	$L1_0$ FePt thin films with tilted and in-plane magnetic anisotropy: A first-principles study . . . . .	18
6.2	Magnetic anisotropy of $L1_0$ FeNi (001), (010), and (111) ultrathin films: A first-principles study . . . . .	31
6.3	First-principles study of the magnetic anisotropy of ultrathin B-, C-, and N-doped FeCo films . . . . .	41

# 1 Aim and motivation

We live in a world where technology surrounds us from all sides and is constantly developing. Magnetic materials, including  $\text{Nd}_2\text{Fe}_{14}\text{B}$ ,  $\text{Sm}_5\text{Co}_2$ , Fe-Si alloys, ferrites, and others, are used in many areas, including electric energy transfer, renewable energy solutions, measuring equipment, medicine, or automotive. Electric transformer cores are made of soft magnets, whereas hard disc drivers (HDD) or electric generators contain permanent magnets.

Different properties of magnetic materials are of interest depending on the application. For example, both hard and soft magnets are used in turbines or electric motors. Rotors have soft magnetic cores, and stators are made of hard magnetic materials. Those should resist over-magnetization in the fields generated by electromagnets. Similarly, in HDDs, a hard magnetic material with appropriate thermal stability is used in memory cells. It ensures the durability of the recorded data in the operating conditions of computer components. On the other hand, the material used to make the recording/reading head is a soft magnetic material with high magnetization to ensure a rapid magnetic field switching and, hence, high recording speed. At the same time, it generates a magnetic field that is high enough to change the magnetization direction of the memory cell.

It is good to mention the research on magnetoresistive random-access memory (MRAM) here. In HDDs and MRAMs, the tunnel magnetoresistance (TMR) effect is used to read the recorded information. This phenomenon occurs in multilayer systems built of the pinned layer (with a fixed magnetization direction), the insulating layer, and the free layer. In the latter, the magnetization direction is changed during information recording. During the information reading, the change in resistance is measured. It depends on the relative direction of the magnetization in the pinned and free magnetic layers and stems from the differences in scattering on parallelly and antiparallelly arranged magnetic moments.

One of the main directions of electronics development is the increasing miniaturization of circuits and components. This also applies to progress in miniaturizing storage devices and increasing their recording density. The main problem that scientists and designers struggle with is the so-called *magnetic recording trilemma* [1].

This trilemma is related to the competition between recording density, thermal stability, and recording capability. Increasing the recording density requires reducing the grain size. These grains can store limited energy, proportional to the grain volume and the uniaxial magnetocrystalline anisotropy constant ( $K_u$ ). The magnetic energy stored in such a grain must be higher than the energy of thermal vibrations at the operating temperature. If we want to maintain the thermal stability of the recorded information while reducing the volume of the recording unit, we need to increase  $K_u$ .  $K_u$  describes how much energy must be supplied to the material to change its magnetization direction. An appropriately strong magnetic field is used to switch this direction; therefore, increasing  $K_u$  of the material storing information can prevent switching between physical – and, hence, logical – states of the system and, consequently, prevent recording. Several proposals have been developed to solve the presented problem. Two of them are discussed below.

One of the proposed approaches is energy-assisted magnetic recording, a variant of which is heat-assisted magnetic recording (HAMR) [2]. The general idea of this method is based on the temperature dependence of magnetocrystalline anisotropy energy (MAE).

By raising the grain temperature to a point close to the Curie temperature ( $T_C$ ) of the material, we may reduce its MAE value. This leads to a significant decrease in the magnetic field required for the reorientation of the magnetization of the memory cell. Then, the grain temperature drops, the MAE value returns to its original value, and the grain's thermal stability returns with it. Although this concept is relatively simple, the technological solutions needed to produce recording heads, for example, are not trivial. Nevertheless, Seagate have made the first magnetic memories based on HAMR technology [3].

Another concept was presented by Albrecht *et al.* in 2005 [4]. In this case, the reduction of the magnetic field required for recording occurs by changing the angle between the magnetic field vector of the recording head and the magnetization axis in the material. The mentioned tilt can be obtained by changing the angle of the generated magnetic field in the recording head and by using structures with a tilt of the magnetic easy axis with respect to the vector perpendicular to the surface of the magnetic layer. In the case of the mentioned experiment, the magnetic film was Co/Pd layers deposited on polystyrene beads with a diameter of the order of nanometers, and the tilt of the magnetic field direction to the magnetization axis of the material by at least  $45^\circ$  caused a decrease of the required field value by about 30%. This type of recording could potentially be used in both HDD and MRAM.

Significant progress in the miniaturization of electronic devices has been achieved by using nanostructures. A structure can be considered nanoscale when at least one of its dimensions is smaller than about 100 nm. This is a rather general definition. More specifically, this length must be comparable to a given material's characteristic lengths. In the case of magnetic nanostructures, such characteristic lengths may be the width of the domain wall, the exchange length, the maximum dimension of a single-domain particle, or the superparamagnetic blocking radius. For nanostructures considered because of electron transport, such characteristic lengths will be the mean free path, the inelastic scattering length, or the spin-diffusion length. These characteristic lengths take on different values, even below 1 nm and significantly above the mentioned 100 nm [5]. Structures in this scale often have entirely different properties than the same materials in the bulk phase. This is why examining structures in their intended dimensions is essential.

In this dissertation, I present the properties of ultrathin magnetic films based on Fe: L1<sub>0</sub> FePt, L1<sub>0</sub> FeNi, and Fe<sub>0.7</sub>Co<sub>0.3</sub>. The underlying research focused on investigating the effect of modification of these films on the fundamental magnetic properties: MAE, spin ( $m_s$ ), and orbital ( $m_l$ ) magnetic moments. The effect of changing the layer thickness in L1<sub>0</sub> structures and doping with B, C, and N atoms in octahedral interstitial positions in the Fe<sub>0.7</sub>Co<sub>0.3</sub> alloy was considered.

The following guide briefly describes the studied groups of materials: the L1<sub>0</sub> phase and Fe-Co alloys (Section 2), basic topics concerning calculation methods in general, density functional theory (DFT), the used full-potential local-orbital (FPLO) code, potential errors and discrepancies with results present in the literature (Section 3) and a summary of each article included in the thesis (Section 4). Section 4 also describes initial research on L1<sub>0</sub> FePt bulk phase published in Ref. [6]. This research is not a part of the dissertation. It provides an introduction to L1<sub>0</sub> FePt ultrathin films description, as these calculations are based on parameters obtained in [6]. This guide ends with final conclusions to the presented publications (Section 5). Reprints of publications included in the thesis (Section 6) and listed below.

## Articles included in the dissertation

- <sup>I</sup>J. Marciniak and M. Werwiński, “L1<sub>0</sub> FePt thin films with tilted and in-plane magnetic anisotropy: a first-principles study”, *Phys. Rev. B* **108**, 214406 (2023).
- <sup>II</sup>J. Marciniak and M. Werwiński, “Magnetic anisotropy of L1<sub>0</sub> FeNi (001), (010), and (111) ultrathin films: a first-principles study”, *J. Magn. Magn. Mater.* **609**, 172455 (2024).
- <sup>III</sup>J. Marciniak, M. Werwiński, and J. Rychły-Gruszecka, “First-principles study of the magnetic anisotropy of ultrathin B-, C-, and N-doped FeCo films”, *J. Magn. Magn. Mater.* **589**, 171563 (2023).

This guide provides a broader context for the research being conducted than what is contained in the publications themselves.

## 2 Researched materials

In the previous chapter, I presented the general context of my research, including a discussion on thin-film ferromagnetic materials with high MAE used in data recording. I also pointed out the need to investigate models with reduced dimensionality instead of simpler bulk-phase materials. In this chapter, I will briefly describe the L1<sub>0</sub> phases and present studies on the FeCo alloys.

The L1<sub>0</sub> phases are an interesting alternative to traditional magnetic materials used in modern technology, especially as material for high-density magnetic recording. L1<sub>0</sub> is an ordered tetragonal structure in which the precursor is the close-packed face-centered cubic (fcc) cell. In this phase, successive monolayers of two (or more) chemical elements are alternately stacked, usually resulting in a minor tetragonal strain. It can be represented in the space group  $P4/mmm$ . In the most general sense, the substituted phase of the composition ABC<sub>2</sub>, where planes of C atoms are sandwiched by A and B atoms layers, can also be called L1<sub>0</sub>. In the framework of this dissertation, only diatomic phases [7–9] were considered. These phases are attractive when designing hard magnetic materials. In that case, at least one of the elements belongs to the 3d transition metals group. The other atom can belong to 3p, 4p, 4d, or 5d groups (as Mn, Ga, Pt, Pd). The alternating atomic monolayers of elements A and B result in structural anisotropy of the chemical environment of the atoms, which then affects the magnetization. It also explains why, for these alloys, the order parameter is so crucial for magnetic properties, especially for MAE [7, 9]. This phase can emerge, e.g., during precisely controlled cooling processes, from disordered fcc structure.

The structure of L1<sub>0</sub> allows for various magnetic orderings. These are both ferromagnetic materials with the easy axis of magnetization oriented along the [001] tetragonal direction and various antiferromagnets, including those with non-collinear spin orientations. Moreover, ferromagnetic and antiferromagnetic ordering in these materials can compete with each other. An example is L1<sub>0</sub> FePt. Both states were obtained as ground states with a slight energy difference in calculations from first principles. However, the results of the experiment contradict these predictions. This is explained by the presence of various types of structural imperfections in the real samples, such as a small amount of Fe bridges that can compensate for the weak antiferromagnetic interlayer coupling [7, 10].



Another group of materials that attracts broad attention are FeCo alloys, which have the highest magnetization among transition metal-based alloys. In 2004, Burkert *et al.* [11] presented DFT results for disordered  $\text{Fe}_{1-x}\text{Co}_x$  alloys with uniaxial strain that predicted MAE maximum for Co concentration of about 60% and a  $c/a$  ratio of 1.20-1.25. This discovery led to a significant increase in interest in these tetragonal alloys.

Unfortunately, attempts to obtain FeCo thin films with such strain failed. The layers quickly relaxed to a body-centered cubic structure when their thickness exceeded about 15 monolayers [12, 13]. Additionally, even for highly strained structures, the experimentally obtained MAE values were below those predicted by Burkert *et al.* [11]. Subsequent DFT studies of FeCo alloys were performed by Turek *et al.* [14] using the more accurate yet more demanding coherent potential approximation (CPA). It showed 3-4 times lower MAE values, which are much closer to those obtained in experiments. At the same time, as presented by Turek *et al.*, the MAE maximum covers a wider range of Fe/Co concentrations than in Ref. [11]. A more detailed description of the FeCo alloys is presented in Refs [15, 16].

In this dissertation, I present results for ultrathin films of two magnetic materials with the  $\text{L1}_0$  phase: FePt and FeNi, see Refs. [I] and [II]. Furthermore, I show findings for  $(\text{Fe}_{0.7}\text{Co}_{0.3})_{18}$  and  $(\text{Fe}_{0.7}\text{Co}_{0.3})_{18}\text{X}$  ( $\text{X} = \text{B}, \text{C}, \text{N}$ ) films with a thickness of nine atomic monolayers, see Ref. [III].

## 3 Methods

The following chapter provides a basic overview of the methods used in the presented studies. It will also address shortcomings and limitations resulting from the assumptions underlying these methods.

### 3.1 Brief overview on computational methods

Calculations allow for predicting various material properties, such as electronic, magnetic, mechanical, or tribological. It can be done for both new hypothetical materials and those already synthesized and tested by experimental techniques. By considering problems *in silico*, we can limit the pool of samples to be prepared for experimental and prototype tests. Such an approach often significantly reduces the financial outlays for research and design. It should be noted that many computational methods exist, with many more specific implementations. In natural sciences, computational methods are divided according to how they approach matter. We can examine matter at a fully macroscopic scale, the nanoscale of small particles reaching for the classical treatment of atoms, or the atomic level considered in a fully quantum way.

The finite element method (and its improvements) is a representative of macroscale methods. In this method, any structure or its element, such as a metal bridge construction, a ceiling beam, an engine part, or a composite material is viewed as an object made of continuous material or with specified parts made from different materials. It is widely used in civil and mechanical engineering, but it can also be implemented in the microscale (e.g. auxetics, plasmons) [17–19]. Such calculations require many parameters specific to the model, e.g., object geometry, bending strength, tensile strength, yield

strength, etc. [20]. It provides a challenge in studying the properties of unmanufactured and untested materials yet is computationally less demanding and sufficient in most cases.

The computational method that reaches the atomic scale is molecular dynamics. In its framework, we assume that matter consists of tiny particles. These can be atoms or larger particles, such as amino acids or repeat units of polymers [21]. During these simulations, Newtonian equations of motion are solved for even tens of millions of these particles. Molecular dynamics allows us to look at the system's evolution in time on the order of up to miliseconds [22]. The force acting on these particles is determined using so-called force fields. These parameter sets often describe two-body or three-body interactions, and interactions with further elements are frequently added via correction factors [23, 24]. Potentials are derived from experimental studies or DFT calculations by strict fitting procedures [25, 26], with the addition of recently appearing machine learning interatomic potentials [21]. Although these methods allow for simulating changes in systems such as heat transfer [23], conformational changes<sup>a</sup> [24], phase transitions [21] or shock wave propagation [27], they usually do not include direct electrons treatment and therefore do not allow for observing changes in properties based on electron interactions such as conductivity or magnetic properties.

With a further decrease in scale, we reach the quantum physics and chemistry methods. The most popular approaches in this scale are based on the Hartree-Fock method and the previously mentioned density functional theory (DFT) based on the Kohn-Sham equations. Both methods rely on solving the energy eigenstate equation of the system – Schrödinger or Schrödinger-like equation [28]:

$$\hat{\mathcal{H}}|\psi\rangle = E|\psi\rangle, \quad (3.1)$$

where  $\hat{\mathcal{H}}$  is a Hamiltonian operator and  $E$  is the energy eigenstate value of  $|\psi\rangle$  wavefunction.

The Hartree-Fock method is based on solving the time-independent many-body equation. In this method, several approximations must be applied to overcome the many-body problem. First, a molecule's wave function is assumed to be a linear combination of atomic orbitals (LCAO) [29], and the effect of correlations between electrons is not considered. Secondly, we assume that atomic nuclei are so heavy and their vibrations so small in relation to electrons that we consider them as stationary lattice points generating an external potential in which electrons move (Born-Oppenheimer approximation) [28]. Finally, each energy eigenfunction is assumed to be describable by a single basis functions product, called the Slater determinant [30]. The last approximation especially leads to the omission of part of the electron correlation energy related to coulombic interaction. The Hartree-Fock method is often used in quantum chemistry [31].

## 3.2 Density functional theory and its application

The DFT method is based on the Hohenberg-Kohn theorems. The first one states that, quoting them directly, *"the full many-particle ground state is a unique functional of  $n(\mathbf{r})$ "*, where  $n(\mathbf{r})$  is the electron density [32]. The second theorem defines the energy functional and states that the actual electron density of the ground state minimizes it.

---

<sup>a</sup> *conformation* is a relative spatial arrangement of atoms and/or groups of atoms (e.g., amino acids)

This allows for determining the electronic structure of the system in the ground state without identifying the exact wave function of the ground state [31].

Kohn and Sham proposed the density-based Schrödinger-like equation 3.1, in which the problem of many interacting electrons in an external potential resulting from the presence of atomic nuclei was reduced to the problem of non-interacting electrons moving in an effective potential. It is important to mention that the electron density does not change; neither the interacting nor non-interacting electrons are assumed. This effective potential includes both the part describing the interaction of electrons with atomic nuclei and the exchange and correlation interactions between electrons. Thus, the functional describing the energy is reduced to the form:

$$E[n] = T[n] + U[n] + E_{XC}[n], \quad (3.2)$$

where the obtained energy is the sum of the kinetic energy of non-interacting electrons ( $T[n]$ ), the potential energy ( $U[n]$ ), which incorporates Hartree potential and the external potential (minimally the interaction of electrons with atomic nuclei), and the energy due to exchange-correlation interactions between electrons ( $E_{XC}[n]$ ) [33] mapping the electrons movement into the non-interacting picture. While it is possible to derive a universal analytical description of  $T[n]$  and  $U[n]$ , so far, no such description of  $E_{XC}[n]$  has been found that would be at the same time universal and analytical [30].

The above equation corresponds to the non-relativistic Schrödinger equation. However, for some properties of matter, such as MAE or magneto-optical effects, the spin-orbit interaction must be taken into account. For this purpose, it is necessary to solve the Kohn-Sham-Dirac equation for a crystal, which can be written in the collinear approximation as:

$$\hat{\mathcal{H}}|\phi\rangle = [-ic\boldsymbol{\alpha} \cdot \boldsymbol{\nabla} + \beta c^2 + V^{\text{cr}} + \beta \Sigma_z \mathbf{B}^{\text{cr}}] |\phi\rangle = |\phi\rangle \varepsilon, \quad (3.3)$$

where the Hamilton operator of the system relies on exchange-correlation field  $\mathbf{B}^{\text{cr}} \equiv B^{\text{cr}} \hat{z}$  that is directed along the  $\hat{z}$ -axis;  $c$  is a light speed in vacuum;  $\varepsilon$  is an eigenstate energy value;  $\phi$  is Dirac spinor orbitals; the Hartree potential, the external nuclear potential, and the exchange-correlation potential are represented by the effective crystal potential  $V^{\text{cr}}$ ;  $\boldsymbol{\alpha}$  is composed of the  $2 \times 2$  sigma matrices as  $\boldsymbol{\alpha} = \begin{pmatrix} 0_2 & \boldsymbol{\sigma} \\ \boldsymbol{\sigma} & 0_2 \end{pmatrix}$ ;  $\beta$  is the Dirac matrix in terms

of  $2 \times 2$  identity matrices:  $\beta = \begin{pmatrix} I_2 & 0_2 \\ 0_2 & -I_2 \end{pmatrix}$ , and  $\Sigma_z$  is the spin matrix:  $\Sigma_z = \begin{pmatrix} \boldsymbol{\sigma} & 0_2 \\ 0_2 & \boldsymbol{\sigma} \end{pmatrix}$ .  $I_n$  denotes the identity matrix and  $0_n$  a zero matrix of the rank  $n$ .  $\boldsymbol{\sigma}$  are  $2 \times 2$  Pauli spin matrices. Solving this equation is computationally more expensive than solving the Kohn-Sham equation for the same system [34]. Regardless of whether one solves the Kohn-Sham equation or the Kohn-Sham-Dirac equation, the solutions are obtained iteratively in a self-consistent manner.

Many DFT codes implement the solution of the Kohn-Sham and Kohn-Sham-Dirac equations. They differ primarily in the choice of the set of basis functions and whether they use full potential or pseudopotentials. Linear combination of basis functions provide a way to express the system's wave function. Hence, the choice of basis significantly impacts system representation accuracy. Simultaneously, a highly localized basis provides for better accuracy *versus* efficiency balance when calculating highly inhomogeneous systems – such as thin films in vacuum – compared to plane waves filling the computational cell

homogeneously. Whether a given code uses full potential or pseudopotentials describes how core electrons are treated. In full-potential methods, the effective single-electron potential is determined using a full set of orbitals, i.e., core and valence [35]. In the case of pseudopotentials, it is assumed that only valence electrons are *active*, and the interaction of valence and core electrons can be reduced to the effective core potential. At this point, it is also worth mentioning that pseudopotentials can have a semi-empirical origin [36].

Another important topic concerning the DFT calculations is the selection of the exchange-correlation functional formulation. DFT codes usually provide multiple such functionals, and it is up to the user to choose the most appropriate one for the studied material, considering the properties he wants to investigate. The most popular groups of functionals include local density approximation (LDA) and generalized gradient approximation (GGA). LDA assumes that the energy of the exchange-correlation interactions for the local density of states is the same as for a homogeneous electron gas of the same density. GGA, on the other hand, introduces additional dependence of the exchange-correlation interaction energy on the electron density gradient. It is important to note here that – in contrast to the LDA, which predicts for Fe a nonmagnetic hexagonal structure – the GGA functional correctly predicts the magnetic body-centered cubic (bcc) structure as the most stable phase of Fe [35]. Hence, in our studies, we use the GGA functional (with the Perdew-Burke-Ernzerhof (PBE) [37] parameterization) whenever possible.

It should also be mentioned that GGA has further improvements, but they do not provide such considerable advantages in our case. Particular attention should be paid to hybrid functionals. They combine the part of the functional describing the correlation interaction with the functional describing the exchange interaction, as, for example, in the Hartree-Fock method [35].

### 3.3 Practical aspects of the calculations

When starting to perform DFT calculations, a number of decisions must be made that will ultimately affect the calculated values of physical properties and the time it takes to obtain these values. The first of them is the choice of the computational code. Specific parameter values are often selected rigorously enough to obtain satisfactory accuracy, while loose enough to minimize the required computational cost. One such parameter is a reciprocal space integration  $\mathbf{k}$ -points mesh density - the larger it is, the better the reciprocal space is sampled at the expense of longer single iteration time. The situation is similar for the electron density and/or system energy convergence criterion. Another decision that must be made is the choice of the exchange-correlation potential. One must also answer whether it is necessary to perform fully relativistic calculations or not.

The choice of the computational cell type and size does not automatically impact the calculated physical properties values, but it can affect the time of a single iteration. This is due to both the number of symmetry operations and nonequivalent atoms. Finally, the mixing parameter determines the impact the last result will have on the next iteration. This parameter and choice of the integration method will influence the speed of obtaining convergence and avoiding falling into a local minimum. All the mentioned aspects are not trivial, as particular choices may lead to obtaining the desired convergence in less but more computationally demanding steps. Proper tests are necessary for each use case to

estimate expected resources usage.

Like any computational method, DFT calculations, regardless of implementation, introduce some errors and discrepancies with the experiment. Discrepancies can appear even within a single DFT code. They mainly result from the choice of different potentials, parameters such as a mesh of  $\mathbf{k}$ -points, convergence criterion, relativity treatment, integration method, and the like [6]. In addition, the discrepancies in the values of considered property will differ between codes even when using identical parameters, potentials, and other options because there will be variances in the technical aspects of the implementation of a given method.

Another concern is the discrepancies between DFT calculations and experiments. Both approaches have their own limitations. DFT calculations are most often performed based on an idealized model: an infinite film, an infinite bulk phase, and an ideal arrangement of atoms. This choice is intended to take advantage of periodic boundary conditions, the use of which greatly speeds up calculations. Additionally, in the basic DFT approach, all systems are in their energetic ground state at a temperature of 0 K. We usually do not study any thermodynamical ensemble as we do not consider the system's evolution in time. On the other hand, experiments are performed on finite samples, often containing grains, sometimes arrangement errors, dislocations, and/or other defects or alloy samples. Hence, the experimental sample does not reflect the final commercial realization. In fact, a sample suitable for some experimental measurements, e.g., homogenous enough, could not be obtainable. In addition, many measurements are often conducted at realistic temperatures. Hence, one cannot expect full agreement between the calculation results and the experiment. It is worth striving for such an agreement, as both approaches complement each other. Cooperation on both sides allows for a better understanding of phenomena at a much lower scale based on theoretical explanations of the experiment's observations.

It should also be noted here that the research I conducted has another factor that makes it difficult to compare my results with experimental outcomes. All models are placed in a vacuum and do not have a substrate or cap layer. Interactions with these layers can introduce changes in the properties of the magnetic film, both due to the introduction of stress in the layers close to the interfaces and by modifying the chemical environment of the atoms at this place. The decision to abandon the consideration of the substrate and cap layer influence resulted from the limitation of the calculations' complexity level and the desire to isolate the changes in properties resulting solely from the dimensionality reduction. In this view, the ability to calculate the properties of a thin film without an additional substrate can be considered an advantage, as it allows separating the physical properties stemming from the effect of the substrate, which would be tricky to implement experimentally.

Many computational codes implement periodic boundary conditions to utilize efficient real to wave vector space transforms. Thus, a vacuum must be added in a selected direction when modeling ultrathin film systems to avoid the influence of the layer image on the modeled properties. I have used the full-potential local-orbital (FPLO) code in my research. It provides a highly localized basis for full potential treatment, which allows for highly accurate yet efficient calculations of magnetic films. Moreover, it is highly optimized at the cost of being only single-threaded, which provides for efficient resource usage. Additionally, it allows for the fully relativistic calculations as presented in Eq. 3.3.

## 4 Research description

This part of the guide will briefly present the scientific publications that constitute the dissertation. It is divided into subsections, in which the publications that make up the dissertation are discussed individually. The first subsection briefly describes my work on  $L1_0$  FePt bulk phase. As mentioned at the end of Section 1, this article is not part of the presented dissertation but provides an introduction for  $L1_0$  FePt ultrathin films research. Additionally, this research on ultrathin films was based on parameters obtained there.

Each subsection will present a detailed description of the contribution of individual authors and conclusions from a given publication. The works will not be presented in chronological order according to the date of publication, but according to the chronology of the beginning of the research. Such an arrangement should also facilitate a later understanding of conclusions to the entire research conducted.

The subject of this dissertation, as it was initially presented in the previous chapters, is the study of the effect of modification of ultrathin films on their basic magnetic properties: MAE,  $m_s$ , and  $m_l$ . More precisely, the modification of films in these studies consists of changing their thickness or doping with B, C, and N atoms in octahedral interstitial positions. I focused on the ferromagnetic materials based on Fe that do not contain rare-earth elements:  $L1_0$  FePt [I],  $L1_0$  FeNi [II] and  $\text{Fe}_{0.7}\text{Co}_{0.3}$  [III]. The studies are discussed in this order below.

### 4.1 DFT calculation of intrinsic properties of magnetically hard phase $L1_0$ FePt

Although the main topic of the dissertation is research on ultrathin magnetic films, at the beginning of my research, I was engaged in the study of bulk phase  $L1_0$  FePt as part of the publication: J. Marciniak, W. Marciniak, M. Werwiński *DFT calculation of intrinsic properties of magnetically hard phase  $L1_0$  FePt*, J. Magn. Magn. Mater., **556**, 169347 (2022). First, the optimized bulk phase structure served as a basis for the development of layer models. Second, the research I provided and presented in this publication was the basis for my master's thesis in the field of Materials Engineering at the Faculty of Materials Engineering and Technical Physics of the Poznań University of Technology. Therefore, the results discussed in this subsection are not the dissertation's part but an essential introduction. In this work, we focused on investigating the dependence of MAE on the value of the magnetic moment ( $m$ ), determining the values of  $m$ , the magnetic anisotropy constants  $K_1$  and  $K_2$ ,  $m$ , the Curie temperature ( $T_C$ ), and the magnetostriction coefficient  $\lambda_{001}$ .

The obtained values of the sum of magnetic moments in the formula unit are in the range between 3.17 and  $3.512 \mu_B$ , which gives a discrepancy of about 10%.  $T_C$  obtained based on the disordered local moment theory are in the range of 430 to 900 K, while  $T_C$  obtained using FPLO5 (except for the *Exchange-only* potential) are within 3% error with respect to the value obtained in the experiment. It should be noted, however, that the applied approach is known to overestimate the value of  $T_C$  significantly, and therefore, higher values would be expected. At the same time, the obtained  $T_C$  for the Vosko-Wilk-Nusair (VWN) potential suggests that the LDA is not the right choice to

properly represent the exchange interactions and  $T_C$ . Interestingly, the LDA *Exchange-only* approach in FPLO seems to be sufficient ( $T_C = 878$  K).

Calculations of the coefficients  $K_1$  and  $K_2$  show that the full-potential approach provides better agreement with the experiment. The differences between the results for the exchange-correlation potential of PBE implemented in FPLO and a spin polarized relativistic Korringa-Kohn-Rostoker (SPR-KKR) are related to the implemented basis. Additionally, convergence tests suggest that this system's minimum angular momentum expansion is  $l_{max} = 4$  (the parameter NL = 5 in the SPR-KKR configuration file). Raising this value to  $l_{max} = 5$  gives further noticeable improvement.

The calculations of the MAE( $m$ ) dependence for different exchange-correlation potentials in the vicinity of equilibrium values show that all potentials studied (except *Exchange-only*) give very similar curves, with a maximum of MAE values around  $20.3 \text{ MJ m}^{-3}$  for  $m$  around  $2.9 \mu_B$ . The optimized solutions lie to the right of the maximum, in the range of higher  $m$  values. Their arrangement suggests that the differences in the obtained MAE values may result from different values of  $m$  obtained using different exchange-correlation potentials.

All calculations using the FPLO18 and FPLO5 codes, i.e. MAE( $m$ ), MAE,  $m$ ,  $K_1$ ,  $K_2$ ,  $T_C$  and the magnetostriction coefficient, were performed by me. Preparing graphs, analyzing results, and writing the first version of the manuscript were also my tasks. I am also the corresponding author of the discussed publication.

## 4.2 L1<sub>0</sub> FePt thin films with tilted and in-plane magnetic anisotropy: A first-principles study

The first publication on ultrathin films is J. Marciniak, M. Werwiński, *L1<sub>0</sub> FePt thin films with tilted and in-plane magnetic anisotropy: A first-principles study*, Phys. Rev. B, **108**, 214406 (2023). In this work, we looked at the influence of the thickness of ultrathin L1<sub>0</sub> FePt films on their magnetic properties in the range from 4 to 16 atomic layers with (111) and (010) surfaces in vacuum. The distances between atoms in the axis perpendicular to the film surface were kept fixed as in the bulk. In the case of (111) films, the calculated properties were the direction of the magnetic easy axis,  $m_s$  and  $m_l$ . Whereas, for (010) films, MAE and spin and orbital magnetic moments are analyzed. Moreover, for L1<sub>0</sub> FePt (010), the influence of two types of modifications of the outer atomic monolayers on the MAE value was studied, considering the removal of Fe/Pt atoms and substitution of Fe atoms with Pt atoms. Furthermore, the  $m_l$  distribution in 16 atomic monolayers FePt (010) thick film was determined. In the case of the (111) surface, the distributions of excess electrons and  $m_s$  and  $m_l$  in 16 atomic monolayers film were studied.

Regardless of the type of surface, whether (111) or (010), the highest values of the average magnetic moment were observed for the thinnest layers and converged asymptotically to the value of the average bulk phase magnetic moment L1<sub>0</sub> FePt. Generally, higher values of magnetic moments were obtained for (111) layers. In (111) layers, the most significant changes in the value of the magnetic moment are visible on the outer atoms of the model; however, in (010) layers, these changes in values occur mainly for the average value of  $m_s$  and  $m_l$ . Therefore, it can be concluded that while in the (010) layer, the magnetic moment on the outer and central atoms does not change significantly with the

change in thickness, the influence of the change in thickness and the presence of the surface is observed on several layers closest to the surface. The main source of magnetic moment fluctuations, especially in the case of three atomic layers closest to the surface, is charge transfer.

In the (010) L1<sub>0</sub> FePt films, it was noticed that it has an easy axis of magnetization in the plane of the film, consistent also with the [001] direction of the L1<sub>0</sub> phase, and therefore consistent with the direction of the alternating Fe and Pt atomic monolayers. In this case, however, we have two MAE values - one related to the change of the magnetization direction in the (100) plane and the other related to the change of the magnetization direction in the (010) plane, and the first one is higher. Therefore, these layers are more manageable in remagnetizing between directions in the plane of the layer than in the direction normal to the surface. With the change of thickness, we observe fluctuations of both MAE values, approaching the MAE value obtained for the bulk phase L1<sub>0</sub> FePt. The difference between the MAE values in different planes for most of the obtained results remains approximately constant in the studied scale of thickness changes. These films have not received much attention in the literature and have no practical applications to date. However, the observed preferred magnetization axis may allow using L1<sub>0</sub> FePt (010) as a pinning layer. We would expect a similar effect in other L1<sub>0</sub> (010) phases, such as FePd, CoPt, or FeNi.

We have shown in our studies that the easy axis of magnetization of the L1<sub>0</sub> FePt (111) phase tends to coincide with the [001] direction of the bulk phase. This is consistent with the experimental results present in the literature. Interestingly, the direction of the easy axis depends on the layer thickness, and for the thinnest layers, it is closer to the normal to the layer surface. The value of the tilt angle of the magnetization easy axis converges to the [001] direction of the L1<sub>0</sub> bulk phase with the increase of the layer thickness. It gives about 45° for a layer 6 atomic monolayers thick, i.e., about 1.3 nm.

When modifying the surface of the (010) L1<sub>0</sub> FePt films, the MAE value in the (100) plane is noticeably higher for the thinnest films when Fe atoms have been removed from the surface than for the ideal L1<sub>0</sub> FePt (010) film. The other modifications caused a decrease in both MAE values, with the substitution of Fe atoms by Pt atoms causing a more significant decrease in the MAE value. This modification also caused a relative change between the MAE in the (100) and (010) films, so switching between the emphasized direction in the layer plane and the direction perpendicular to the plane is easier than changing the direction in the plane.

The publication was prepared in cooperation with my supervisor, Dr. Mirosław Werwiński, with each dealing with different parts of the work. Models of layers with a thickness of 16 atomic monolayers were prepared by Dr. Mirosław Werwiński based on the bulk phase optimized as part of the publication [6] by me. I used these models to generate the remaining thicknesses. I did the calculations that allow investigating the dependence of the energy of systems with a thickness of 10 atomic layers, distributions of  $m_s$  (for (111)) and  $m_l$  (for (010)) on individual atoms in systems with a thickness of 16 atomic layers, changes in the values of  $m_s$  and  $m_l$ , MAE (for (010)) and the direction of the magnetic easy axis (for (111)) depending on the layer thickness. The graphical representation of the results obtained from my calculations, their analysis and interpretation (excluding the distributions of  $m_s$  (for (111)) and  $m_l$  (for (010)) on individual atoms in systems with 16 atomic layers) were also performed by me. I wrote the first version of the manuscript and



was responsible for the correspondence with the journal.

### 4.3 Magnetic anisotropy of L1<sub>0</sub> FeNi (001), (010), and (111) ultrathin films: A first-principles study

The next presented publication will be about L1<sub>0</sub> FeNi layers: J. Marciniak, M. Werwiński *Magnetic anisotropy of L1<sub>0</sub> FeNi (001), (010), and (111) ultrathin films: A first-principles study*, J. Magn. Magn. Mater., **609**, 172455 (2024). The work focuses on DFT studies of ultrathin L1<sub>0</sub> FeNi(001), (010), and (111) films with thicknesses from 4 to 16 atomic monolayers, analogous to the publication described in subsection 4.2. Atomic positions in the axis perpendicular to the surface of the layers have been optimized. In this work, we presented the analysis of the stability of individual layers, the MAE changes in (010) and (001) layers with thickness, the dependence of the tilt angle of the magnetic easy axis in (111) layers on the layer thickness, the distribution of  $m_s$  and  $m_l$  and electron transfer in 16-atom-thick layers. Apart from the studies of the ultrathin layers themselves, the work was supplemented with the results of the fixed spin moment method for the bulk phase L1<sub>0</sub> FeNi, the density of states of this phase, and the band structure along the  $\Gamma$ -Z path for both selected (010) and bulk phase layers.

The analysis of the obtained results in the publication begins with the analysis of the results of the fixed spin moment calculations for the L1<sub>0</sub> FeNi bulk phase. They explain one of the sources of the discrepancy between the results of DFT calculations using different exchange-correlation potentials and the experiment, described in more detail in Section 3. They also repeat analogous calculations for the L1<sub>0</sub> FePt bulk phase [6]. An extension of this analysis is to look at the density of states distribution, which makes it possible to explain the relationship between the MAE and the magnetic moment.

In the further part of the publication, calculations for ultrathin L1<sub>0</sub> FeNi layers are analyzed. We found that the total energy of the systems calculated per atom is higher than for the bulk phase and converges to its value with increasing layer thickness. The energy of the (111) layers is the lowest, while the differences between the (001) and (010) layers are slightly in favor of the (010) layers. This allows us to conclude that the stability of the (111), (010), and (001) layers decreases in this order. Also, the differences between the energies of individual layers of a given thickness decrease with increasing thickness. To further assess the stability of the layers, we also looked at the range of charge fluctuations at the surface of the layers. The charge transfer in the L1<sub>0</sub> FeNi layers is noticeably lower than in the L1<sub>0</sub> FePt layers.

As in the case of L1<sub>0</sub> FePt layers, we observe an increase in magnetic moments in the first three monolayers, passing in the center of the film to values close to those observed for the bulk phase. It is also observed that the (010) layers have higher moments on the outer layers than in the other models. The only exception in this case is the Ni atom forming the asymmetric (001) film's outermost monolayer.

Again, calculations of the MAE dependence on the layer thickness for (010) layers showed oscillations converging to the bulk phase MAE value. It also indicates a preference for switching between the in-plane directions of the layer than between [001] (in-plane) and [010] (normal to the layer surface). The energy difference between the in-plane directions of the layer is much lower than in (010) L1<sub>0</sub> FePt layers, which gives reason to expect that this difference will disappear at higher temperatures. At the same time, the

results obtained for the bulk phase by the fixed spin moment method give hope that this difference may increase, giving a stable, distinguished direction in the layer plane.

Also, the MAE for the (001) layers shows oscillations, although they are closer to the MAE value for the bulk phase than the (010) layer in the (100) plane. Such oscillatory behavior has already been observed in our previous work [I], as well as in other computational works [38, 39]. However, our MAE calculation results do not allow us to state with certainty that the direction of magnetization of the (001) layers is perpendicular to the layer surface because the obtained values do not exceed the shape anisotropy energy. This is an important criterion for magnetic stability. However, it should be taken into account that the calculations are performed at 0 K, and the final applications will probably occur at room temperature. Increasing the temperature causes a decrease in the value of the magnetic moment, and our results of the fixed spin moment suggest that this will cause an increase in the MAE.

The last topic discussed in the publication is the easy direction of magnetization in the (111) layer. After studying the (111) L1<sub>0</sub> FePt [I] layers, we expected a tilt of the easy axis direction. The tilt of the easy axis in the L1<sub>0</sub> FeNi layers grows more linearly and converges faster to the [001] bulk phase. Moreover, for a layer 4 atomic monolayers thick, the tilt of the easy axis is less than 10°. Therefore, it is possible that the formation of an ultrathin L1<sub>0</sub> FeNi (111) layer will allow obtaining a layer with a more stable out-of-plane direction. Here, too, the shape anisotropy energy will play an important role, and again, our results from the PBE exchange-correlation potential do not meet the condition of exceeding this value. Nevertheless, it is necessary to remember the influence of temperature on the magnetic moment and MAE mentioned in the previous paragraph.

Dr. Mirosław Werwiński prepared models of 16-atom-thick films based on the bulk phase optimized as part of the publication [40]. On their basis, I prepared models of thinner films and converged all layered systems. I presented and analyzed the results for ultrathin layers and wrote part of the manuscript.

#### 4.4 First-principles study of the magnetic anisotropy of ultrathin B-, C-, and N-doped FeCo films

The last work included in my dissertation is on 9 atomic monolayers thick FeCo-(B/C/N) films: J. Marciniak, M. Werwiński, J. Rychły-Gruszecka, *First-principles study of the magnetic anisotropy of ultrathin B-, C-, and N-doped FeCo films*, J. Magn. Magn. Mater., **589**, 171563 (2024). This publication focuses on the influence of B, C, and N dopants in the octahedral position located in the middle of the film on the magnetic properties of the Fe<sub>0.7</sub>Co<sub>0.3</sub> alloy films. As far as we know, it was the first approach to perform calculations of ultrathin film systems with dopants in interstitial positions. DFT calculations and the virtual crystal approximation (VCA) were used. As in the case of the publication on the L1<sub>0</sub> FeNi [II] layers, the atomic positions in the axis perpendicular to the layer surface were optimized. In addition to presenting the results for doped systems, calculations were also performed for the pure Fe and Fe<sub>0.7</sub>Co<sub>0.3</sub> layers to compare the obtained values. We analyzed the calculated MAE values, charge transfer, density of states, and the values and distribution of  $m_s$  and  $m_l$ .

Optimization of positions in the  $z$ -axis allowed us to observe the stretching of structures containing dopants. Interestingly, the B atom in the octahedral position causes a

greater deformation of the structure than C or N, which give very similar model thicknesses. The charge transfer behaves in the opposite manner - we obtained a lower charge on the B atom than on the C and N atoms (again, values very similar to each other). In all doped models, we observe electron transfer from the dopant mainly to atoms near the dopant and gradual relaxation of the excess charge towards the surface. Additionally, charge transfer shows that in  $\text{Fe}_{0.7}\text{Co}_{0.3}$  layers, in the context of charge transfer, the presence of the dopant is much more important than the surface for the charge distribution. It should be noted that even in the models without dopants, we observe lower charge fluctuations near the surface than in the  $\text{L1}_0$  FePt [I] or  $\text{L1}_0$  FeNi [II] layers.

When we look at the  $m_s$  values, we see that the presence of the surface changes the moment on the first two monolayers from the surface in both the undoped layers (Fe and  $\text{Fe}_{0.7}\text{Co}_{0.3}$ ) and in the doped layers. However, again, the presence of the dopant causes larger changes than those associated with the presence of the surface. The  $m_s$  is induced on the dopants with the opposite direction to the other atoms, and its absolute value decreases in the order B, C, and N. This trend is reversed for  $m_l$  - the magnetic orbital moments on the dopants are in the same direction as the other atoms, and their magnitude increases in the order B, C, and N. It should also be noted that while the presence of the dopant does not significantly affect the  $m_s$  value of the other atoms, it does decrease the value of  $m_l$  relative to  $m_l$  in the undoped  $\text{Fe}_{0.7}\text{Co}_{0.3}$  layer.

The addition of the dopant significantly reduces the MAE value. The B dopant causes negative magnetic anisotropy, which indicates magnetic anisotropy in the layer plane. The highest MAE value among the doped layers is obtained for the N-doped layer.

The density of states graphs presented in the publication [III] show the change in the magnetic character first by creating an alloy  $(\text{Fe}_{0.7}\text{Co}_{0.3})_{18}$  with respect to  $\text{Fe}_{18}$ , and then doping  $\text{Fe}_{0.7}\text{Co}_{0.3}$  with B, C and N atoms with respect to pure  $(\text{Fe}_{0.7}\text{Co}_{0.3})_{18}$ . We observe a progressive separation of states from majority and minority channels. Additionally, doping does not cause the appearance of sharp peaks, which allows us to conclude that the dopant atoms form chemical bonds with the alloy atoms.

As part of this work, I performed all calculations based on models provided by my supervisor, Dr. Mirosław Werwiński. I prepared the obtained results. I also partly prepared the graphical representation of the results and the analysis. I wrote part of the manuscript at the review stage.

## 5 Summary

In the above guide, I briefly presented my research background, both in the context of materials: applications of magnetic materials and thin films, data recording techniques, and the method used. I also started with the broad context of computational and simulation methods, further describing the basis of DFT calculations, approximations used by FPLO code, and possible sources of discrepancies between results. Then, I briefly described subsequent works, starting with the publication on bulk phase  $\text{L1}_0$  FePt [6] as an introduction to the work on  $\text{L1}_0$  FePt film. The first paper included in the dissertation is the publication on ultrathin films  $\text{L1}_0$  FePt [I]. Then, the work on ultrathin  $\text{L1}_0$  FeNi [II] films is described, and finally, the publication on  $\text{Fe}_{0.7}\text{Co}_{0.3}$  and  $\text{Fe}_{0.7}\text{Co}_{0.3}$ -X (X = B, C, N) layers [III] is presented.

The obtained results for  $\text{L1}_0$  phases indicate that the production of (111) films may

allow the creation of a system with a tilted magnetization direction. The tilt can be controlled by changing the film's thickness because the tilt angle increases with increasing thickness. Additionally, in the thinnest films tested  $L1_0$  (111), the easy axis of magnetization is almost perpendicular, especially in the case of  $L1_0$  FeNi. Hence, (111)  $L1_0$  films may be a non-intuitive method of producing layers with a perpendicular magnetization axis.

The (010)  $L1_0$  films exhibit in-plane anisotropy along the tetragonal [001]  $L1_0$  phase direction, with the MAE between in-plane directions being lower than with respect to the direction perpendicular to the film. Therefore, the change in the magnetization direction should be more accessible in the film's plane. In the case of  $L1_0$  FeNi, the preferred in-plane direction is most likely not thermally stable. Furthermore, the observed MAE changes in the  $L1_0$  layers are nonmonotonic.

The introduction of surface changes ( $L1_0$  FePt [I] films) as well as adding an extra atom in an octahedral position in the center of the film ( $\text{Fe}_{0.7}\text{Co}_{0.3}\text{-B/C/N}$  [III] films) leads to a significant change in the magnetocrystalline anisotropy energy value relative to the ideal models. However, only one of the modifications caused an increase in MAE - the removal of Fe atoms from the surface of the  $L1_0$  FePt (010) layers.

In summary, modifications of ultrathin films, regardless of their type, significantly affect magnetic properties. In the materials studied, the main differences occurred in the magnetocrystalline anisotropy energy and orbital magnetic moments values. Additionally, the type of surface affected the direction of the easy magnetization axis. The use of the (111) surface allowed for the tilted magnetization direction to be obtained, and changing the thickness of the layer with the (111) surface allowed for the setting of a specific tilt value. The above observations may contribute to the future development of electronic systems.

## 6 Copies of the articles

**$L1_0$  FePt thin films with tilted and in-plane magnetic anisotropy: A first-principles study**Joanna Marciniak<sup>\*</sup> and Mirosław Werwiński*Institute of Molecular Physics, Polish Academy of Sciences, M. Smoluchowskiego 17, 60-179 Poznań, Poland*

(Received 29 March 2023; revised 3 November 2023; accepted 21 November 2023; published 7 December 2023)

Ultrathin  $L1_0$  FePt films with different  $c$ -axis orientations relative to the film plane are promising candidates for data storage materials. In this work, within the framework of density functional theory, we calculated the magnetic properties of ultrathin  $L1_0$  FePt (111) and (010) films with thicknesses ranging from 4 to 16 atomic monolayers (from about 0.8 to 3.5 nm). The highest average magnetic moments are observed for the thinnest films considered and, with increasing film thickness, the values converge towards the magnetic moment for bulk. The observed increase comes mainly from enhanced moments in the two atomic monolayers closest to the surface of the films. The easy axis of magnetization of (111) films prefers an alignment close to the tetragonal axis—an example of tilted magnetic anisotropy. The 6-monolayer (111) film (about 1.3 nm thick) inclines the easy axis of magnetization of about  $45^\circ$  to the film plane, which can find use in applications. The (010) films show an in-plane easy magnetization axis in a unique  $L1_0$  tetragonal direction. This is an unusual type of in-plane anisotropy, as the particular direction preference is very strong. The computational results encourage further experimental studies of  $L1_0$  systems with tilted and in-plane fixed magnetic anisotropy.

DOI: [10.1103/PhysRevB.108.214406](https://doi.org/10.1103/PhysRevB.108.214406)**I. INTRODUCTION**

The increase in data recording density is made possible by using new materials. One of the approaches is using magnetic materials as thin films for this purpose because structuring can significantly improve the desired properties [1,2]. One of the characteristic parameters defining the potential of a given ferromagnetic material for use in data storage media is magnetocrystalline anisotropy energy (MAE). An example of a material with a very high positive MAE value, indicating strong uniaxial anisotropy, is the  $L1_0$  FePt phase. The experimental MAE value of the FePt  $L1_0$  phase is about  $11 \text{ MJ m}^{-3}$  at 4.2 K and  $8 \text{ MJ m}^{-3}$  at 300 K, while its Curie temperature is about 750 K [3]. The density functional theory (DFT) calculations performed for the bulk phase show that the MAE can be in the range of  $13.03\text{--}21.29 \text{ MJ m}^{-3}$  at 0 K [4–6] and that the spin magnetic moments are equal to  $2.95\mu_B$  on the Fe and  $0.22\mu_B$  on the Pt site. The temperature dependence of the MAE in FePt can be used in heat-assisted magnetic recording (HAMR)-based memory devices, which can provide both density and speed improvements in data processing [7–11]. Magnetic data storage application of  $L1_0$  FePt films have been discussed in a review article by Lyubina *et al.* [12].

Pioneering experiments using ordered tetragonal FePt magnetic thin films for data storage date back to the 1970s [13]. But the most intensive research and technological

development of methods for obtaining and analyzing FePt thin films for applications in spintronic devices occurred in the 1990s and the first two decades of the 21st century [14–16]. In most of the studies conducted, the FePt films have a thickness ranging from 10 nm to tens of nm [14–26], in contrast to work focusing on ultrathin FePt films with thicknesses of single nanometers [17,27–31]. In the early 1990s, epitaxial thin films (about 50 nm thick) of FePt (001) with perpendicular magnetic anisotropy were obtained [14]. In numerous cases, FePt films were deposited on a conventional MgO substrate [14,21,24,28,29,31], quite often on silver [19], oxidized silicon [18,25,32], and other glassy substrates [33,34]. Experimentally obtained  $L1_0$  FePt thin films are usually not continuous but granular, which provides an additional degree of freedom that can be controlled to improve the desired properties and achieve dedicated patterned surface films [20]. The main factor distinguishing FePt films from other materials is that they possess one of the highest coercivity values [35]. For example, Takahashi *et al.* obtained a huge coercivity of 42 kOe (4.2 T) for FePt films with a thickness of 10 nm [21]. In addition to the intrinsic properties of FePt, Takahashi *et al.* attributed this high value to the complete magnetic isolation of the nanoscale grains and the excellent uniaxial alignment of the  $c$  axis perpendicular to the film plane [21]. Such a high coercive field value is comparable to those obtained for extremely strong samarium-cobalt permanent magnets.

An important factor affecting the magnetic properties of the compound is the degree of ordering of the  $L1_0$  phase. Optimal selection of technical parameters, such as the type and temperature of the substrate during deposition and the time and temperature of annealing, makes it possible to obtain FePt films with very high ordering parameter reaching 0.95 [16,20,22].

<sup>\*</sup>Corresponding author: [joanna.marciniak@ifmpan.poznan.pl](mailto:joanna.marciniak@ifmpan.poznan.pl)Published by the American Physical Society under the terms of the [Creative Commons Attribution 4.0 International](https://creativecommons.org/licenses/by/4.0/) license. Further distribution of this work must maintain attribution to the author(s) and the published article's title, journal citation, and DOI.

The studies mentioned above of several nanometer-thick ultrathin FePt films reveal details of their granular microstructure [28–31]. For example, for 2 nm thick films, the average grain size is about 8 nm and the coercivity is about 17 kOe (1.7 T) with a degree of order ( $S$ ) of about 0.6–0.7 [28]. Highly ordered ( $S = 0.95$ ) highly textured granular films with grain diameters well below 5 nm achieve huge coercivity up to 7.3 T at room temperature [29]. In contrast, reducing the nominal thickness to 0.5 nm decreases coercivity to 0.2 T [29]. Zhang *et al.* for a FePt film thickness of 2.6 nm determined an averaged grain diameter of 4.3 nm [31] and shown that the Curie temperature differs between the grains of different sizes and increases rapidly with decreasing grain diameter. The magnetic anisotropy constant ( $K_u$ ) measured for 5 nm thick FePt film is equal to  $4.2 \text{ MJ m}^{-3}$ , while saturation magnetization is equal to  $980 \text{ emu cm}^{-3}$  ( $0.98 \text{ MA m}^{-1}$ ) [31].

Due to their tetragonal structure,  $L1_0$  FePt films are often obtained with a unique tetragonal  $c$  axis perpendicular to the plane of the film. This makes it possible to produce FePt films with perpendicular magnetic anisotropy that can be used in recording systems. However, in 2005, Albrecht *et al.* experimentally obtained [36] a system that, going beyond the standard configuration of longitudinal or perpendicular anisotropy, made it possible to achieve a magnetization direction tilted to the plane of the film, thus initiating a new path in the development of recording media [36,37]. At the same time, it was confirmed that tilting the magnetization direction to  $45^\circ$  minimizes the value of the switching field [36]. Since then, several other ways of achieving a film with tilted magnetization have been considered, such as ferromagnetic coupling of a tilted top Co layer with an in-plane magnetized bottom Co layer [38]. Much attention has been paid in particular to  $L1_0$  FePt and CoPt films [32,39], which can be deposited on the substrate in such a way that the unique tetragonal axis is strongly deviated from the plane of the film, as in the case of the growth of the FePt films with a (111) surface [33,34,40,41]. The  $L1_0$  FePt (111) films in the aforementioned experiments have a thickness of 20 to 60 nm. In contrast, the fabricated (111)-oriented CoPt single layer had a thickness of 5 nm [32]. The  $L1_0$  FePt (111) films were deposited on oxidized Si (001) and (100) surfaces [25,42], Si (100) covered with 5 nm MgO [15], Ta [40], and metallic glasses such as CoFeTaB [33] and FeHfNbYB [34]. The measured magnetization direction of the  $L1_0$  FePt(111) film is tilted by  $33\text{--}36^\circ$  out of plane to the film plane [40], roughly in the tetragonal axis of the alternating Fe and Pt atomic monolayers. FePt (111) films were also used in experimental pseudo spin valves [40], indicating a noticeable magnetoresistance, followed by a theoretical analysis of a spin valve with conical magnetization [43]. To directly measure angles of tilted magnetic anisotropy, Pişkin *et al.* proposed a new experimental method using anomalous and planar Hall effects together and called it angle-resolved Hall effect signals (ARHES) [39].

Although the possibility of aligning the tetragonal crystallographic axis of the  $L1_0$  FePt film in a direction [111] inclined to the film plane is relatively well studied, the alignment of the tetragonal  $c$  axis in the plane of the film appears less frequently in the literature [19,20,44–46]. This alignment of the  $c$  axis results in a magnetization oriented in a specific

direction in the plane. Such a uniaxial configuration could be called in-plane fixed magnetic anisotropy, as opposed to conventional in-plane magnetic anisotropy, when the approximately free rotation of the magnetization direction in the plane of the film is allowed.

All previous first-principles calculations of  $L1_0$  FePt films assumed a (001) surface (atomic Fe and Pt monolayers lying in the film plane) [47–54]. The FePt films considered were up to 19 atomic monolayers thick [54]. The effect of film thickness on magnetic properties was investigated and parameters such as surface magnetic anisotropy and bulk magnetic anisotropy were determined [47]. In addition, the properties of FePt films coated with Fe and Pt layers [47,49,52] and FePt films on MgO substrate with Cu and Pt overlays [50,51] were also studied from first principles. The hard magnetic properties of large FePt grains were also modeled [55], and the possibility of ferroelectric control of magnetic anisotropy in FePt/BaTiO<sub>3</sub> [48] and FePt/PbTiO<sub>3</sub> [53] heterostructures was computationally analyzed.

In the present work, we focus on the first-principles study of  $L1_0$  FePt thin films with (111) and (010) surfaces, limiting ourselves to freestanding FePt films surrounded on the top and bottom sides by vacuum (without including the substrate material and overlayer).

## II. CALCULATIONS' DETAILS

The starting point for the preparation of thin film models was the bulk phase crystallographic unit cell of  $L1_0$  FePt (space group  $P4/mmm$ ,  $a' = 3.872/\sqrt{2} = 2.738 \text{ \AA}$ , and  $c = 3.763 \text{ \AA}$ ), which we optimized earlier [6]. Based on the tetragonal unit cell, two sets of films ranging from 4 to 16 atomic monolayers were generated with (111) and (010) surfaces; see Fig. 1. The complete structural data of the  $L1_0$  FePt films with (111) and (010) surfaces with the extreme thicknesses of the 16 atomic monolayers are presented in Table I. The vacuum space in the direction normal to the film is added so that films of different thicknesses have a constant value of the unit cell lattice parameter  $c$ . The minimum height of vacuum space in the unit cell is about  $22 \text{ \AA}$  in 16-monolayer systems. The film models with smaller thicknesses were obtained by subtracting the outer monolayers. None of the structures considered were subjected to film geometry optimization. Such a simplification can be justified by results from Hammar *et al.* [54], where optimization of the geometry of the FePt film showed that mainly the positions of only three outer atomic monolayers change. The change in the distance between these layers is only about 1–2% and does not significantly affect the magnetic properties. All structure representations were prepared using VESTA code [56].

First-principles calculations were performed using the full-potential local-orbital code (FPLO18.00-52) developed to solve the Kohn-Sham equations of density functional theory [57,58]. The Perdew-Burke-Ernzerhof exchange-correlation potential (PBE) [59] was used. For each model, self-consistent scalar-relativistic calculations were performed with a  $60 \times 30 \times 5$   $\mathbf{k}$ -point mesh, a density convergence criterion of  $10^{-6}$ , and the tetrahedron method chosen for integration over the Brillouin zone. Finally, to find the magnetic anisotropy

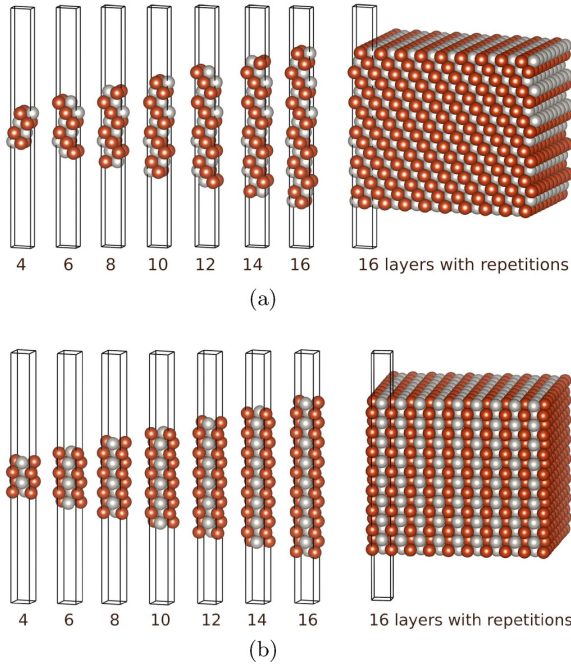


FIG. 1. Compilation of unit cells of  $L1_0$  FePt thin films with (111) (a) and (010) (b) surfaces and thicknesses ranging from 4 to 16 atomic monolayers [from about 0.9 to 3.5 nm for (111) films and from 0.78 to 3.1 nm for (010) films]. On the right, fragments of infinite films are generated by duplicating 16-monolayer unit cells several times in directions in the film plane.

energy, one fully relativistic iteration [58] was performed for each of the selected quantization directions of the considered films.

The calculations of the complete energy dependence of the systems on the magnetization direction were carried out for 10-monolayer structures with surfaces (111) and (010). To remove energy discrepancies between different magnetization directions due to variation in the choice of  $\mathbf{k}$ -mesh symmetry, these particular calculations were performed using computational unit cells with the space group reduced to  $P1$ . The magnetization direction was determined for a set of films with a surface (111) in the following way. Having found that the energy minimum must be in the plane (100) for each film thickness, calculations were made for directions in this plane varying every  $2^\circ$ . Based on five such results, the direction of the easy axis of magnetization was determined using a third-degree polynomial fit.

Below, we discuss some of the approximations adopted in this work, resulting from the need to reduce the computational complexity of the systems. These approximations can be divided into groups concerning crystallographic and electronic structure. The first group involves the assumption of infinite periodicity of the model in the film plane. This leads to a failure to incorporate finite layer and grain sizes of real materials in the magnetic shape anisotropy. Furthermore, magnetic films are usually deposited on substrates and coated with a cap layer in practical applications. Interactions

TABLE I. Structural data of  $L1_0$  FePt thin films with 16 atomic monolayers and surfaces (111) and (010). The unit cell parameters  $c$  specify the height of the computational unit cell, including the vacuum. The thicknesses of the (111) and (010) films themselves are 35.47 and 30.99 Å, respectively.

Element	(111) thin film			(010) thin film		
	$P12/m1$			$Pmma$		
	$a$ (Å)	$b$ (Å)	$c$ (Å)	$a$ (Å)	$b$ (Å)	$c$ (Å)
Fe	2.738	4.654	53.638	3.872	3.763	48.914
Pt	0.000	-0.173	-0.479	0.250	0.000	0.480
Pt	0.500	0.327	-0.479	-0.250	0.500	0.480
Fe	0.000	0.481	-0.438	-0.250	0.000	0.441
Pt	-0.500	-0.019	-0.438	0.250	0.500	0.441
Fe	0.000	0.135	-0.397	0.250	0.000	0.401
Pt	0.500	-0.365	-0.397	-0.250	0.500	0.401
Fe	0.000	-0.212	-0.356	-0.250	0.000	0.361
Pt	-0.500	0.288	-0.356	0.250	0.500	0.361
Fe	0.000	0.442	-0.314	0.250	0.000	0.322
Pt	0.500	-0.058	-0.314	-0.250	0.500	0.322
Fe	0.000	0.096	-0.273	-0.250	0.000	0.282
Pt	-0.500	-0.404	-0.273	0.250	0.500	0.282
Fe	0.000	-0.250	-0.232	0.250	0.000	0.243
Pt	0.500	0.250	-0.232	-0.250	0.500	0.243
Fe	0.000	0.404	-0.190	-0.250	0.000	0.203
Pt	-0.500	-0.096	-0.190	0.250	0.500	0.203

of the magnetic film with the substrate and overlayer can significantly affect the properties of the system. However, our models do not consider the substrate or overlayer. This assumption was due to the need to constrain the models to allow accurate, fully relativistic calculations to determine magnetic anisotropy energies. Another assumption is the fully ordered arrangement of atoms. Therefore, defects such as atom swapping or extra atoms in interstitial positions are not accounted for. Additionally, the models assume no other phases, no grains, and a perfect, atomically smooth surface of the films. Subsequently, it was also necessary to use approximations within the electronic structure. Several of these have been mentioned previously, but we will bring up two more. DFT calculations were performed for the ground state, meaning that the films' properties were determined for the temperature of 0 K. The obtained results of such quantities as magnetic moments and magnetic anisotropy may, therefore, differ from those observed at room temperature. In addition, we also assumed a collinear arrangement of magnetic moments, which may not be well met for the film surfaces.

Despite the series of approximations summarized above, the results obtained for  $L1_0$  FePt (111) and (010) films represent a significant step toward a better understanding of these structured materials. The presented calculations also represent the first attempt to model  $L1_0$  FePt films with an arrangement of atomic monolayers other than in the plane of the films. They are one of the first to study the thickness dependence of the magnetic properties of FePt films.



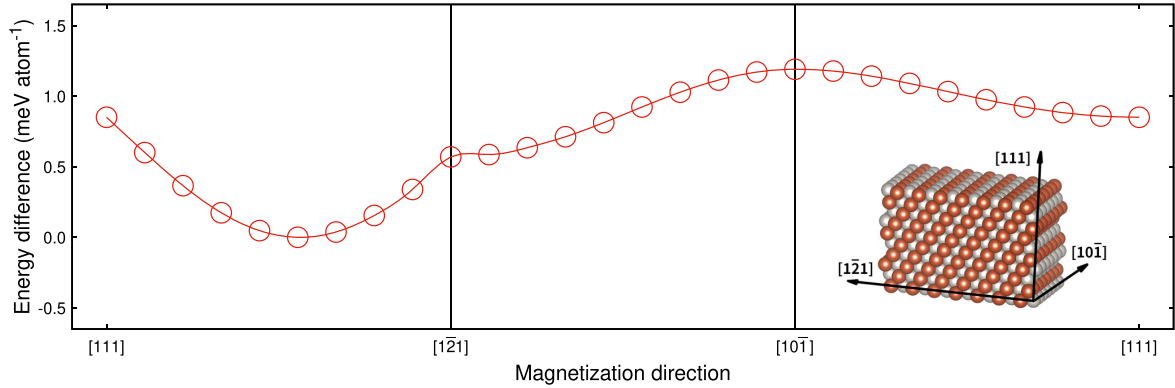


FIG. 2. Evolution of magnetic anisotropy energy with change in magnetization direction for a 10-monolayer  $L1_0$  FePt film with (111) surface. The energy difference is determined between the total energies for a given direction and the direction of the axis of easy magnetization (energy minimum). The energy minimum occurs at an angle of about  $50.0^\circ$  relative to the [111] direction. Calculations were performed with the PBE exchange-correlation potential using the FPLO18 code.

### III. RESULTS AND DISCUSSION

Among the magnetic compounds with the  $L1_0$  layered structure, FePt, FePd, FeNi, and CoPt are of especially interesting. In particular, their potential use for data storage makes them intensively studied, especially in the form of thin films. The thickness of experimentally investigated  $L1_0$  films is sometimes less than 1 nm (about five atomic monolayers) [29]. Several experimental studies also cover the range of ultrathin FePt films with thicknesses on the order of single nanometers. Among  $L1_0$  FePt films, systems with Fe and Pt monolayers arranged in the [001] direction are the most commonly studied. However, in the second decade of the 21st century, a lot of attention has also been paid by experimenters to  $L1_0$  FePt (111) films due to the observed tilted magnetic anisotropy and much less to  $L1_0$  FePt (010) films with the direction of alternating Fe/Pt monolayers perpendicular to the film plane. These two types of surfaces are also important from a practical point of view because, as previous calculations have shown, the energetically most stable  $L1_0$  FePt surface is (111), followed by (100/010), and only the third most stable is (001) [60]. So far, however, no computational analysis of the  $L1_0$  FePt (111) and (010) films has been performed under first-principles calculations. Since we are convinced this knowledge gap is worth filling, below we will present the computational results for ultrathin films (111) and (010) with thicknesses ranging from about 0.8 to 3.5 nm.

#### A. Thin films of $L1_0$ FePt (111)

We will begin by discussing the results obtained for films (111) as systems already better-recognized experimentally [33,34,40,41]. We will present computational results on how magnetic moments and magnetization direction change with the film thickness.

Figure 1(a) shows a set of prepared unit cells of  $L1_0$  FePt (111) with thicknesses ranging from 4 to 16 atomic monolayers. Since the models are infinitely periodic, the shown unit cells describe films infinite in a plane. The thickness of the 16-monolayer film is 3.5 nm, corresponding to a distance

of 0.22 nm between atomic monolayers in the [111] direction. Thus the thinnest 4-monolayer (111) film's thickness is 0.88 nm.

We begin the analysis of  $L1_0$  FePt films with (111) surface by determining the total energy dependence of the system as a function of magnetization direction for a film with a thickness of 10 atomic monolayers; see Fig. 2. Calculations were made for magnetization directions changing every  $10^\circ$  along the path [111]  $\rightarrow$  [121]  $\rightarrow$  [101]  $\rightarrow$  [111]. The selected 10-monolayer film shows an energy minimum at an angle of about  $50^\circ$  to the [111] direction. This means that the determined direction of magnetization is not precisely parallel to the direction of alignment of the Fe and Pt monolayers, which is equal to  $53.96^\circ$  (counting from the [111] direction, not from the plane of the film, as done

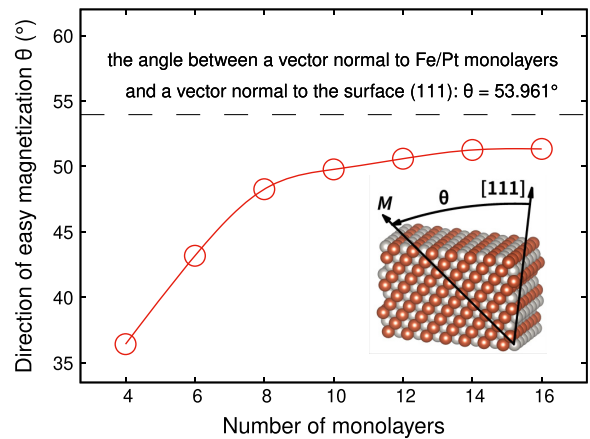


FIG. 3. Easy magnetization axis direction ( $\theta$ ) as a function of the thickness of  $L1_0$  FePt films with a surface (111). The angle between the vector normal to the Fe/Pt monolayers and the vector normal to the film surface ( $53.961^\circ$ ) is indicated as a dashed line. Calculations were performed with the PBE exchange-correlation potential using the FPLO18 code.



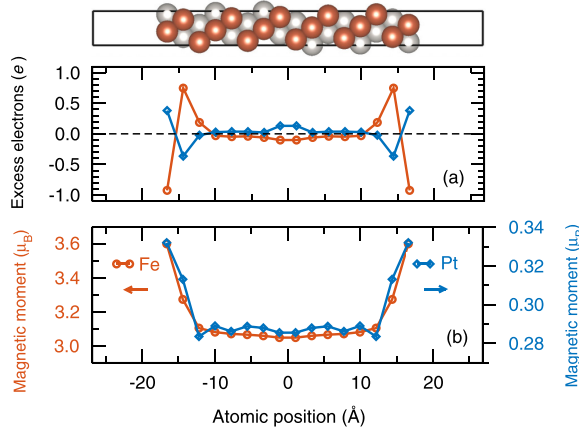


FIG. 4. Charge transfer (a) and spin magnetic moment (b) in a 16-monolayer (111) film of  $L1_0$  FePt, together with the unit cell shown on top as a function of atomic position in a direction perpendicular to the film plane. Calculations were performed with the PBE exchange-correlation potential in scalar-relativistic formalism using the FPLO18 code.

in Ref. [40]). The energy difference between the easy magnetization direction and the direction normal to the films is about  $0.85 \text{ meV atom}^{-1}$  ( $\sim 10 \text{ MJ m}^{-3}$ ), which is smaller than the  $1.38 \text{ meV atom}^{-1}$  for bulk FePt [6], but still implies very high magnetic anisotropy, as seen in Fig. 2.

Figure 3 shows the dependence of the easy magnetization direction on film thickness. For larger thicknesses, the magnetization angle converges in the direction of the alignment of Fe and Pt monolayers ( $\theta = 53.96^\circ$ ). However, for thinner films, the direction of magnetization deviates in the out-of-plane direction. For films with a thickness of six atomic monolayers (1.3 nm), the angle of easy magnetization is about  $45^\circ$ , which is the direction that minimizes the value of the switching field in systems with tilted magnetic anisotropy [36,37]. However, magnetically hard FePt films alone are not best suited for switching. Instead, it is conceivable that a magnetically hard film would be coupled to a magnetically soft layer, which can be switched much more easily.

Figure 4 shows two more characteristics relatively universal for the entire set of (111) films under consideration: the distributions of charge transfer and spin magnetic moment in an example film with a thickness of 16 monolayers. The sample's unit cell parameter  $c$  equals  $53.6 \text{ Å}$  and the film thickness is  $35.4 \text{ Å}$ . Since we chose to make the  $x$  axis centered at zero, the scale extends by  $26.8 \text{ Å}$  in both directions. The charge transfer plot reveals significant deviations for the three monolayers near the surface and electron deficiency on Fe atoms is compensated for on Pt atoms; see Fig. 4(a). Like the excess electrons, the spin magnetic moments of several monolayers near the surface stand out clearly. Moreover, the spin magnetic moments induced on Pt are proportional to those on Fe. The central and surface spin magnetic moments on Fe atoms are significantly elevated relative to the value for bcc Fe of  $2.15 \mu_B$  [61].

Figures 5 and 6 show the dependence of component and average magnetic moments on film thickness. The fully

relativistic values of the spin (orbital) magnetic moment on the surface of the 16-monolayer film are  $3.42$  ( $0.11$ ) and  $0.29$  ( $0.03$ )  $\mu_B \text{ atom}^{-1}$  for Fe and Pt atoms, respectively. They are elevated compared to the bulk  $L1_0$  FePt values, for which the spin (orbital) magnetic moments are equal to  $2.95$  ( $0.065$ ) and  $0.22$  ( $0.057$ )  $\mu_B \text{ atom}^{-1}$  for Fe and Pt atoms, respectively [6]. On the other hand, as we can see in Fig. 5, the values of magnetic moments we observe in the center of the film are comparable to the bulk values. However, additional noticeable changes in the values of magnetic moments are observed for the thinnest films with a thickness of fewer than 10 monolayers. Particularly for the 4-monolayer film, we observe a significant increase in the spin and orbital magnetic moments on Pt atoms on the surface. The average spin (total) magnetic moment of  $1.58$  ( $1.64$ )  $\mu_B \text{ atom}^{-1}$  is also elevated relative to the bulk values and increases further with decreasing film thickness. This is due to elevated magnetic moments on the film surface, whose contribution to the average becomes more significant with decreasing film thickness. An analogous dependence of the magnetic moment on the layer thickness was observed for ultrathin Fe films, both experimentally and theoretically [62,63].

In summary, we have shown that the ultrathin  $L1_0$  FePt (111) films are characterized by high-valued and tilted magnetic anisotropy and relatively high values of magnetic moments. Such strongly tilted magnetic anisotropies can find use, for example, as hard magnetic films for coupling with soft magnetic films, inducing tilted magnetization in the latter.

#### B. Thin films of FePt $L1_0$ (010)

In the second part, we discuss the computational results for  $L1_0$  FePt films with a tetragonal  $c$  direction oriented in the film plane; see Fig. 1(b). So far, usually on the occasion of more comprehensive studies, experimenters have observed islands/grains and areas of (100) and (010)  $L1_0$  FePt phase [19,20,44,45]. In those studies, films from 10 to 40 nm thick with areas of (100) and (010) surfaces were deposited on Ag, MgO (001), and  $\text{MgAl}_2\text{O}_4$  substrates. Sepehri-Amin *et al.* found that (100) and (010) FePt grains give an in-plane component in the magnetization curves [45]. As far as we have determined, there has been no detailed study of individual FePt (100) grains and their magnetic properties. However, intuition suggests that, at least for thicker (100) films, the magnetization should be directed in-plane and have a strong preference for alignment in the direction of the tetragonal axis. Such a uniaxial configuration can be called in-plane fixed magnetic anisotropy. Since the [100] and [010] tetragonal axis orientations are equivalent when FePt islands form on the substrate, the effective magnetization and in-plane anisotropy can average for larger sample areas. Nevertheless, we expect individual grains with (100) and (010) surfaces to exhibit strong in-plane fixed magnetic anisotropy.

Of the two symmetrically equivalent configurations [(100) and (010)], we arbitrarily chose the one with a (010) surface for the film models we prepared. The thickness of the 16-monolayer FePt (010) film is  $3.1 \text{ nm}$ , corresponding to a distance of  $0.194 \text{ nm}$  between atomic monolayers, which is half of the lattice parameter  $a$  of the bulk  $L1_0$  FePt. The

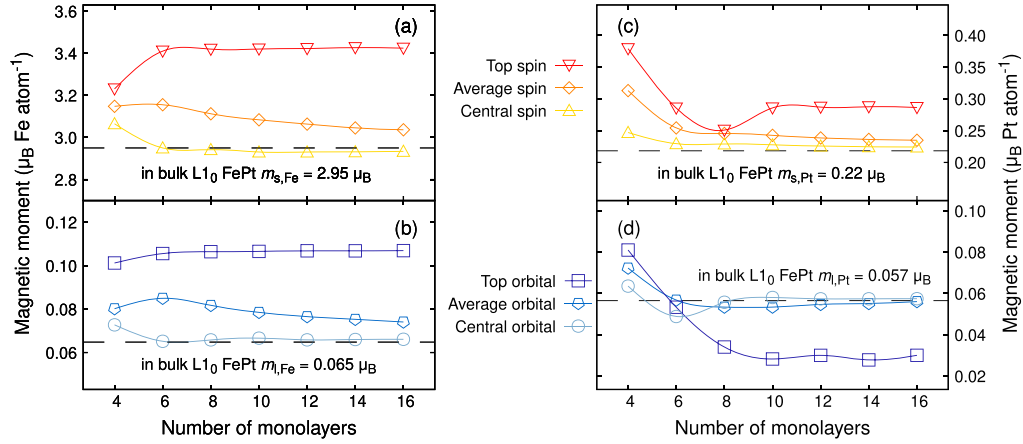


FIG. 5. Spin and orbital magnetic moments at Fe (a), (b) and Pt (c), (d) atoms as a function of the number of monolayers in  $L1_0$  FePt films with (111) surface obtained for easy magnetization direction. Magnetic moments at specified atoms for the bulk  $L1_0$  FePt system are indicated as dashed horizontal lines. The calculations were performed with the PBE exchange-correlation potential using the FPLO18 code.

thickness of the thinnest 4-monolayer (010) film considered is 0.78 nm.

To computationally determine the preferred magnetization direction in ultrathin  $L1_0$  FePt (010) films, for an example film with a thickness of 10 atomic monolayers, we have performed calculations of the dependence of the energy of the system on the direction of magnetization. The direction was changed according to the path of  $[010] \rightarrow [001] \rightarrow [100] \rightarrow [010]$  every  $10^\circ$  and the calculated results are presented in Fig. 7. The easy magnetization direction lies in the plane of the film and follows the direction of alternating Fe and Pt monolayers  $[001]$ . The energy difference between the easy

magnetization direction and the direction normal to the film is about  $1.2 \text{ meV atom}^{-1}$  ( $\sim 13 \text{ MJ m}^{-3}$ ), which is smaller than the  $1.38 \text{ meV atom}^{-1}$  for bulk FePt [6], but still very high. The energy difference between the two orthogonal in-plane magnetization directions ( $[001]$  and  $[100]$ ) is similarly very high, confirming the intuitive expectation of a strong fixed magnetic anisotropy in the plane of the film.

After a complete analysis of the energy-angle dependence for the 10-monolayer film, other thicknesses were considered in the range of 4 to 16 monolayers and the energies were calculated only for the unique magnetization directions  $[100]$ ,  $[010]$ , and  $[001]$ . Figure 8 shows the calculated energy differences  $E_{010} - E_{001}$  and  $E_{100} - E_{001}$  for the full range of film thicknesses taken into account. All the energy differences are positive and relatively high, which implies a high in-plane fixed magnetic anisotropy. Except for the 10-monolayer film, the energy difference of  $E_{010} - E_{001}$  is larger than  $E_{100} - E_{001}$  by about  $0.2 \text{ meV atom}^{-1}$ , indicating that the magnetization direction perpendicular to the film plane has the highest energy and is, therefore, the least preferred. In addition, the general trend shows a decrease in magnetic anisotropy with decreasing film thickness. However, the dependence on film thickness is not monotonic over the entire range considered, which is not surprising since many previous calculations for ultrathin films showed characteristic MAE oscillations [47,64–67]. Experimentally, oscillations of uniaxial magnetic anisotropy, with a period of 5.9 and 2.3 monolayers, were observed, for example, for ultrathin films of bcc Fe and fcc Co, respectively [68]. Detailed theoretical analysis has established that the observed oscillations result from the presence of quantum-well states located in the vicinity of the Fermi level [68] and originating from the so-called quantum size effect occurring in systems of sufficiently small size, in our case films on the order of single nanometers thick.

In addition to magnetic anisotropy, the average magnetic moment of the film is an important parameter for potential

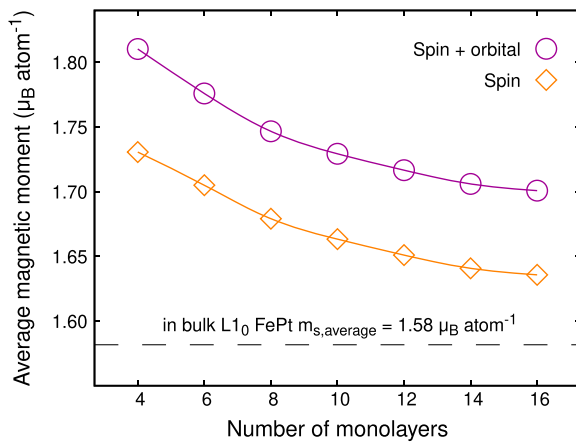


FIG. 6. Average total (spin + orbital) and spin magnetic moments for easy magnetization direction versus a number of atomic monolayers in  $L1_0$  FePt film with (111) surface. A dashed horizontal line indicates the average spin magnetic moment for a bulk  $L1_0$  FePt phase. The calculations were performed with the PBE exchange-correlation potential using the FPLO18 code.

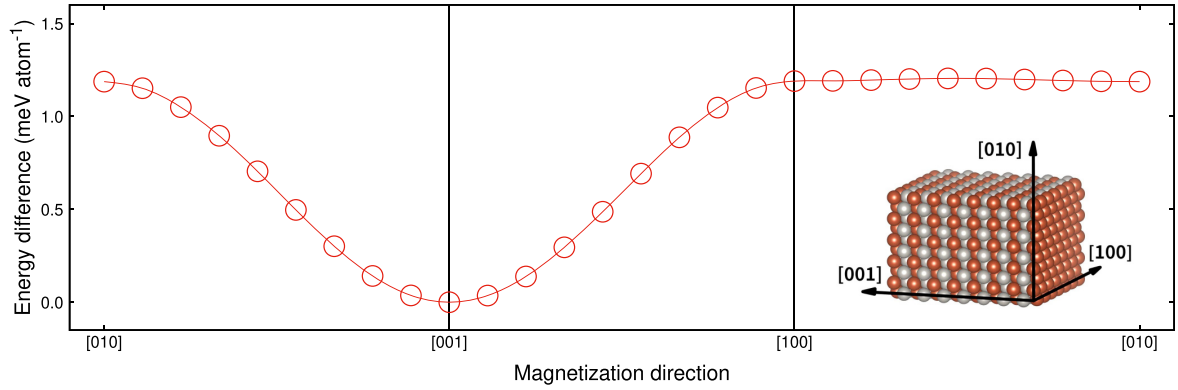


FIG. 7. Evolution of magnetic anisotropy energy with change in magnetization direction for a 10-monolayer film of  $L1_0$  FePt with (010) surface. The energy difference is determined between the total energies for a given direction and the direction of the axis of easy magnetization (energy minimum). Calculations were performed with PBE exchange-correlation potential using the FPLO18 code.

applications. Figures 9 and 10 show the dependence of magnetic moments on film thickness. The average total and spin magnetic moments decrease monotonically as the number of monolayers increases. They tend to reach values for the bulk  $L1_0$  FePt of  $1.58\mu_B \text{ atom}^{-1}$  for the spin magnetic moment and  $1.64\mu_B \text{ atom}^{-1}$  for the total magnetic moment [6]. The values of the average magnetic moments observed for the (010) films are slightly lower than for the (111) films (by about  $0.1\mu_B$ ); compare Figs. 6 and 9.

A more detailed analysis of the magnetic moments of Fe and Pt is shown in Fig. 10. As the thickness of the film increases, both the average moments and the moments on the atoms in the center of the film tend to be the values determined for the bulk phase [6]. The magnetic moments on Fe on the surface monolayer change noticeably less than the moments on the central monolayer and the average values.

They also remain approximately constant regardless of the film thickness. The observed nonmonotonic changes in spin magnetic moments on Pt atoms are related to the variations in the energy differences presented in Fig. 8.

Magnetocrystalline anisotropy energy (MAE) and orbital magnetic moment are related according to the formula of Bruno [69]:

$$\text{MAE} \sim \pm \frac{\xi}{4} \Delta m_L, \quad (1)$$

where  $\xi$  is the spin-orbit constant and  $\Delta m_L$  is the anisotropy of the orbital magnetic moment defined as

$$\Delta m_L = m_L^{\parallel} - m_L^{\perp}, \quad (2)$$

where  $m_L^{\parallel}$  and  $m_L^{\perp}$  are orbital magnetic moments calculated in two perpendicular magnetization directions.

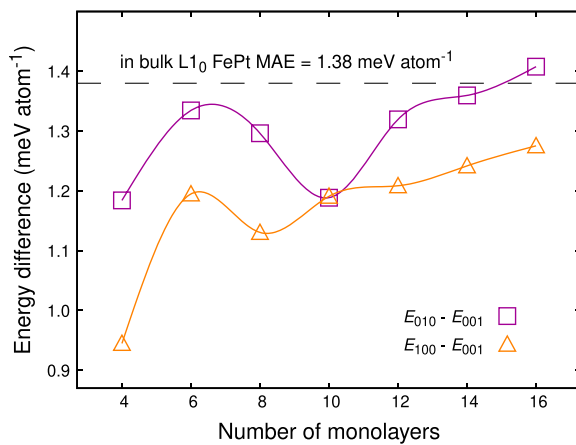


FIG. 8. Energy differences  $E_{010} - E_{001}$  and  $E_{100} - E_{001}$  as a function of thickness of  $L1_0$  FePt films with (010) surface. The energies  $E_{001}$ ,  $E_{010}$ , and  $E_{100}$  were determined for the corresponding magnetization directions using the FPLO18 with the PBE exchange-correlation potential.

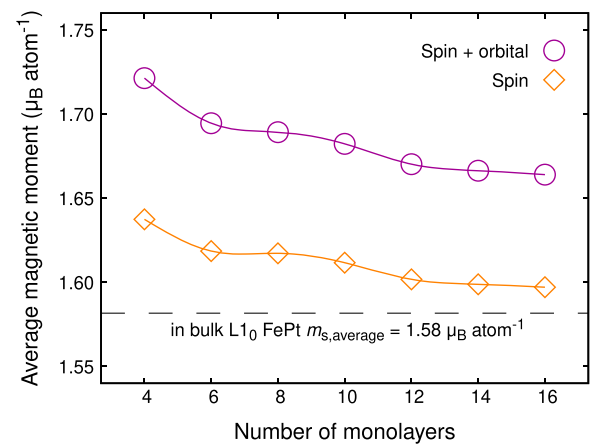


FIG. 9. Average total (spin + orbital) and spin magnetic moments versus the number of atomic monolayers in  $L1_0$  FePt (010) film. A dashed horizontal line indicates the average spin magnetic moment for the bulk  $L1_0$  FePt phase. Calculations were performed with the PBE exchange-correlation potential using the FPLO18 code.

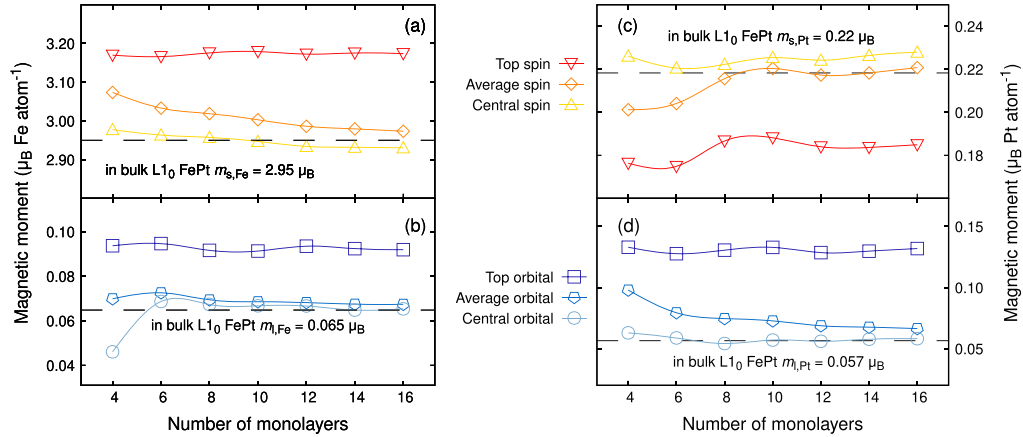


FIG. 10. Spin and orbital magnetic moments on Fe (a), (b) and Pt (c), (d) atoms as a function of the number of monolayers in  $L1_0$  FePt films with (010) surface. Magnetic moments on specified atoms for bulk  $L1_0$  FePt are indicated as dashed horizontal lines. Calculations were performed with the PBE exchange-correlation potential using the FPLO18 code.

For bulk  $L1_0$  FePt the calculated orbital magnetic moments are  $0.0648\mu_B$  ( $0.0590\mu_B$ ) for Fe in [001] ([110]) magnetization direction and  $0.0565\mu_B$  ( $0.0719\mu_B$ ) for Pt in [001] ([110]) direction. The calculated orbital magnetic moment differences are then  $\Delta m_L(Fe) = -0.0058\mu_B$  and  $\Delta m_L(Pt) = 0.0153\mu_B$ , which leads to the total  $\Delta m_L$  equal to  $0.0095\mu_B$  f.u.<sup>-1</sup>. The normalized contributions to  $\Delta m_L$  from Fe and Pt are then  $-0.61$  and  $1.61$ , respectively. The above result is in qualitative agreement with the sublattice-resolved MAE calculated by Ke for  $L1_0$  FePt using perturbation theory in a tight binding approach, which gives  $-0.16$  and  $1.16$  contributions for Fe and Pt (for MAE calculated as  $1.25$  meV atom<sup>-1</sup>) [70]. According to the formula of Bruno, we expect the same values of contributions for the MAE.

Following the above line of reasoning, in Fig. 11 we present the site-resolved orbital magnetic moments and their differences calculated for two magnetization directions ([001] and [010]) for an exemplary 16-monolayer thick  $L1_0$  FePt (010) film. We observe that in the central part of the film the values of orbital magnetic moments ( $m_l$ ) and their differences for two perpendicular magnetization directions ( $\Delta m_l$ ) are about the same as the values for bulk  $L1_0$  FePt. However, the orbital magnetic moments at the film's surfaces differ significantly from the values for the bulk [similar to the previously discussed site-resolved spin magnetic moments in the FePt (111) film]. A comparable pattern emerges also for orbital magnetic moments' differences, where for about five surface atomic monolayers we observe significant deviations from the values for the central part of the film. Assuming the applicability of Bruno's formula, we conclude that contributions of analogous proportions would also be obtained for decomposed MAE. This indicates mainly positive dominating contributions from Pt sites and smaller negative contributions from Fe sites. This means that, especially for films thinner than ten monolayers, modifications of individual surface monolayers may have the most significant effect on the total magnetic anisotropy of the film.

To demonstrate the impact of surface layer modification on the value of magnetic anisotropy energy, we modified one

monolayer located on the surface by (1) removing Pt atoms from it, (2) removing Fe atoms from it, and (3) replacing Fe atoms with Pt atoms. The calculations show that, for all considered films with modified surfaces, the average magnetic

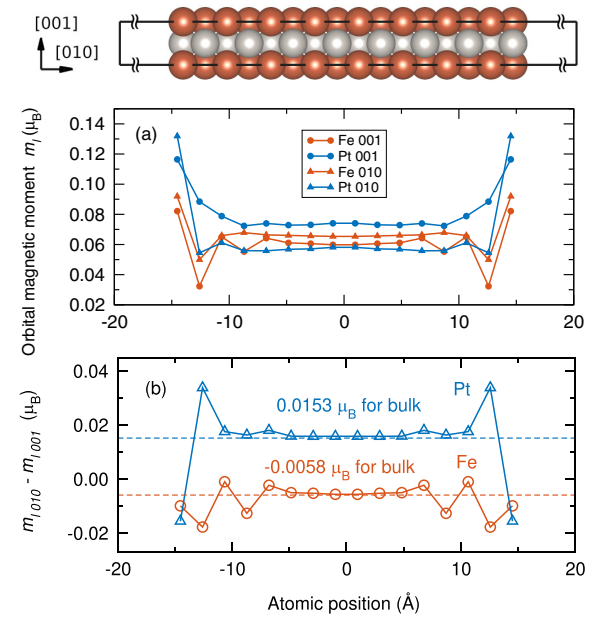


FIG. 11. Orbital magnetic moments on the atomic sites along the direction perpendicular to the film plane for 16-monolayer thick  $L1_0$  FePt (010) film calculated for [001] and [010] magnetization directions (a). Difference of orbital magnetic moments calculated between magnetization directions [010] and [001] (b). Dashed lines indicate Fe and Pt contributions calculated for bulk  $L1_0$  FePt. On top, a side view of the unit cell of 16-monolayer FePt (010) film. The calculations were performed with the FPLO18 code with the PBE exchange-correlation potential.

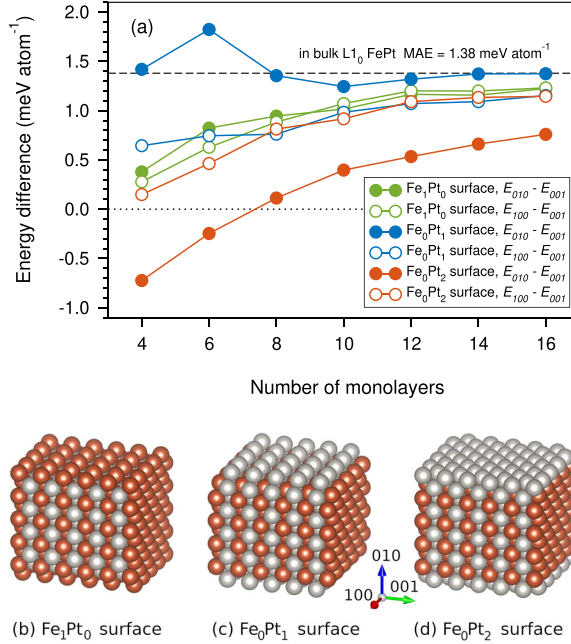


FIG. 12. Energy differences  $E_{010} - E_{001}$  and  $E_{100} - E_{001}$  as a function of the thickness of  $L1_0$  FePt films with (010) surface and modified top monolayer (a). Models of exemplary FePt (010) films of 10 monolayers thick with a modified surface single monolayer represented as unit cells multiplied several times in the directions of the film plane (b)–(d). Models include surface monolayer with removed Pt atoms (a), with removed Fe atoms (b), and with Fe replaced by Pt atoms (c). The energies  $E_{001}$ ,  $E_{010}$ , and  $E_{100}$  were determined for the corresponding magnetization directions using the FPLO18 with the PBE exchange-correlation potential.

moment per Fe atom decreases with increasing film thickness (not shown), similar to the results presented earlier for ideal films. Figure 12 shows our models and results of calculating the energy differences depending on the film thickness. The presented dependencies resemble the trends observed for perfect films (without modification), see Fig. 8, where we observe a tendency for the anisotropy energy to saturate with increasing film thickness. However, significant quantitative differences are observed for magnetic anisotropy energies  $E_{010} - E_{001}$  for films with surface monolayers that do not contain Fe [ $\text{Fe}_0\text{Pt}_1$  and  $\text{Fe}_0\text{Pt}_2$ ; see Figs. 12(c) and 12(d)]. For the  $\text{Fe}_0\text{Pt}_1$  films, the thinnest ones do not show a substantial decrease in anisotropy energy. In contrast, for the  $\text{Fe}_0\text{Pt}_2$  films, the observed energy difference values are significantly shifted toward lower ones, resulting in negative values for films with thicknesses below eight monolayers, which indicates a change in magnetization direction preference from fixed in-plane to out-of-plane. The above results confirm that the value of magnetic anisotropy energy determined for ideal FePt films can change considerably under the influence of modification of even a single monolayer on the film surface and that the most pronounced differences can be observed in FePt films with the smallest thickness of several monolayers.

$L1_0$  FePt thin films and grains with the direction of the tetragonal axis aligned in the plane with respect to the substrate have great application potential and have not yet been sufficiently investigated experimentally. It would be desirable to continue the previous studies [19,20,44,45] to obtain  $L1_0$  FePt grains with the (010)/(100) surface and the high value of the ordering parameter and characterizing the magnetic properties of individual grains. Furthermore, we also expect a similar magnetization direction anisotropy as for  $L1_0$  FePt (010) films for other  $L1_0$  phases, such as FePd, FeNi, and CoPt. We want to emphasize that the in-plane anisotropy observed for the (010) films is unusual, as it strongly distinguishes a specific in-plane direction. We associate the vertical alignment of the Fe and Pt monolayers relative to the film plane with books stacked on a shelf. Hence perhaps this type of  $L1_0$  film geometry could be referred to as a *bookshelf* configuration, as opposed to what is usually referred to as a *sandwich* geometry of a film specifying several layers arranged in a plane.

#### IV. SUMMARY AND CONCLUSIONS

This paper presented the results of density functional theory calculations of self-standing ultrathin  $L1_0$  FePt films with (111) and (010) surfaces. We looked at two sets of films with thicknesses from about 0.8 nm to 3.5 nm (from 4 to 16 atomic monolayers). All considered systems show a significant increase in the magnetic moment on the two near-surface atomic monolayers, leading to an increase in the average magnetic moment value relative to the value obtained for the bulk phase. This value decreases asymptotically with increasing film thickness. The presented dependencies of spin and orbital magnetic moments on Fe and Pt atoms on film thickness reveal additional deviations from the trends for the thinnest films regarded, with a thickness of around 1.0 nm (4–6 atomic monolayers). Furthermore, we observed higher magnetic moment values on surfaces (111) than on surfaces (010).

The observed increase in magnetic moments near the surface relates to the apparent charge transfer, especially in the three near-surface monolayers. In the case of  $L1_0$  FePt (111) thin films, the alignment of the easy magnetization axis in the unique direction of the  $L1_0$  tetragonal structure was experimentally confirmed earlier. Calculations for ultrathin  $L1_0$  FePt (111) films also indicate a tilted magnetic anisotropy. Moreover, calculations have shown that reducing the thickness of the (111) films to about a few atomic monolayers leads to a further tilt of the easy direction toward the out-of-plane. However, an optimal angle of 45° from the point of view of potential applications is observed for a thickness of 6 monolayers (about 1.3 nm).

In the case of the  $L1_0$  FePt (010) films, we showed that the easy magnetization axis is located in the plane of the film in a unique tetragonal direction, consistent with the direction of the ordering of the Fe/Pt monolayers. The calculations also allowed for the determination of the value of the magnetic anisotropy energy in the film plane, which turned out to be only slightly lower than the value observed for bulk  $L1_0$  FePt. This means that the  $L1_0$  FePt (010) films have an in-plane magnetic anisotropy with a very strong preference for



a distinct in-plane direction, as opposed to a regular in-plane magnetic anisotropy when all magnetization directions are energetically nearly equivalent.

The  $L1_0$  FePt (010) films have not yet received much attention and have found no practical application. However, we hope that the predicted high value of in-plane fixed magnetic anisotropy will also make it possible to find a use for (010) films, e.g., as a substrate for pinning soft magnetic layers in a fixed in-plane direction. Intuitively, we predict that analogous preferences for the directions of the easy magnetization axes can also be found in films of other  $L1_0$  phases, such as FePd, FeNi, and CoPt.

# ACKNOWLEDGMENTS

We acknowledge the financial support of the National Science Centre Poland under the decision DEC-2018/30/E/ST3/00267. We thank P. Leśniak and D. Depcik for compiling the scientific software and administration of the computing cluster at the Institute of Molecular Physics, Polish Academy of Sciences. We also thank J. Rychły-Gruszecka and J. Snarski-Adamski for reading the manuscript and providing valuable comments and discussion. We want to thank D. Kiphart for reading the manuscript and for his comments on the language.

- [1] R. W. Siegel, Synthesis and properties of nanophase materials, *Mater. Sci. Eng. A* **168**, 189 (1993).
- [2] M. Gell, Application opportunities for nanostructured materials and coatings, *Mater. Sci. Eng. A* **204**, 246 (1995).
- [3] N. Hai, N. Dempsey, and D. Givord, Magnetic properties of hard magnetic FePt prepared by cold deformation, *IEEE Trans. Magn.* **39**, 2914 (2003).
- [4] S. Ayaz Khan, P. Blaha, H. Ebert, J. Minár, and O. Šipr, Magnetocrystalline anisotropy of FePt: A detailed view, *Phys. Rev. B* **94**, 144436 (2016).
- [5] M. Wolloch, D. Suess, and P. Mohn, Influence of antisite defects and stacking faults on the magnetocrystalline anisotropy of FePt, *Phys. Rev. B* **96**, 104408 (2017).
- [6] J. Marciniak, W. Marciniak, and M. Werwiński, DFT calculation of intrinsic properties of magnetically hard phase  $L1_0$  FePt, *J. Magn. Magn. Mater.* **556**, 169347 (2022).
- [7] J. A. Christodoulides, Y. Huang, Y. Zhang, G. C. Hadjipanayis, I. Panagiotopoulos, and D. Niarchos, CoPt and FePt thin films for high density recording media, *J. Appl. Phys.* **87**, 6938 (2000).
- [8] J.-U. Thiele, S. Maat, and E. E. Fullerton, FeRh/FePt exchange spring films for thermally assisted magnetic recording media, *Appl. Phys. Lett.* **82**, 2859 (2003).
- [9] O. Hovorka, S. Devos, Q. Coopman, W. J. Fan, C. J. Aas, R. F. L. Evans, X. Chen, G. Ju, and R. W. Chantrell, The Curie temperature distribution of FePt granular magnetic recording media, *Appl. Phys. Lett.* **101**, 052406 (2012).
- [10] D. Weller, G. Parker, O. Mosendz, A. Lyberatos, D. Mitin, N. Y. Safonova, and M. Albrecht, Review Article: FePt heat assisted magnetic recording media, *J. Vac. Sci. Technol. B* **34**, 060801 (2016).
- [11] R. John, M. Berritta, D. Hinzke, C. Müller, T. Santos, H. Ulrichs, P. Nieves, J. Walowski, R. Mondal, O. Chubykalo-Fesenko, J. McCord, P. M. Oppeneer, U. Nowak, and M. Münzenberg, Magnetisation switching of FePt nanoparticle recording medium by femtosecond laser pulses, *Sci. Rep.* **7**, 4114 (2017).
- [12] J. Lyubina, B. Rellinghaus, O. Gutfleisch, and M. Albrecht, Structure and Magnetic Properties of  $L1_0$ -Ordered Fe–Pt Alloys and Nanoparticles, in *Handbook of Magnetic Materials* (Elsevier, Amsterdam, 2011), Vol. 19, pp. 291–407.
- [13] N. N. Evtkhiev, N. A. Ekonomov, A. R. Krebs, N. A. Zamyatina, A. S. Komalov, V. G. Pinko, and L. V. Ivaeva, FePt and CoPt alloy films for magneto-optic storage, *Phys. Status Solidi A* **50**, K153 (1978).
- [14] B. M. Lairson, M. R. Visokay, R. Sinclair, and B. M. Clemens, Epitaxial PtFe(001) thin films on MgO(001) with perpendicular magnetic anisotropy, *Appl. Phys. Lett.* **62**, 639 (1993).
- [15] C. L. Platt, K. W. Wierman, E. B. Svedberg, R. van de Veerdonk, J. K. Howard, A. G. Roy, and D. E. Laughlin,  $L1_0$  ordering and microstructure of FePt thin films with Cu, Ag, and Au additive, *J. Appl. Phys.* **92**, 6104 (2002).
- [16] E. Yang, D. E. Laughlin, and J.-G. Zhu, Correction of order parameter calculations for FePt perpendicular thin films, *IEEE Trans. Magn.* **48**, 7 (2012).
- [17] K. Coffey, M. Parker, and J. Howard, High anisotropy thin films for longitudinal recording, *IEEE Trans. Magn.* **31**, 2737 (1995).
- [18] T. Shimatsu, J. Lodder, Y. Sugita, and Y. Nakamura, Thermal fluctuation of magnetization in nanocrystalline FePt thin films with high coercivity, *IEEE Trans. Magn.* **35**, 2697 (1999).
- [19] Y.-N. Hsu, S. Jeong, D. Lambeth, and D. Laughlin, In situ ordering of FePt thin films by using Ag/Si and Ag/Mn<sub>3</sub>Si/Ag/Si templates, *IEEE Trans. Magn.* **36**, 2945 (2000).
- [20] T. Shima, K. Takanashi, Y. K. Takahashi, and K. Hono, Preparation and magnetic properties of highly coercive FePt films, *Appl. Phys. Lett.* **81**, 1050 (2002).
- [21] Y. K. Takahashi, K. Hono, T. Shima, and K. Takanashi, Microstructure and magnetic properties of FePt thin films epitaxially grown on MgO (001) substrates, *J. Magn. Magn. Mater.* **267**, 248 (2003).
- [22] K. Barmak, J. Kim, L. H. Lewis, K. R. Coffey, M. F. Toney, A. J. Kellock, and J.-U. Thiele, On the relationship of magnetocrystalline anisotropy and stoichiometry in epitaxial  $L1_0$  CoPt (001) and FePt (001) thin films, *J. Appl. Phys.* **98**, 033904 (2005).
- [23] C. Y. You, Y. K. Takahashi, and K. Hono, Particulate structure of FePt thin films enhanced by Au and Ag alloying, *J. Appl. Phys.* **100**, 056105 (2006).
- [24] A. P. Mihai, J. P. Attané, A. Marty, P. Warin, and Y. Samson, Electron-magnon diffusion and magnetization reversal detection in FePt thin films, *Phys. Rev. B* **77**, 060401(R) (2008).
- [25] E. Sallica Leva, R. C. Valente, F. Martínez Tabares, M. Vázquez Mansilla, S. Roshdestwensky, and A. Butera, Magnetic domain crossover in FePt thin films, *Phys. Rev. B* **82**, 144410 (2010).
- [26] S. Matsumoto and T. Shima, Magnetic properties of FePt thin films with multilayered structure, *J. Phys.: Conf. Ser.* **266**, 012038 (2011).

- [27] Y.-C. Wu, L.-W. Wang, and C.-H. Lai, Low-temperature ordering of (001) granular FePt films by inserting ultrathin  $\text{SiO}_2$  layers, *Appl. Phys. Lett.* **91**, 072502 (2007).
- [28] A. Perumal, Y. K. Takahashi, T. O. Seki, and K. Hono, Particulate structure of  $L1_0$  ordered ultrathin FePt films for perpendicular recording, *Appl. Phys. Lett.* **92**, 132508 (2008).
- [29] F. Kurth, M. Weisheit, K. Leistner, T. Gemming, B. Holzapfel, L. Schultz, and S. Fähler, Finite-size effects in highly ordered ultrathin FePt films, *Phys. Rev. B* **82**, 184404 (2010).
- [30] A. Kaidatzis, V. Psycharis, G. Giannopoulos, J. M. García-Martín, and D. Niarchos, Magnetic anisotropy axis reorientation at ultrathin FePt films, *Phys. Status Solidi RRL* **11**, 1600386 (2017).
- [31] Y. Zhang, A. Kalitsov, J. Ciston, O. Mryasov, B. Ozdol, J. Zhu, S. Jain, B. Zhang, B. Livshitz, A. Chernyshov, A. Ajan, P. Dorsey, G. Bertero, R. Acharya, A. Greene, and S. Myers, Microstructure and magnetic properties of ultrathin FePt granular films, *AIP Adv.* **8**, 125018 (2018).
- [32] Z. Li, K. Zhang, L. Shen, X. Xie, W. Chen, Z. Zhou, L. Lu, M. Liu, S. Yan, W. Zhao, and Q. Leng, Field-free magnetization switching induced by bulk spin-orbit torque in a (111)-oriented CoPt single layer with in-plane remanent magnetization, *ACS Appl. Electron. Mater.* **4**, 4033 (2022).
- [33] P. Sharma, N. Kaushik, A. Makino, M. Esashi, and A. Inoue,  $L1_0$  FePt(111)/glassy CoFeTaB bilayered structure for patterned media, *J. Appl. Phys.* **109**, 07B908 (2011).
- [34] Y. Wang, P. Sharma, and A. Makino, Magnetization reversal in a preferred oriented (111)  $L1_0$  FePt grown on a soft magnetic metallic glass for tilted magnetic recording, *J. Phys.: Condens. Matter* **24**, 076004 (2012).
- [35] J. Snarski-Adamski, J. Rychły, and M. Werwiński, Magnetic properties of 3d, 4d, and 5d transition-metal atomic monolayers in Fe/TM/Fe sandwiches: Systematic first-principles study, *J. Magn. Magn. Mater.* **546**, 168828 (2022).
- [36] M. Albrecht, G. Hu, I. L. Guhr, T. C. Ulbrich, J. Boneberg, P. Leiderer, and G. Schatz, Magnetic multilayers on nanospheres, *Nat. Mater.* **4**, 203 (2005).
- [37] J.-P. Wang, Tilting for the top, *Nat. Mater.* **4**, 191 (2005).
- [38] S. Łazarski, W. Skowroński, J. Kanak, Ł. Karwacki, S. Ziętek, K. Grochot, T. Stobiecki, and F. Stobiecki, Field-free spin-orbit-torque switching in Co/Pt/Co multilayer with mixed magnetic anisotropies, *Phys. Rev. Appl.* **12**, 014006 (2019).
- [39] H. Pişkin, E. Demirci, M. Öztürk, and N. Akdoğan, Experimental determination of the orientation of tilted magnetic anisotropy by using angle-resolved hall effect signals, *J. Supercond. Nov. Magn.* **34**, 1435 (2021).
- [40] C. L. Zha, J. Persson, S. Bonetti, Y. Y. Fang, and J. Åkerman, Pseudo spin valves based on  $L1_0$  (111)-oriented FePt fixed layers with tilted anisotropy, *Appl. Phys. Lett.* **94**, 163108 (2009).
- [41] C. Zha and J. Åkerman, Study of pseudo spin valves based on  $L1_0$  (111)-oriented FePt and FePtCu fixed layer with tilted magnetocrystalline anisotropy, *IEEE Trans. Magn.* **45**, 3491 (2009).
- [42] R. A. Ristau, K. Barmak, L. H. Lewis, K. R. Coffey, and J. K. Howard, On the relationship of high coercivity and  $L1_0$  ordered phase in CoPt and FePt thin films, *J. Appl. Phys.* **86**, 4527 (1999).
- [43] R. Matsumoto, H. Arai, S. Yuasa, and H. Imamura, Spin-transfer-torque switching in a spin-valve nanopillar with a conically magnetized free layer, *Appl. Phys. Express* **8**, 063007 (2015).
- [44] M. Ohtake, S. Ouchi, F. Kirino, and M. Futamoto,  $L1_0$  ordered phase formation in FePt, FePd, CoPt, and CoPd alloy thin films epitaxially grown on MgO(001) single-crystal substrates, *J. Appl. Phys.* **111**, 07A708 (2012).
- [45] H. Sepehri-Amin, H. Iwama, T. Ohkubo, T. Shima, and K. Hono, Microstructure and in-plane component of  $L1_0$ -FePt films deposited on MgO and  $\text{MgAl}_2\text{O}_4$  substrates, *Scr. Mater.* **130**, 247 (2017).
- [46] K. Wu, X. Fu, W. Zhu, and X. Huang, Atomic-scale investigation on the origin of in-plane variants in  $L1_0$ -FePt nanoparticles embedded in a single-crystalline MgO matrix, *J. Appl. Phys.* **132**, 175305 (2022).
- [47] H. Zhang, M. Richter, K. Koepernik, I. Opahle, F. Tasnádi, and H. Eschrig, Electric-field control of surface magnetic anisotropy: a density functional approach, *New J. Phys.* **11**, 043007 (2009).
- [48] M. Lee, H. Choi, and Y.-C. Chung, Ferroelectric control of magnetic anisotropy of FePt/BaTiO<sub>3</sub> magnetoelectric heterojunction: A density functional theory study, *J. Appl. Phys.* **113**, 17C729 (2013).
- [49] C. J. Aas, P. J. Hasnip, R. Cuadrado, E. M. Plotnikova, L. Szunyogh, L. Udvardi, and R. W. Chantrell, Exchange coupling and magnetic anisotropy at Fe/FePt interfaces, *Phys. Rev. B* **88**, 174409 (2013).
- [50] W. Zhu, H.-C. Ding, S.-J. Gong, Y. Liu, and C.-G. Duan, First-principles studies of the magnetic anisotropy of the Cu/FePt/MgO system, *J. Phys.: Condens. Matter* **25**, 396001 (2013).
- [51] W. Zhu, D. Xiao, Y. Liu, S. J. Gong, and C.-G. Duan, Picosecond electric field pulse induced coherent magnetic switching in MgO/FePt/Pt(001)-based tunnel junctions: A multiscale study, *Sci. Rep.* **4**, 4117 (2014).
- [52] G. Géranton, F. Freimuth, S. Blügel, and Y. Mokrousov, Spin-orbit torques in  $L1_0$  - FePt/Pt thin films driven by electrical and thermal currents, *Phys. Rev. B* **91**, 014417 (2015).
- [53] T. Liu, X. Wei, and J. Cao, Modulation of magnetocrystalline anisotropy in FePt/PbTiO<sub>3</sub> heterostructures by ferroelectric polarization, *J. Phys.: Condens. Matter* **31**, 395801 (2019).
- [54] K. Hammar, Y. Labaye, L. Messad, and A. Ziane, Theoretical estimation of surface magnetic anisotropy on  $L1_0$ -FePt thin films: Case of perfect and defect surfaces, *Surf. Sci.* **717**, 121999 (2022).
- [55] C. Antoniuk, M. E. Gruner, M. Spasova, A. V. Trunova, F. M. Römer, A. Warland, B. Krumme, K. Fauth, S. Sun, P. Entel, M. Farle, and H. Wende, A guideline for atomistic design and understanding of ultrahard nanomagnets, *Nat. Commun.* **2**, 528 (2011).
- [56] K. Momma and F. Izumi, VESTA: a three-dimensional visualization system for electronic and structural analysis, *J. Appl. Crystallogr.* **41**, 653 (2008).
- [57] K. Koepernik and H. Eschrig, Full-potential nonorthogonal local-orbital minimum-basis band-structure scheme, *Phys. Rev. B* **59**, 1743 (1999).
- [58] H. Eschrig, M. Richter, and I. Opahle, Chapter 12: Relativistic Solid State Calculations, in *Theoretical and Computational Chemistry*, Relativistic Electronic Structure Theory Vol. 14, edited by P. Schwerdtfeger (Elsevier, Amsterdam, 2004), pp. 723–776.

- [59] J. P. Perdew, K. Burke, and M. Ernzerhof, Generalized gradient approximation made simple, *Phys. Rev. Lett.* **77**, 3865 (1996).
- [60] A. Dannenberg, M. E. Gruner, A. Hucht, and P. Entel, Surface energies of stoichiometric FePt and CoPt alloys and their implications for nanoparticle morphologies, *Phys. Rev. B* **80**, 245438 (2009).
- [61] V. L. Moruzzi, P. M. Marcus, K. Schwarz, and P. Mohn, Ferromagnetic phases of bcc and fcc Fe, Co, and Ni, *Phys. Rev. B* **34**, 1784 (1986).
- [62] J. I. Beltrán, L. Balcells, and C. Martínez-Boubeta, Interfacial geometry dependence of the iron magnetic moment: The case of MgO/Fe/MgO, *Phys. Rev. B* **85**, 064417 (2012).
- [63] G. Scheunert, O. Heinonen, R. Hardeman, A. Lapicki, M. Gubbins, and R. M. Bowman, A review of high magnetic moment thin films for microscale and nanotechnology applications, *Appl. Phys. Rev.* **3**, 011301 (2016).
- [64] L. Szunyogh, B. Újfalussy, C. Blaas, U. Pustogowa, C. Sommers, and P. Weinberger, Oscillatory behavior of the magnetic anisotropy energy in Cu(100)/Co<sub>n</sub> multilayer systems, *Phys. Rev. B* **56**, 14036 (1997).
- [65] M. Blanco-Rey, P. Perna, A. Gudin, J. M. Diez, A. Anadón, P. Ollerós-Rodríguez, L. de Melo Costa, M. Valvidares, P. Gargiani, A. Guedeja-Marron, M. Cabero, M. Varela, C. García-Fernández, M. M. Otrokov, J. Camarero, R. Miranda, A. Arnau, and J. I. Cerdá, Large perpendicular magnetic anisotropy in nanometer-thick epitaxial graphene/Co/heavy metal heterostructures for spin-orbitronics devices, *ACS Appl. Nano Mater.* **4**, 4398 (2021).
- [66] P.-H. Chang, W. Fang, T. Ozaki, and K. D. Belashchenko, Voltage-controlled magnetic anisotropy in antiferromagnetic MgO-capped MnPt films, *Phys. Rev. Mater.* **5**, 054406 (2021).
- [67] M. Cinal, Magnetic anisotropy and orbital magnetic moment in Co films and Co/X bilayers (*X* = Pd and Pt), *Phys. Rev. B* **105**, 104403 (2022).
- [68] M. Przybylski, M. Dąbrowski, U. Bauer, M. Cinal, and J. Kirschner, Oscillatory magnetic anisotropy due to quantum well states in thin ferromagnetic films (invited), *J. Appl. Phys.* **111**, 07C102 (2012).
- [69] P. Bruno, Tight-binding approach to the orbital magnetic moment and magnetocrystalline anisotropy of transition-metal monolayers, *Phys. Rev. B* **39**, 865 (1989).
- [70] L. Ke, Intersublattice magnetocrystalline anisotropy using a realistic tight-binding method based on maximally localized Wannier functions, *Phys. Rev. B* **99**, 054418 (2019).





Contents lists available at ScienceDirect

Journal of Magnetism and Magnetic Materials

journal homepage: [www.elsevier.com/locate/jmmm](http://www.elsevier.com/locate/jmmm)

## Research article

Magnetic anisotropy of L1<sub>0</sub> FeNi (001), (010), and (111) ultrathin films: A first-principles study

Joanna Marciniak, Mirosław Werwiński \*

Institute of Molecular Physics, Polish Academy of Sciences, M. Smoluchowskiego 17, 60-179 Poznań, Poland

## ARTICLE INFO

## Keywords:

Magnetic thin films  
DFT  
Magnetocrystalline anisotropy energy  
Perpendicular magnetic anisotropy  
L1<sub>0</sub> FeNi

## ABSTRACT

In previous experiments, L1<sub>0</sub> FeNi thin films with different surfaces, including (001), (110), and (111), were produced and studied. Each surface defines a different alignment of the crystallographic tetragonal axis with respect to the film's plane, resulting in different magnetic anisotropies. In this study, we use density functional theory calculations to examine three series of L1<sub>0</sub> FeNi films with surfaces (001), (010), and (111), and with thicknesses ranging from 0.5 to 3 nm (from 4 to 16 atomic monolayers). Our results show that films (001) have perpendicular magnetic anisotropy, while (010) favor in-plane magnetization, with a clear preference for the tetragonal axis [001]. We proposed calling this type of in-plane anisotropy *fixed in-plane*. A film with a surface (111) and a thickness of four atomic monolayers has a magnetization easy axis almost perpendicular to the plane of the film. As the thickness of the (111) film increases, the direction of magnetization rotates towards a tetragonal axis [001], positioned at an angle of about 45° to the plane of the film. Furthermore, the most significant changes in spin and orbital magnetic moments occur at a depth of about three near-surface atomic monolayers. Ultrathin L1<sub>0</sub> FeNi films with varying magnetic anisotropies may find applications in spintronic devices.

## 1. Introduction

The ordered L1<sub>0</sub> FeNi was first discovered in neutron bombarded specimens [1–3] and later identified in samples cut from meteorites [4, 5]. Studies of natural L1<sub>0</sub> FeNi samples from various meteorites [4–10] are being conducted in parallel with research on ordered FeNi thin films produced in laboratories. Takanashi, co-author of numerous papers on L1<sub>0</sub> FeNi thin films [11–27], summarized investigations of ordered FeNi thin films in a 2017 topical review [28]. The study of Takanashi et al. was complemented by other experimental groups [29–34]. Mandal et al. concluded the experimental characteristics of bulk and thin-film L1<sub>0</sub> FeNi in a 2023 review article [35].

Measurements of L1<sub>0</sub> FeNi films with thickness less than 5 nm [36, 37] give an important context for the calculation results we present in this work. Kojima et al. [37] have presented the dependence of order parameter, magnetization, and magnetic anisotropy on the number of monolayers. For thicknesses of about 10 atomic monolayers (~1.5 nm), low values of both the order parameter and the uniaxial magnetic anisotropy constant were observed [37].

The magnetic properties of the L1<sub>0</sub> FeNi phase are as follows: Curie temperature of about 830 K [9], magnetic moment of about 1.7  $\mu_B$  atom<sup>-1</sup> [32], upper limit of magnetocrystalline anisotropy constants ( $K_1$ ) of 1.3 MJ m<sup>-3</sup> [3,38], and room-temperature coercivity

( $H_c$ ) of 95.5 kA m<sup>-1</sup> (1.2 kOe) [9]. The transformation of FeNi from an ordered to a disordered phase occurs at a temperature of 593 K (320°C) [38,39]. Whereas obtaining samples with high values of the long-range order parameter ( $S$ ) is difficult [28]. Kojima et al. in research on L1<sub>0</sub> FeNi (001) films with a thickness of 50 × (Fe atomic monolayer/Ni atomic monolayer) shown that the uniaxial magnetic anisotropy constant ( $K_u$ ) depends on  $S$  and obtained the highest  $K_u$  value of 0.7 MJ m<sup>-3</sup> ( $7.0 \times 10^6$  erg cm<sup>-3</sup>) for  $S = 0.48$  [15]. Since this value of  $K_u$  is smaller than the shape anisotropy ( $2\pi M_s^2$ ) estimated for FeNi films as 0.9 MJ m<sup>-3</sup> ( $9.0 \times 10^6$  erg cm<sup>-3</sup>), it has not been possible to manufacture FeNi (001) films with a perpendicular magnetic anisotropy so far [28]. However, Takanashi et al. estimated that increasing the order parameter  $S$  above 0.7 should raise the  $K_u$  above the shape anisotropy value [28]. In addition to the lack of complete L1<sub>0</sub> ordering, the films are also not perfectly periodic but contain grains that further negatively affect the magnetic anisotropy. For the L1<sub>0</sub> phase, it is assumed that three basic nanocrystal variants are present in a single sample, and their main crystallographic axes do not necessarily point in the same direction [40].

The properties of the L1<sub>0</sub> FeNi bulk phase were also investigated using density functional theory (DFT) [9,40–53]. The computational

\* Corresponding author.

E-mail address: [werwinski@ifmpan.poznan.pl](mailto:werwinski@ifmpan.poznan.pl) (M. Werwiński).<https://doi.org/10.1016/j.jmmm.2024.172455>

Received 20 June 2024; Received in revised form 2 August 2024; Accepted 21 August 2024

Available online 23 August 2024

0304-8853/© 2024 The Author(s). Published by Elsevier B.V. This is an open access article under the CC BY license (<http://creativecommons.org/licenses/by/4.0/>).

**Table 1**

Structural data of L1<sub>0</sub> FeNi (001), (010), and (111) thin films consisting of 16 atomic monolayers. The *c* parameters of the computational unit cells include a vacuum of at least 30 Å. The thicknesses (without vacuum) of the considered (001), (010), and (111) films are 27, 27, and 31 Å, respectively. Unit cell parameters (*a*, *b*, *c*) are given in Å.

Atom	(001) s.g. <i>P4mm</i>			(010) s.g. <i>Pmma</i>			(111) s.g. <i>P12/m1</i>		
	<i>a</i>	<i>b</i>	<i>c</i>	<i>a</i>	<i>b</i>	<i>c</i>	<i>a</i>	<i>b</i>	<i>c</i>
	2.52	2.52	56.85	3.56	3.58	56.70	2.52	4.38	60.89
Fe	0.00	0.00	-0.484	0.75	0.00	0.484	0.00	0.335	-0.483
Ni	0.50	0.50	0.484	0.25	0.50	0.484	0.50	-0.165	-0.483
Fe	0.00	0.00	0.453	0.25	0.00	0.453	0.00	0.004	-0.449
Ni	0.50	0.50	-0.453	0.75	0.50	0.453	0.50	-0.496	-0.449
Fe	0.00	0.00	-0.422	0.75	0.00	0.422	0.00	-0.327	-0.416
Ni	0.50	0.50	0.422	0.25	0.50	0.422	0.50	0.173	-0.416
Fe	0.00	0.00	0.390	0.25	0.00	0.391	0.00	0.343	-0.382
Ni	0.50	0.50	-0.390	0.75	0.50	0.391	0.50	-0.157	-0.382
Fe	0.00	0.00	-0.359	0.75	0.00	0.360	0.00	0.012	-0.348
Ni	0.50	0.50	0.359	0.25	0.50	0.360	0.50	-0.488	-0.348
Fe	0.00	0.00	0.328	0.25	0.00	0.328	0.00	-0.321	-0.315
Ni	0.50	0.50	-0.328	0.75	0.50	0.328	0.50	0.180	-0.315
Fe	0.00	0.00	-0.296	0.75	0.00	0.297	0.00	0.353	-0.281
Ni	0.50	0.50	0.296	0.25	0.50	0.297	0.50	-0.147	-0.281
Fe	0.00	0.00	0.265	0.25	0.00	0.266	0.00	0.010	-0.248
Ni	0.50	0.50	-0.266	0.75	0.50	0.266	0.50	-0.489	-0.248

method has been used to determine, among others, the magnetocrystalline anisotropy energy (MAE) of a perfect L1<sub>0</sub> FeNi crystal [41–44, 46], to study the effect of chemical disorder [40,47,51,52], and to predict how different substitutions affect the MAE [45,49,50].

Despite extensive experimental work on L1<sub>0</sub> FeNi thin films and numerous computational studies on L1<sub>0</sub> FeNi bulk, L1<sub>0</sub> FeNi magnetic thin films have not been modeled from first principles. Only the adsorption of ethylene (C<sub>2</sub>H<sub>4</sub>) [54] and hydrazine (N<sub>2</sub>H<sub>4</sub>) [55] on the L1<sub>0</sub> FeNi (111) surface were calculated from DFT. In this work, continuing our DFT investigation of L1<sub>0</sub> phases [46,56,57], we study ultrathin L1<sub>0</sub> FeNi films.

In this work, the first-principles calculations were made for ultrathin L1<sub>0</sub> FeNi films with surfaces (001), (010), and (111). The study aims to determine the films' magnetic moments and magnetic anisotropies. Answering the question of how they depend on the thickness and type of surface can help obtain FeNi films with different types of magnetic anisotropy, such as perpendicular, tilted, or fixed in-plane. Although perpendicular magnetic anisotropy is fairly well known, it is worth briefly discussing the other two types.

In 2005, a system with the magnetization direction tilted from the plane of the film was prepared experimentally, and it was shown that deflecting it to 45° minimizes the value of the switching magnetic field [58,59]. Since the magnetization direction of L1<sub>0</sub> crystals agrees with the tetragonal axis, a natural candidate for systems with tilted anisotropy are L1<sub>0</sub> (111) films. Previous experiments on the L1<sub>0</sub> FePt (111) films showed that the direction of magnetization is tilted by 33–36° from the plane of the film, i.e., it points roughly in the direction of the tetragonal axis [60]. In our computational work on FePt ultrathin films, we also addressed this issue [57]. Here, we will determine the magnetization angle for L1<sub>0</sub> FeNi (111) films.

Alignment of the tetragonal axis leads to perpendicular magnetic anisotropy in films (001) and tilted magnetic anisotropy in films (111). In films (010), it results in an unconventional type of in-plane anisotropy with a preferred direction in the film plane. We already postulated that such a uniaxial configuration could be called *fixed in-plane* magnetic anisotropy [57], as opposed to conventional *in-plane*. 20 nm L1<sub>0</sub> FeNi (110) films with a tetragonal axis in the plane of the film were experimentally obtained in 2023 and showed order parameter *S* of 0.6 and magnetic anisotropy constant of 0.55 MJ m<sup>-3</sup> [26]. Experimental work on isostructural L1<sub>0</sub> FePt (010) films are also known [61–65]. In this work, we will determine the magnetic easy axis of L1<sub>0</sub> FeNi (010) films.

## 2. Calculations' details

We prepared models of L1<sub>0</sub> FeNi (001), (010), and (111) thin films in the thickness range from four to sixteen atomic monolayers, see Fig. 1. To keep the concentration of Fe and Ni equal, we considered only films with an even number of monolayers. As a starting point for modeling thin films, we used a unit cell of the L1<sub>0</sub> FeNi bulk phase (s.g. *P4/mmm*, *a*' = 3.56/√2 ~ 2.52 and *c* = 3.58 Å) [46]. We added a minimum of 30 Å vacuum to all unit cells of the thin films in the direction perpendicular to the film plane.

For the prepared models, calculations were performed using the full-potential local-orbital (FPLO18.00-52) code [66,67] within the density functional theory (DFT). The exchange–correlation potential in the Perdew–Burke–Ernzerhof (PBE) form was used [68]. The atomic positions of the films were optimized using forces in a spin-polarized approach in 20 × 20 × 1 k-point mesh, with a convergence criterion of 10<sup>-3</sup> eV Å<sup>-1</sup>. Table 1 shows space groups, calculated Wyckoff positions, and unit cell parameters of the example 16-monolayer films. The prepared (001) and (010) films have thicknesses from 0.5 to 2.7 nm, while the (111) films span from 0.6 to 3.1 nm (all values determined as the distance between the atomic positions of the surface sites).

The k-point mesh was considerably densified in the next step to determine the accurate magnetocrystalline anisotropy energy (MAE) values. For (001) and (010) films, a k-point mesh of 60 × 60 × 5 was assumed, and for (111) films, a k-point mesh of 60 × 30 × 5. For Brillouin zone integration, the tetrahedron method was chosen. For scalar-relativistic calculations, a 10<sup>-6</sup> density convergence criterion was used. After self-consistent scalar-relativistic calculations, one iteration of fully relativistic calculations was performed for the selected quantization axes. Such fully relativistic solutions were used to determine magnetic anisotropy energies and energy dependencies as a function of the quantization axis (magnetization) direction. As demonstrated [69], this approach leads to sufficiently accurate results, significantly reducing computation time.

Calculations of the energy dependence of the magnetization direction were performed for 10-monolayer films (010) and (111) using unit cells with space group *P1*. For (111) films, having established that the energy minimum is in the (100) plane, calculations were carried for directions varying in this plane every 2°. The direction of easy magnetization was then determined using third-degree polynomial fitting.

The unique implementation of the fixed spin moment method in a fully relativistic approach of the FPLO code allowed us to determine the dependence of the magnetocrystalline anisotropy energy on the

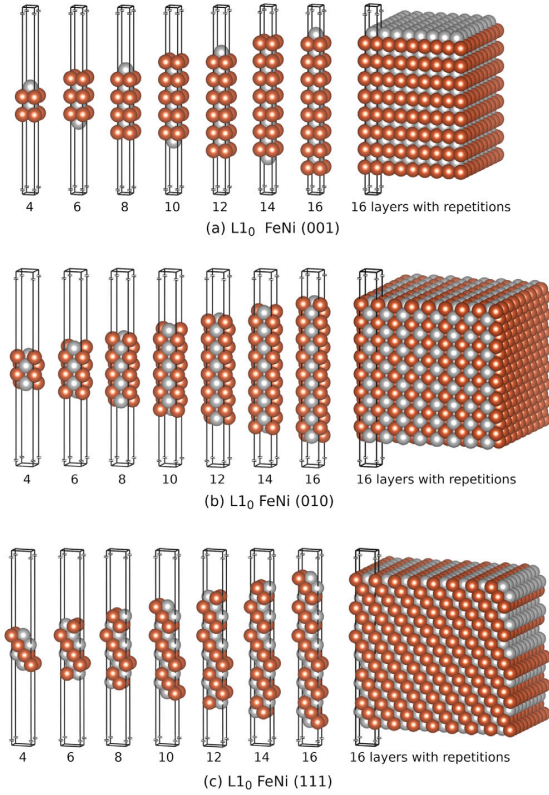


**Fig. 1.** The series of unit cells of L1<sub>0</sub> FeNi thin films with (001), (010), and (111) surfaces and thickness from 4 to 16 atomic monolayers [from 0.5 to 2.7 nm for (001) and (010) films and from 0.6 to 3.1 nm for (111) films]. On the right, 16-monolayer unit cells were repeated several times in two directions in the plane of the film to visualize the layered character of the models. The vacuum height (at least 30 Å) has been reduced in the figures to save space.

spin magnetic moment. We performed these calculations with the PBE exchange–correlation functional in the generalized gradient approximation (GGA), as well as with the Perdew–Wang (PW92) functional in the local density approximation (LDA) [70].

We calculated the  $k$ -point resolved contributions to MAE using the magnetic force theorem [41,71,72] defined by equation:

$$\text{MAE} = E(\theta = 90^\circ) - E(\theta = 0^\circ) = \sum_{\text{occ}'} \epsilon_i(\theta = 90^\circ) - \sum_{\text{occ}'} \epsilon_i(\theta = 0^\circ), \quad (1)$$

where  $E(\theta)$  is the total energy for a specific direction;  $\theta$  is the angle between the direction of magnetization and the  $c$  axis;  $\epsilon_i$  is the band energy of state  $i$ .

Because the implementation of the DFT used in this work is based on the linear combination of atomic orbitals, it was possible to perform population analysis using Mulliken's method [73]. We used the VESTA code to prepare drawings of the structures [74]. In our previous article on ultrathin films of L1<sub>0</sub> FePt, we discussed the limitations of the models adopted and the approximations used [57].

### 3. Results and discussion

Before discussing the calculated results for the films, we will present an analysis of the dependence of the magnetic anisotropy energy on the value of the magnetic moment and the form of the exchange–correlation potential for bulk L1<sub>0</sub> FeNi. This allows us to place in a

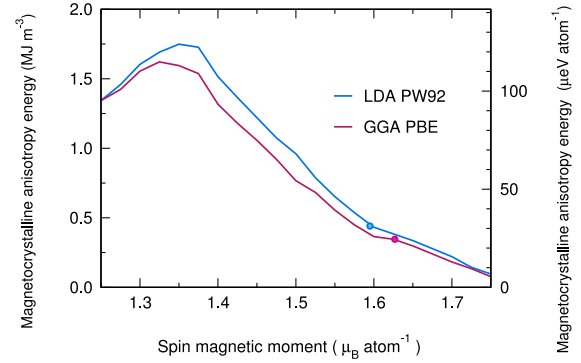


**Fig. 2.** Magnetocrystalline anisotropy energy of the bulk L1<sub>0</sub> FeNi as a function of the spin magnetic moment. Calculations were performed using the FPLO18 code with the LDA PW92 and GGA PBE exchange–correlation potentials. Circles represent equilibrium results.

context the magnetic anisotropy results for ultrathin FeNi films, which in the limit of large thicknesses converge to the values for the bulk.

#### 3.1. Magnetocrystalline anisotropy of bulk L1<sub>0</sub> FeNi

For bulk L1<sub>0</sub> FeNi, the MAE of  $0.34 \text{ MJ m}^{-3}$  ( $24 \text{ } \mu\text{eV atom}^{-1}$ ) determined from the GGA is much lower than the maximum determined values of experimental magnetic anisotropy constants of up to  $1.3 \text{ MJ m}^{-3}$  [38]. The discrepancy may be due to the temperature for which the DFT calculations are done (by definition, 0 K) or the limitations of the GGA. In our work on bulk L1<sub>0</sub> FePt, we pointed out that the values of MAE and magnetic moment are correlated [56], and the latter depends on the choice of the exchange–correlation potential. To show this correlation also for bulk L1<sub>0</sub> FeNi, we performed calculations of the dependence of MAE on a fixed spin moment for LDA and GGA functional. Fig. 2 shows that for L1<sub>0</sub> FeNi the equilibrium values of magnetic moments and MAEs obtained in the PW92 and PBE approximations differ only slightly. Moreover, the MAE value depends on the magnetic moment, and in both approximations, it has a maximum above  $1.5 \text{ MJ m}^{-3}$  for a reduced magnetic moment of about  $1.35 \text{ } \mu_B \text{ atom}^{-1}$ . The presented relation of MAE and magnetic moment may partially explain the discrepancy between the experimentally determined  $K_u$  values above  $1 \text{ MJ m}^{-3}$  at room temperature and the calculated MAE values below  $0.5 \text{ MJ m}^{-3}$  at 0 K. Namely,  $K_u$  can also indirectly depend on temperature via temperature-mediated reduction of magnetization. Such interpretation is supported by calculations of the MAE dependence on temperature for L1<sub>0</sub> Fe<sub>0.56</sub>Ni<sub>0.44</sub>, showing lowered MAE at low temperatures and MAE maximum near room temperature [40]. Furthermore,  $K_u$  measurements of L1<sub>0</sub> FeNi films performed at 35 K reveal much lower  $K_u$  values ( $< 0.2 \text{ MJ m}^{-3}$ ) than typical results obtained at room temperature [31].

To understand the dependence of the MAE on the spin magnetic moment, we look at the density of states and the band structure of the bulk L1<sub>0</sub> FeNi. Fig. 3 presents the equilibrium solutions (without fixed spin moment) of these properties. The energy range in Fig. 3 covers most of the valence band. The majority spin channel (red) is mostly occupied, while the minority spin channel (blue) has empty states above the Fermi level.

#### 3.2. L1<sub>0</sub> FeNi ultrathin films

In the following subsection, we discuss magnetic moments, magnetization directions, and magnetic anisotropy energies of considered films.

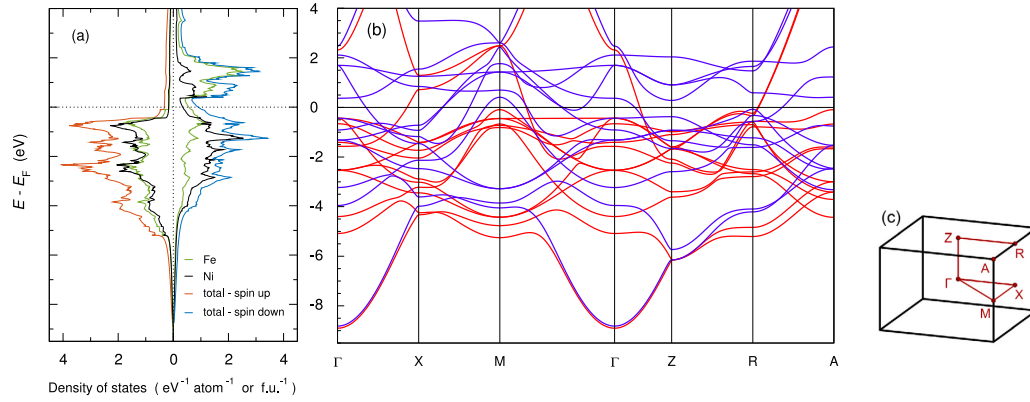


Fig. 3. Density of states (a) and band structure (b) of L1<sub>0</sub> FeNi bulk. Red and blue bands denote contributions from majority and minority spin channels, respectively. Calculations were performed with the FPLO18 code using the PBE functional and a scalar-relativistic approach. Brillouin zone with high symmetry points is also shown (c).

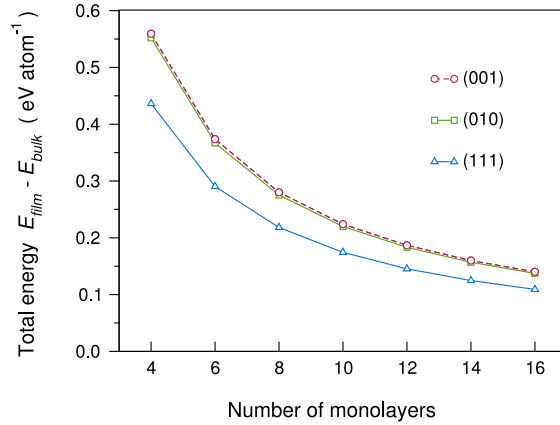


Fig. 4. Differences between film energy and bulk energy, calculated for L1<sub>0</sub> FeNi films with (001), (010), and (111) surfaces. Calculations were performed using the FPLO18 code with the PBE exchange–correlation functional.

### 3.2.1. Energetic stability, magnetic moments, and excess electrons of ultrathin films

The total energy of the films decreases with thickness, tending asymptotically to the bulk value, see Fig. 4. Over the considered range, the most energetically stable films are (111), then (010), and last (001), with the energy of the (111) surface being much lower than the other two. Previously, the same order was determined for the surfaces of L1<sub>0</sub> FePt and L1<sub>0</sub> CoPt films [75]. This result identifies a suboptimal energy condition for (001) surface formation.

Fig. 5 shows excess electrons on Fe and Ni atoms along the thickness of films, which were calculated using Mulliken's approach [73]. The deviations in excess electrons on FeNi surfaces (ranging from about −0.02 to 0.15 on Fe sites) are much smaller than those calculated previously for FePt surfaces (ranging from about −1.0 to 1.0 on Fe sites) [57]. This indicates higher stability of FeNi surfaces in comparison to L1<sub>0</sub> FePt ultrathin films. As we look closer at this plot, the excess electron (hole) values are close to those for bulk FeNi in the central region of the films, while for about three surface monolayers, they show large deviations from the bulk value. We observed similar behavior in the results of additional calculations performed without spin polarization, confirming the primary role of charge transfer in the formation of perturbations in the near-surface monolayers.

Fig. 5 also presents the spin and orbital magnetic moments on individual atoms along film thickness. We can see a similar increase in magnetic moments on about three surface monolayers and values close to the bulk value in the central region [46]. The highest values of magnetic moments are on the surface (010). Magnetic moments on the surfaces are elevated throughout the thickness range considered; the central region vanishes only below about six monolayers. Unlike the (010) and (111), the model of (001) film has asymmetrical *top* and *bottom* surfaces (one side ends in an Fe monolayer and the other in Ni). Hence, the observed asymmetry in the (001) results in Fig. 5.

### 3.2.2. Magnetic anisotropy of ultrathin films

For ultrathin films of L1<sub>0</sub> FeNi, we observed an increase in the average magnetic moment only to about 5% over the bulk value. However, the magnetic anisotropy of thin films differs much more. In the case of magnetic anisotropy, we are interested in both the value of the magnetic anisotropy energy and the direction of magnetization relative to the plane of the film (magnetic easy axis). We expect that since the films under consideration have an L1<sub>0</sub> structure with a unique tetragonal axis, the direction of magnetization will be along or close to this axis. This means that perpendicular, in-plane, and tilted magnetic anisotropy should be observed for the films (001), (010), and (111), respectively.

We will begin our discussion of the magnetic anisotropy of L1<sub>0</sub> FeNi films with the most studied (001) films. As in the previous experiments [11–28], we also expect for them the perpendicular magnetic anisotropy. The relation of total energy and magnetic moment to the number of monolayers suggests that we should also expect a dependence on magnetic anisotropy energy that converges asymptotically to the bulk value. However, as we can see in Fig. 6, although the anisotropy energy of the (001) films converges to the bulk value, this is accompanied by pronounced oscillations. This type of MAE behavior has been observed in several previous calculations for ultrathin films [57,76–80]. Oscillations of uniaxial magnetic anisotropy have also been observed experimentally for ultrathin bcc Fe and fcc Co films with periods of 5.9 and 2.3 atomic monolayers, respectively [81]. They are due to quantum well states situated around the Fermi level [81] and come from the quantum size effect appearing in small enough systems. The positive values of the magnetic anisotropy energies for films (001), defined as energy difference  $E_{010} - E_{001}$ , indicate a preference for orientation of the magnetization direction perpendicular to the plane of the (001) film. However, the result obtained does not clearly identify perpendicular anisotropy, since for this, the uniaxial anisotropy energy must exceed the energy of shape anisotropy ( $2\pi M_s^2 \sim 0.9 \text{ MJ m}^{-3}$  [37]). This criterion is not met in the case of our computational results. Nevertheless, uniaxial anisotropy is still expected to overcome the shape



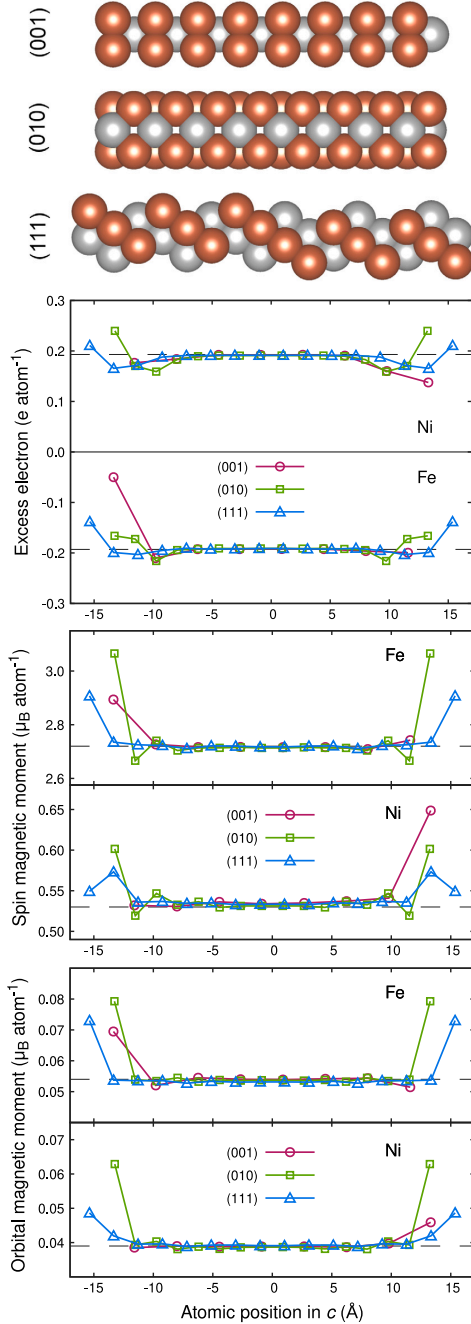


Fig. 5. Excess electrons and spin and orbital magnetic moments in 16-monolayer films of L1<sub>0</sub> FeNi with surfaces (001), (010), and (111). Dashed lines indicate bulk values: spin magnetic moments on Fe (Ni) equal to 2.72  $\mu_B$  (0.53  $\mu_B$ ), orbital magnetic moments on Fe (Ni) equal to 0.054  $\mu_B$  (0.039  $\mu_B$ ), and excess electron of  $\pm 0.193$   $e$ . Calculations were performed using the FPLO18 code with the PBE exchange–correlation potential. Above the charts are the side views of the film unit cells.

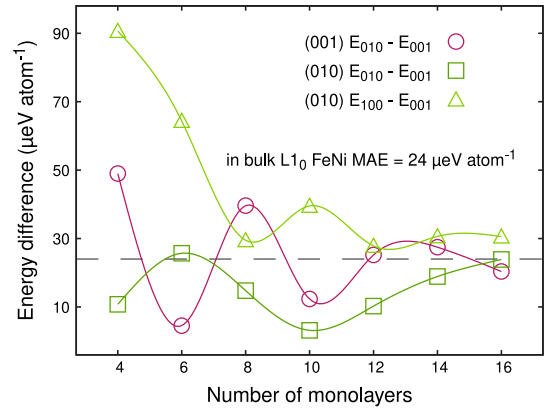


Fig. 6. Magnetic anisotropy energies as a function of the number of atomic monolayers of L1<sub>0</sub> FeNi (001) and (010) ultrathin films. The dashed horizontal line indicates the magnetocrystalline anisotropy energy (MAE) calculated for bulk L1<sub>0</sub> FeNi (24  $\mu\text{eV atom}^{-1}$ ) [46]. The energies  $E_{001}$ ,  $E_{010}$ , and  $E_{100}$  were determined for the corresponding magnetization directions using the FPLO18 code with the PBE exchange–correlation functional.

anisotropy in experiments at room temperature, where the determined  $K_u$  value is up to three times higher than the GGA value calculated here.

For films (010) with Fe/Ni monolayers aligned perpendicular to the plane of the film (*bookshelf* arrangement), we expect an easy magnetization axis in the direction of the crystallographic tetragonal axis, that is, in the plane of the film. Indeed, this magnetization direction is the most energetically stable in this case, see Figs. 6 and 8. However, since magnetization has a clear preference in the direction of the tetragonal axis [001], this is not a typical case of in-plane magnetic anisotropy. The corresponding phenomenon observed in FePt (010) films we proposed to call *fixed in-plane* magnetic anisotropy [57]. As in the case of the (001) films discussed above, we also observe oscillations in the magnetic anisotropy energy due to the quantum size effect. Furthermore, as mentioned, *bookshelf*-type FeNi films with a (110) surface were obtained in 2023 experimentally, but the dependence of the magnetization anisotropy in the plane of the films was not investigated [26]. It is then not clear how shape anisotropy will affect uniaxial anisotropy in this case.

To give an idea of the physical origins of magnetic anisotropy in (010) films, below we will present an analysis of the difference in orbital moments based on Bruno's formula [82] for an example film with a thickness of 16 monolayers, and present images of the band structure for (010) films of different thicknesses.

Fig. 9 presents the evolution of the band structure (along the  $\Gamma$ -Z  $k$ -path) with the thickness of the (010) films. Both similarities and differences between film and bulk solutions are noticeable. The number of bands increases with the thickness of the film increases, which is due to an increase in the number of non-equivalent sites in the system. In the limit of larger thicknesses, the solution includes contributions from the central part of the film (similar to the solution for bulk), contributions from atoms in the near-surface layers, and also quantum well states [81]. The change in band structure with film thickness consequently leads to oscillation of the MAE with film thickness. In turn, in the limit of large thicknesses, the film's MAE converges to the value for bulk material and the surface contributions are negligible.

MAE contributions can be analyzed from the perspective of real space, using Bruno's formula [82] linking the magnetic anisotropy energy to the anisotropy in orbital magnetic moments:

$$\text{MAE} \sim \pm \frac{\epsilon}{4} \Delta m_L, \quad (2)$$

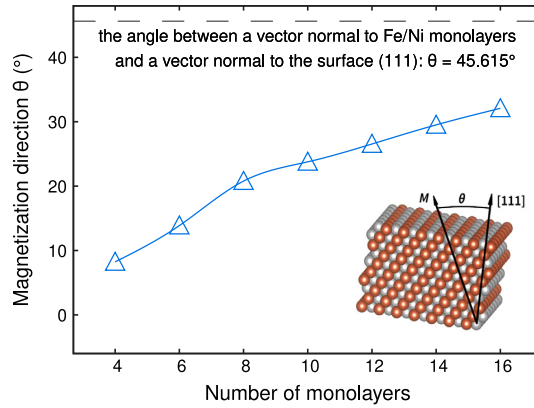


Fig. 7. Magnetization direction as a function of the number of atomic monolayers of  $L1_0$  FeNi (111) thin films. The calculations were performed using the FPLO18 code with PBE exchange–correlation potential. The horizontal dashed line indicates the angle value between the vector [001] normal to the plane of the Fe/Ni atomic monolayers and the vector [111] normal to the film's surface.

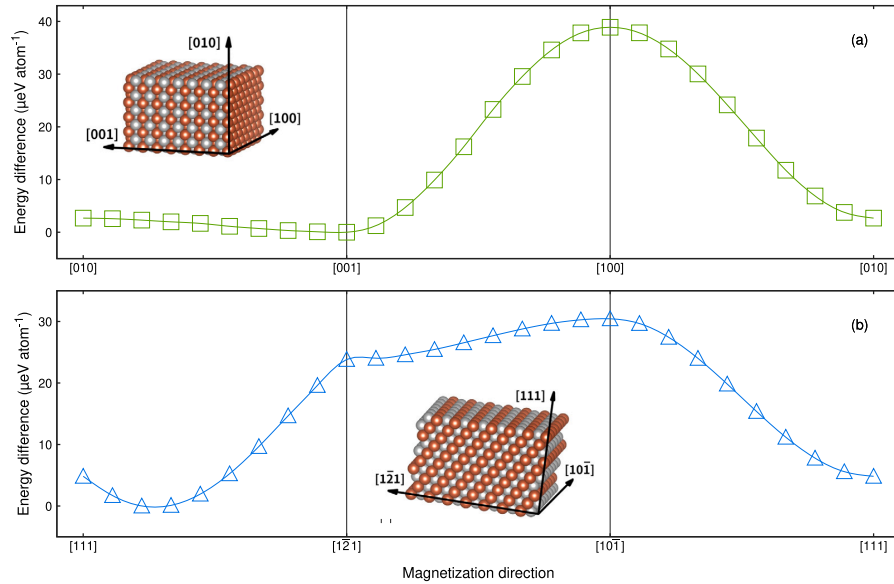


Fig. 8. Evolution of magnetic anisotropy energy with magnetization direction for 10-monolayer films of  $L1_0$  FeNi (010) (a) and (111) (b). The calculations were performed using the FPLO18 code with PBE exchange–correlation functional.

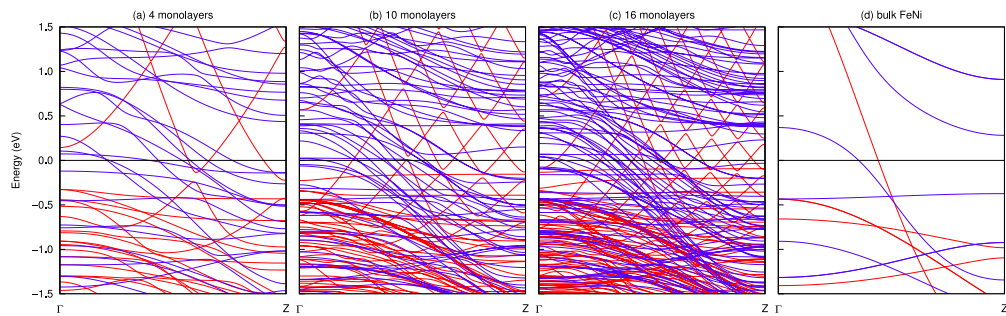


Fig. 9. Band structure along  $\Gamma$ -Z  $k$ -path calculated for selected  $L1_0$  FeNi (010) thin films (a-c) and  $L1_0$  FeNi bulk (d). Red and blue bands denote majority and minority spin channels. Calculations were performed with the FPLO18 code using the PBE functional and a scalar-relativistic approach.

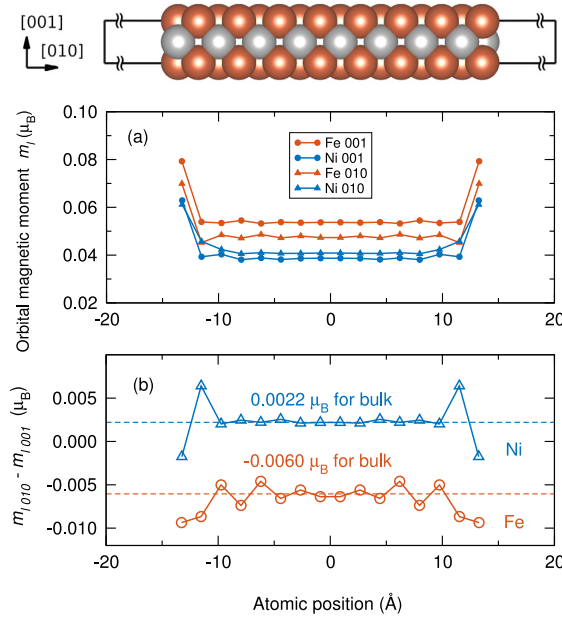


Fig. 10. Orbital magnetic moments at atomic sites along the direction perpendicular to the plane of the film for a 16-monolayer-thick L1<sub>0</sub> FeNi (010) film, calculated for magnetization directions [001] and [010] (a). Difference in orbital magnetic moments calculated between magnetization directions [010] and [001] (b). Dashed lines indicate the solutions for Fe and Ni calculated for the L1<sub>0</sub> FeNi bulk. Above, a side view of the unit cell of the 16-monolayer FeNi (010) film. The calculations were performed with the FPLO18 code and the PBE functional.

where  $\xi$  is the spin-orbit constant and  $\Delta m_L$  is the difference in the orbital magnetic moment defined as:

$$\Delta m_L = m_L^{\parallel} - m_L^{\perp}, \quad (3)$$

where  $m_L^{\parallel}$  and  $m_L^{\perp}$  are the orbital magnetic moments calculated for two perpendicular quantization axes. For bulk L1<sub>0</sub> FeNi, the calculated orbital magnetic moments for Fe are 0.054  $\mu_B$  (0.048  $\mu_B$ ) in [001] ([110]) magnetization direction and for Ni they are 0.038  $\mu_B$  (0.041  $\mu_B$ ) in [001] ([110]) direction. The calculated differences in the orbital magnetic moment are  $\Delta m_L(\text{Fe}) = -0.0060 \mu_B$  and  $\Delta m_L(\text{Ni}) = 0.0022 \mu_B$ , leading to a total  $\Delta m_L$  equal to  $-0.0038 \mu_B \text{ f.u.}^{-1}$ . The normalized contributions of Fe and Ni to  $\Delta m_L$  are 1.58 and  $-0.58$ , respectively. The above values are consistent with the sublattice-resolved MAE calculated by Ke for L1<sub>0</sub> FeNi using perturbation theory in the tight-binding approach, resulting in contributions of 1.57 and  $-0.57$  for Fe and Ni, respectively (for MAE calculated as 33  $\mu\text{eV atom}^{-1}$ ) [83]. In Fig. 10, we show the orbital magnetic moments and their differences calculated for the two magnetization directions for an example 16-monolayer L1<sub>0</sub> FeNi (010) film. In several near-surface layers, we see the largest deviations of orbital magnetic moments and differences of orbital magnetic moments from the values in the central part of the film. At the same time, the values of orbital magnetic moment differences in the central part are close to the values for bulk L1<sub>0</sub> FeNi.

Finally, we will discuss the magnetic anisotropy of (111) films. We do not present for them the dependence of the anisotropy energy on the number of monolayers, because the direction of magnetization changes with film thickness. For L1<sub>0</sub> FeNi (111) films, the angle of the normal to the alternating Fe and Ni monolayers (the tetragonal axis [001]) to the out-of-plane direction [111] is 45.615°. This value also specifies the easy magnetization axis within the limits of thick films. For ultrathin films, however, we expect the magnetic easy axis

to deviate from the tetragonal axis [001]. The determined direction of the magnetic easy axis for the (111) film with a thickness of 10 atomic monolayers (1.85 nm) is deviated from the [111] direction by 23.8°, see Fig. 8. Furthermore, Fig. 7 shows that the direction of the easy axis indeed converges asymptotically to the hypothetical value of 45.615° for the thick (111) films. Whereas, for the thinnest films, the easy axis approaches the out-of-plane direction [111].

Although it might be counterintuitive, perhaps it is the ultrathin L1<sub>0</sub> FeNi films (111), rather than films (001), that will allow for the practical realization of perpendicular magnetic anisotropy? In their favor is the highest energy stability among the three surfaces considered, and the positive results of recent experiments confirming the high values of both the order parameter  $S$  and the anisotropy constant  $K_u$  (1.15 MJ m<sup>-3</sup>) [34]. On the other hand, with the uniaxial anisotropy constant tuned in such a way that it only slightly exceeds the shape anisotropy and the direction of the easy axis at about 45° to the surface, the L1<sub>0</sub> FeNi (111) thin films can become excellent systems for devices with switching magnetic field [58,59]. There are, however, limitations related to the demagnetization effect, which may prevent the magnetization direction in the films from being set in the easy axis predicted from DFT [84,85]. Skomski and Coey pointed out that for a magnet of any shape (including film) to resist demagnetization, the anisotropy field must exceed the demagnetizing field, for which the condition is  $K_1 > 1/2\mu_0 M_s^2$  [85]. In case of our models calculated at 0 K, with saturated total magnetic moment of bulk L1<sub>0</sub> FeNi equal to 3.34  $\mu_B \text{ f.u.}^{-1}$  ( $M_s = 1.36 \text{ MA m}^{-1}$ ), we estimate that to resist demagnetization the  $K_1$  (MAE) should exceed 1.16 MJ m<sup>-3</sup> (about 80  $\mu\text{eV atom}^{-1}$ ). Unfortunately, this condition is not fulfilled, as our 0 K PBE value of MAE is only 0.34 MJ m<sup>-3</sup> (24  $\mu\text{eV atom}^{-1}$ ) for bulk L1<sub>0</sub> FeNi, and stay around it also for considered thin films. This indicates that the demagnetization effect will not allow easy magnetization axes of the films to be fixed in the directions predicted from DFT calculations. However, the condition  $K_1 > 1/2\mu_0 M_s^2$  might be fulfilled in practice. The measured magnetization of the FeNi films is lower than that predicted from PBE, leading to a reduction in the  $K_1$  value necessary to meet the demagnetization resistance condition below 1.0 MJ m<sup>-3</sup>. At the same time, some measured MAE values, such as for FeNi (111) films, are as high as 1.15 MJ m<sup>-3</sup> [34].

#### 4. Summary and conclusions

The computational results presented here extend previous research on L1<sub>0</sub> FeNi films to include the thinnest films with thickness from 0.5 to 3 nm. Among the films with (001), (010) and (111) surfaces, the latter is the most energetically preferable. Reducing the thickness of ultrathin films raises the magnetic moment by about 5%. Furthermore, in films (001) and (010), the easy magnetization direction follows the direction of the crystallographic tetragonal axis and is perpendicular to and in the plane of the film, respectively. At the same time, the alignment of the easy axis in the (010) film plane is unusual because it is strongly anisotropic in the plane, clearly preferring the direction of the tetragonal axis [001]. For thicker (111) films, the easy magnetization direction is consistent with the tetragonal axis direction [001] (at the angle of about 45° to the normal to the plane). However, for ultrathin (111) films, it deviates from [001] towards [111] direction (normal to the plane). By this, the magnetic anisotropy of the thinnest (111) films resembles perpendicular anisotropy.

The unique anisotropic properties of L1<sub>0</sub> FeNi films may find application in new spintronic devices, as in the case of L1<sub>0</sub> FePt films. However, the uniaxial magnetic anisotropy for the L1<sub>0</sub> FeNi films is an order of magnitude lower than for the L1<sub>0</sub> FePt films and competes with the shape anisotropy. Still, the lower magnetic anisotropy constant may be preferable for some applications, and the significant price difference between nickel and platinum may also favor FeNi films.

## CRediT authorship contribution statement

**Joanna Marciniak:** Writing – original draft, Visualization, Validation, Software, Methodology, Investigation, Formal analysis, Data curation, Conceptualization. **Miroslaw Werwiński:** Writing – original draft, Visualization, Validation, Supervision, Software, Resources, Project administration, Methodology, Investigation, Funding acquisition, Formal analysis, Data curation, Conceptualization.

## Declaration of competing interest

The authors declare that they have no known competing financial interests or personal relationships that could have appeared to influence the work reported in this paper.

## Data availability

Data will be made available on request.

## Acknowledgments

We acknowledge the financial support of the National Science Centre Poland under the decision DEC-2018/30/E/ST3/00267. Part of the computations were performed using resources provided by the Poznan Supercomputing and Networking Center (PSNC). We thank P. Leśniak and D. Depcik for compiling the scientific software and administration of the computing cluster at the Institute of Molecular Physics, Polish Academy of Sciences. We also thank Z. Śniadecki and J. Snarski-Adamski for reading the manuscript and providing valuable comments.

## References

- [1] J. Paulevé, D. Dautreppe, J. Laugier, L. Néel, Une nouvelle transition ordre-désordre dans Fe-Ni (50-50), *J. Phys. Radium* 23 (10) (1962) 841–843, <http://dx.doi.org/10.1051/jphysrad:019620023010084100>.
- [2] L. Néel, J. Paulevé, R. Pauthenet, J. Laugier, D. Dautreppe, Magnetic properties of an iron-nickel single crystal ordered by neutron bombardment, *J. Appl. Phys.* 35 (3) (1964) 873–876, <http://dx.doi.org/10.1063/1.1713516>.
- [3] J. Paulevé, A. Chamberod, K. Krebs, A. Bourret, Magnetization curves of Fe-Ni (50–50) single crystals ordered by neutron irradiation with an applied magnetic field, *J. Appl. Phys.* 39 (2) (1968) 989–990, <http://dx.doi.org/10.1063/1.1656361>.
- [4] J.F. Petersen, M. Aydin, J.M. Knudsen, Mössbauer spectroscopy of an ordered phase (Superstructure) of FeNi in an iron meteorite, *Phys. Lett. A* 62 (3) (1977) 192–194, [http://dx.doi.org/10.1016/0375-9601\(77\)90023-8](http://dx.doi.org/10.1016/0375-9601(77)90023-8).
- [5] R.S. Clarke, E.R.D. Scott, Tetraetaenite—Ordered FeNi, a new mineral in meteorites, *Am. Mineral.* 65 (7–8) (1980) 624–630.
- [6] P. Wasilewski, Magnetic characterization of the new magnetic mineral tetraetaenite and its contrast with isochemical taenite, *Phys. Earth Planet. Inter.* 52 (1) (1988) 150–158, [http://dx.doi.org/10.1016/0031-9201\(88\)90063-5](http://dx.doi.org/10.1016/0031-9201(88)90063-5).
- [7] M. Kotsugi, C. Mitsumata, H. Maruyama, T. Wakita, T. Taniuchi, K. Ono, M. Suzuki, N. Kawamura, N. Ishimatsu, M. Oshima, Y. Watanabe, M. Taniguchi, Novel magnetic domain structure in iron meteorite induced by the presence of L1<sub>0</sub>-FeNi, *Appl. Phys. Express* 3 (1) (2010) 013001, <http://dx.doi.org/10.1143/APEX.3.013001>.
- [8] M. Kotsugi, H. Maruyama, N. Ishimatsu, N. Kawamura, M. Suzuki, M. Mizumaki, K. Osaka, T. Matsumoto, T. Ohkuchi, T. Ohtsuki, T. Kojima, M. Mizuguchi, K. Takanashi, Y. Watanabe, Structural, magnetic and electronic state characterization of L1<sub>0</sub>-type ordered FeNi alloy extracted from a natural meteorite, *J. Phys.: Condens. Matter* 26 (6) (2014) 064206, <http://dx.doi.org/10.1088/0953-8984/26/6/064206>.
- [9] L.H. Lewis, A. Mubarak, E. Poirier, N. Bordeaux, P. Manchanda, A. Kashyap, R. Skomski, J. Goldstein, F.E. Pinkerton, R.K. Mishra, R.C. Kubie Jr., K. Barnak, Inspired by nature: Investigating tetraetaenite for permanent magnet applications, *J. Phys.: Condens. Matter* 26 (6) (2014) 064213, <http://dx.doi.org/10.1088/0953-8984/26/6/064213>.
- [10] E. Poirier, F.E. Pinkerton, R. Kubie, R.K. Mishra, N. Bordeaux, A. Mubarak, L.H. Lewis, J.I. Goldstein, R. Skomski, K. Barnak, Intrinsic magnetic properties of L1<sub>0</sub> FeNi obtained from meteorite NWA 6259, *J. Appl. Phys.* 117 (17) (2015) 17E318, <http://dx.doi.org/10.1063/1.4916190>.
- [11] T. Shima, M. Okamura, S. Mitani, K. Takanashi, Structure and magnetic properties for L1<sub>0</sub>-ordered FeNi films prepared by alternate monatomic layer deposition, *J. Magn. Magn. Mater.* 310 (2, Part 3) (2007) 2213–2214, <http://dx.doi.org/10.1016/j.jmmm.2006.10.799>.
- [12] M. Mizuguchi, S. Sekiya, K. Takanashi, Characterization of Cu buffer layers for growth of L1<sub>0</sub>-FeNi thin films, *J. Appl. Phys.* 107 (9) (2010) 09A716, <http://dx.doi.org/10.1063/1.3337649>.
- [13] T. Kojima, M. Mizuguchi, K. Takanashi, L1<sub>0</sub>-ordered FeNi film grown on Cu-Ni binary buffer layer, *J. Phys. Conf. Ser.* 266 (2011) 012119, <http://dx.doi.org/10.1088/1742-6596/266/1/012119>.
- [14] M. Mizuguchi, T. Kojima, M. Kotsugi, T. Koganezawa, K. Osaka, K. Takanashi, Artificial fabrication and order parameter estimation of L1<sub>0</sub>-ordered FeNi Thin Film Grown on a AuNi buffer layer, *J. Magn. Soc. Jpn.* 35 (4) (2011) 370–373, <http://dx.doi.org/10.3379/msjmag.1106R008>.
- [15] T. Kojima, M. Mizuguchi, T. Koganezawa, K. Osaka, M. Kotsugi, K. Takanashi, Magnetic anisotropy and chemical order of artificially synthesized L1<sub>0</sub>-ordered FeNi films on Au-Cu-Ni buffer layers, *Japan. J. Appl. Phys.* 51 (1R) (2012) 010204, <http://dx.doi.org/10.1143/JJAP.51.010204>.
- [16] M. Kotsugi, M. Mizuguchi, S. Sekiya, M. Mizumaki, T. Kojima, T. Nakamura, H. Osawa, K. Kodama, T. Ohtsuki, T. Ohkuchi, K. Takanashi, Y. Watanabe, Origin of strong magnetic anisotropy in L1<sub>0</sub>-FeNi probed by angular-dependent magnetic circular dichroism, *J. Magn. Magn. Mater.* 326 (2013) 235–239, <http://dx.doi.org/10.1016/j.jmmm.2012.09.008>.
- [17] M. Ogiwara, S. Iihama, T. Seki, T. Kojima, S. Mizukami, M. Mizuguchi, K. Takanashi, Magnetization damping of an L1<sub>0</sub>-FeNi thin film with perpendicular magnetic anisotropy, *Appl. Phys. Lett.* 103 (24) (2013) 242409, <http://dx.doi.org/10.1063/1.4845035>.
- [18] T. Ohtsuki, M. Kotsugi, T. Ohkuchi, S. Lee, Z. Horita, K. Takanashi, Nanoscale characterization of FeNi alloys processed by high-pressure torsion using photoelectron emission microscope, *J. Appl. Phys.* 114 (14) (2013) 143905, <http://dx.doi.org/10.1063/1.4824372>.
- [19] T. Kojima, M. Mizuguchi, T. Koganezawa, M. Ogiwara, M. Kotsugi, T. Ohtsuki, T.-Y. Tashiro, K. Takanashi, Addition of Co to L1<sub>0</sub>-ordered FeNi films: Influences on magnetic properties and ordered structures, *J. Phys. Appl. Phys.* 47 (42) (2014) 425001, <http://dx.doi.org/10.1088/0022-3727/47/42/425001>.
- [20] K. Mibu, T. Kojima, M. Mizuguchi, K. Takanashi, Local structure and magnetism of L1<sub>0</sub>-type FeNi alloy films with perpendicular magnetic anisotropy studied through <sup>57</sup>Fe nuclear probes, *J. Phys. Appl. Phys.* 48 (20) (2015) 205002, <http://dx.doi.org/10.1088/0022-3727/48/20/205002>.
- [21] T. Ueno, K. Saito, N. Inami, T. Kojima, M. Mizuguchi, N. Miyata, K. Akutsu, M. Takeda, K. Takanashi, K. Ono, Structural and magnetic depth profile analysis of L1<sub>0</sub> FeNi Film by polarized neutron reflectometry, in: *Proc. 2nd Int. Symp. Sci. J-PARC, Journal of the Physical Society of Japan, Tsukuba, Ibaraki, Japan, 2015*, <http://dx.doi.org/10.7566/JPSCP.8.034008>.
- [22] T. Kojima, M. Mizuguchi, K. Takanashi, Growth of L1<sub>0</sub>-FeNi thin films on Cu(001) single crystal substrates using oxygen and gold surfactants, *Thin Solid Films* 603 (2016) 348–352, <http://dx.doi.org/10.1016/j.tsf.2016.02.040>.
- [23] T. Tashiro, M. Mizuguchi, T. Kojima, T. Koganezawa, M. Kotsugi, T. Ohtsuki, K. Sato, T. Konno, K. Takanashi, Fabrication of L1<sub>0</sub>-FeNi phase by sputtering with rapid thermal annealing, *J. Alloys Compd.* 750 (2018) 164–170, <http://dx.doi.org/10.1016/j.jallcom.2018.02.318>.
- [24] K. Ito, M. Hayashida, H. Masuda, T. Nishio, S. Goto, H. Kura, T. Koganezawa, M. Mizuguchi, Y. Shimada, T.J. Konno, H. Yanagihara, K. Takanashi, Epitaxial L1<sub>0</sub>-FeNi films with high degree of order and large uniaxial magnetic anisotropy fabricated by denitriding FeNi films, *Appl. Phys. Lett.* 116 (24) (2020) 242404, <http://dx.doi.org/10.1063/5.0011875>.
- [25] T. Nishio, H. Kura, K. Ito, K. Takanashi, H. Yanagihara, Fabrication of L1<sub>0</sub>-FeNi films with Island structures by nitrogen insertion and topotactic extraction for improved coercivity, *APL Mater.* 9 (9) (2021) 091108, <http://dx.doi.org/10.1063/5.0062692>.
- [26] K. Ito, T. Ichimura, M. Hayashida, T. Nishio, S. Goto, H. Kura, R. Sasaki, M. Tsujikawa, M. Shirai, T. Koganezawa, M. Mizuguchi, Y. Shimada, T.J. Konno, H. Yanagihara, K. Takanashi, Fabrication of L1<sub>0</sub>-ordered FeNi films by denitriding FeNi(001) and FeNiN(110) films, *J. Alloys Compd.* 946 (2023) 169450, <http://dx.doi.org/10.1016/j.jallcom.2023.169450>.
- [27] T. Nishio, K. Ito, H. Kura, K. Takanashi, H. Yanagihara, Uniaxial magnetic anisotropy of L1<sub>0</sub>-FeNi films with island structures on LaAlO<sub>3</sub>(110) substrates by nitrogen insertion and topotactic extraction, *J. Alloys Compd.* 976 (2024) 172992, <http://dx.doi.org/10.1016/j.jallcom.2023.172992>.
- [28] K. Takanashi, M. Mizuguchi, T. Kojima, T. Tashiro, Fabrication and characterization of L1<sub>0</sub>-ordered FeNi thin films, *J. Phys. Appl. Phys.* 50 (48) (2017) 483002, <http://dx.doi.org/10.1088/1361-6463/aa8ff6>.
- [29] Z. Chen, S. Li, T. Lai, Laser-induced transient strengthening of coupling in L1<sub>0</sub>-FePt/FeNi exchange-spring film, *J. Phys. Appl. Phys.* 48 (14) (2015) 145002, <http://dx.doi.org/10.1088/0022-3727/48/14/145002>.
- [30] A. Svalov, B. González Asensio, A. Chlenova, P. Savin, A. Larrañaga, J. Gonzalez, G. Kurylanskaya, Study of the effect of the deposition rate and seed layers on structure and magnetic properties of magnetron sputtered FeNi films, *Vacuum* 119 (2015) 245–249, <http://dx.doi.org/10.1016/j.vacuum.2015.05.037>.



- [31] A. Frisk, B. Lindgren, S.D. Pappas, E. Johansson, G. Andersson, Resonant X-Ray diffraction revealing chemical disorder in sputtered L1<sub>0</sub> FeNi on Si(0 0 1), *J. Phys.: Condens. Matter* 28 (40) (2016) 406002, <http://dx.doi.org/10.1088/0953-8984/28/40/406002>.
- [32] A. Frisk, T.P.A. Hase, P. Svedlindh, E. Johansson, G. Andersson, Strain engineering for controlled growth of thin-film FeNi L1<sub>0</sub>, *J. Phys. Appl. Phys.* 50 (8) (2017) 085009, <http://dx.doi.org/10.1088/1361-6463/aa5629>.
- [33] G. Giannopoulos, G. Barucca, A. Kaidatzis, V. Psycharis, R. Salikhov, M. Farle, E. Koutsouflakis, D. Niarchos, A. Mehta, M. Scuderi, G. Nicotra, C. Spinella, S. Laureti, G. Varvaro, L1<sub>0</sub>-FeNi films on Au-Cu-Ni buffer-layer: A high-throughput combinatorial study, *Sci. Rep.* 8 (1) (2018) 15919, <http://dx.doi.org/10.1038/s41598-018-34296-9>.
- [34] V.Q. Nguyen, B.-H. Jun, Y.-B. Chun, J.H. Lee, Ordered L1<sub>0</sub>-FeNi (111) epitaxial thin film on Al<sub>2</sub>O<sub>3</sub> (0001) substrate: Molecular beam epitaxy growth and characterizations, *Thin Solid Films* 780 (2023) 139962, <http://dx.doi.org/10.1016/j.tsf.2023.139962>.
- [35] S. Mandal, M. Debata, P. Sengupta, S. Basu, L1<sub>0</sub> FeNi: A promising material for next generation permanent magnets, *Crit. Rev. Solid State Mater. Sci.* 48 (6) (2023) 703–725, <http://dx.doi.org/10.1080/10408436.2022.2107484>.
- [36] M. Sakamaki, K. Amemiya, Effect of structural strain on magnetic anisotropy energy of each element in alternately layered FeNi thin films, *Phys. Rev. B* 87 (1) (2013) 014428, <http://dx.doi.org/10.1103/PhysRevB.87.014428>.
- [37] T. Kojima, M. Ogiwara, M. Mizuguchi, M. Kotsugi, T. Koganezawa, T. Ohtsuki, T.-Y. Tashiro, K. Takanashi, Fe–Ni composition dependence of magnetic anisotropy in artificially fabricated L1<sub>0</sub>-ordered FeNi films, *J. Phys.: Condens. Matter* 26 (6) (2014) 064207, <http://dx.doi.org/10.1088/0953-8984/26/6/064207>.
- [38] L.H. Lewis, F.E. Pinkerton, N. Bordeaux, A. Mubarak, E. Poirier, J.I. Goldstein, R. Skomski, K. Barmak, De magnetite et meteorite: Cosmically motivated materials, *IEEE Magn. Lett.* 5 (2014) 1–4, <http://dx.doi.org/10.1109/LMAG.2014.2312178>.
- [39] C.W. Yang, D.B. Williams, J.I. Goldstein, A revision of the Fe–Ni phase diagram at low temperatures (<400 °C), *J. Phase Equilibria* 17 (6) (1996) 522–531, <http://dx.doi.org/10.1007/BF02665999>.
- [40] C.D. Woodgate, C.E. Patrick, L.H. Lewis, J.B. Staunton, Revisiting Néel 60 years on: The magnetic anisotropy of L1<sub>0</sub> FeNi (Tetraenite), *J. Appl. Phys.* 134 (16) (2023) 163905, <http://dx.doi.org/10.1063/5.0169752>.
- [41] R. Wu, A.J. Freeman, Spin-orbit induced magnetic phenomena in bulk metals and their surfaces and interfaces, *J. Magn. Magn. Mater.* 200 (1–3) (1999) 498–514, [http://dx.doi.org/10.1016/S0304-8853\(99\)00351-0](http://dx.doi.org/10.1016/S0304-8853(99)00351-0).
- [42] P. Ravindran, A. Kjekshus, H. Fjellvåg, P. James, L. Nordström, B. Johansson, O. Eriksson, Large magnetocrystalline anisotropy in bilayer transition metal phases from first-principles full-potential calculations, *Phys. Rev. B* 63 (14) (2001) 144409, <http://dx.doi.org/10.1103/PhysRevB.63.144409>.
- [43] Y. Miura, S. Ozaki, Y. Kuwahara, M. Tsujikawa, K. Abe, M. Shirai, The origin of perpendicular magneto-crystalline anisotropy in L1<sub>0</sub> FeNi under tetragonal distortion, *J. Phys.: Condens. Matter* 25 (10) (2013) 106005, <http://dx.doi.org/10.1088/0953-8984/25/10/106005>.
- [44] A. Edström, J. Chico, A. Jakobsson, A. Bergman, J. Ruzs, Electronic structure and magnetic properties of L1<sub>0</sub> binary alloys, *Phys. Rev. B* 90 (1) (2014) 014402, <http://dx.doi.org/10.1103/PhysRevB.90.014402>.
- [45] P. Manchanda, R. Skomski, N. Bordeaux, L.H. Lewis, A. Kashyap, Transition-metal and metalloid substitutions in L1<sub>0</sub>-ordered FeNi, *J. Appl. Phys.* 115 (17) (2014) 17A710, <http://dx.doi.org/10.1063/1.4862722>.
- [46] M. Werwiński, W. Marciniak, Ab initio study of magnetocrystalline anisotropy, magnetostriiction, and Fermi surface of L1<sub>0</sub> FeNi (Tetraenite), *J. Phys. Appl. Phys.* 50 (49) (2017) 495008, <http://dx.doi.org/10.1088/1361-6463/aa958a>.
- [47] L.-Y. Tian, H. Levämäki, O. Eriksson, K. Kokko, A. Nagy, E.K. Dölczeg-Czirják, L. Vitos, Density functional theory description of the order-disorder transformation in Fe–Ni, *Sci. Rep.* 9 (1) (2019) 8172, <http://dx.doi.org/10.1038/s41598-019-44506-7>.
- [48] L.-Y. Tian, O. Eriksson, L. Vitos, Pressure effect on the order–disorder transformation in L1<sub>0</sub> FeNi, *Sci. Rep.* 10 (1) (2020) 14766, <http://dx.doi.org/10.1038/s41598-020-71551-4>.
- [49] L.-Y. Tian, O. Gutfleisch, O. Eriksson, L. Vitos, Alloying effect on the order-disorder transformation in tetragonal FeNi, *Sci. Rep.* 11 (1) (2021) 5253, <http://dx.doi.org/10.1038/s41598-021-84482-5>.
- [50] D. Tuvshin, T. Tsevelmaa, S. Hong, D. Odkhui, Fe–Ni–N based alloys as rare-earth free high-performance permanent magnet across  $\alpha''$  to L1<sub>0</sub> phase transition: A theoretical insight, *Acta Mater.* 210 (2021) 116807, <http://dx.doi.org/10.1016/j.actamat.2021.116807>.
- [51] M. Si, A. Izardar, C. Ederer, Effect of chemical disorder on the magnetic anisotropy in L1<sub>0</sub> FeNi from first-principles calculations, *Phys. Rev. Res.* 4 (3) (2022) 033161, <http://dx.doi.org/10.1103/PhysRevResearch.4.033161>.
- [52] Z. Qiao, M. Tsujikawa, M. Shirai, The effect of chemical disorder on magnetic properties of FeNi and Fe<sub>2</sub>Ni<sub>2</sub>N alloys, *J. Magn. Magn. Mater.* 568 (2023) 170362, <http://dx.doi.org/10.1016/j.jmmm.2023.170362>.
- [53] S. Yamashita, A. Sakuma, Finite-temperature second-order perturbation analysis of magnetocrystalline anisotropy energy of L1<sub>0</sub>-type ordered alloys, *Phys. Rev. B* 108 (5) (2023) 054411, <http://dx.doi.org/10.1103/PhysRevB.108.054411>.
- [54] S. Simonetti, G. Brizuela, A. Juan, Study of the adsorption, electronic structure and bonding of C<sub>2</sub>H<sub>4</sub> on the FeNi(111) surface, *Appl. Surf. Sci.* 256 (21) (2010) 6459–6465, <http://dx.doi.org/10.1016/j.apsusc.2010.04.035>.
- [55] Y.-B. He, J.-F. Jia, H.-S. Wu, First-principles investigation of the molecular adsorption and dissociation of hydrazine on Ni–Fe alloy surfaces, *J. Phys. Chem. C* 119 (16) (2015) 8763–8774, <http://dx.doi.org/10.1021/acs.jpcc.5b01605>.
- [56] J. Marciniak, W. Marciniak, M. Werwiński, DFT calculation of intrinsic properties of magnetically hard phase L1<sub>0</sub> FePt, *J. Magn. Magn. Mater.* 556 (2022) 169347, <http://dx.doi.org/10.1016/j.jmmm.2022.169347>.
- [57] J. Marciniak, M. Werwiński, L1<sub>0</sub> FePt thin films with tilted and in-plane magnetic anisotropy: A first-principles study, *Phys. Rev. B* 108 (21) (2023) 214406, <http://dx.doi.org/10.1103/PhysRevB.108.214406>.
- [58] M. Albrecht, G. Hu, I.L. Guhr, T.C. Ulbrich, J. Boneberg, P. Leiderer, G. Schatz, Magnetic multilayers on nanospheres, *Nature Mater.* 4 (3) (2005) 203–206, <http://dx.doi.org/10.1038/nmat1324>.
- [59] J.-P. Wang, Tilting for the top, *Nature Mater.* 4 (3) (2005) 191–192, <http://dx.doi.org/10.1038/nmat1344>.
- [60] C.L. Zha, J. Persson, S. Bonetti, Y.Y. Fang, J. Åkerman, Pseudo spin valves based on L1<sub>0</sub> (111)-oriented FePt fixed layers with tilted anisotropy, *Appl. Phys. Lett.* 94 (16) (2009) 163108, <http://dx.doi.org/10.1063/1.3123003>.
- [61] Y.-N. Hsu, S. Jeong, D. Lambeth, D. Laughlin, In situ ordering of FePt thin films by using Ag/Si and Ag/Mn<sub>2</sub>Si/Ag/Si templates, *IEEE Trans. Magn.* 36 (5) (2000) 2945–2947, <http://dx.doi.org/10.1109/20.908636>.
- [62] T. Shima, K. Takanashi, Y.K. Takahashi, K. Hono, Preparation and magnetic properties of highly coercive FePt films, *Appl. Phys. Lett.* 81 (6) (2002) 1050–1052, <http://dx.doi.org/10.1063/1.1498504>.
- [63] M. Ohtake, S. Ouchi, F. Kirino, M. Futamoto, L10 ordered phase formation in FePt, FePd, CoPt, and CoPd alloy thin films epitaxially grown on MgO(001) single-crystal substrates, *J. Appl. Phys.* 111 (7) (2012) 07A708, <http://dx.doi.org/10.1063/1.3672856>.
- [64] H. Sepehri-Amin, H. Iwama, T. Ohkubo, T. Shima, K. Hono, Microstructure and in-plane component of L1<sub>0</sub>-FePt films deposited on MgO and MgAl<sub>2</sub>O<sub>4</sub> substrates, *Scr. Mater.* 130 (2017) 247–251, <http://dx.doi.org/10.1016/j.scriptamat.2016.12.018>.
- [65] K. Wu, X. Fu, W. Zhu, X. Huang, Atomic-scale investigation on the origin of in-plane variants in L1<sub>0</sub>-FePt nanoparticles embedded in a single-crystalline MgO matrix, *J. Appl. Phys.* 132 (17) (2022) 175305, <http://dx.doi.org/10.1063/5.0109411>.
- [66] K. Koepernik, H. Eschrig, Full-potential nonorthogonal local-orbital minimum-basis band-structure scheme, *Phys. Rev. B* 59 (3) (1999) 1743–1757, <http://dx.doi.org/10.1103/PhysRevB.59.1743>.
- [67] I. Opahle, K. Koepernik, H. Eschrig, Full-potential band-structure calculation of iron pyrite, *Phys. Rev. B* 60 (20) (1999) 14035, <http://dx.doi.org/10.1103/PhysRevB.60.14035>.
- [68] J.P. Perdew, K. Burke, M. Ernzerhof, Generalized gradient approximation made simple, *Phys. Rev. Lett.* 77 (18) (1996) 3865–3868, <http://dx.doi.org/10.1103/PhysRevLett.77.3865>.
- [69] W. Marciniak, M. Werwiński, Structural and magnetic properties of Fe–Co–C alloys with tetragonal deformation: A first-principles study, *Phys. Rev. B* 108 (21) (2023) 214433, <http://dx.doi.org/10.1103/PhysRevB.108.214433>.
- [70] J.P. Perdew, Y. Wang, Accurate and simple analytic representation of the electron-gas correlation energy, *Phys. Rev. B* 45 (23) (1992) 13244–13249, <http://dx.doi.org/10.1103/PhysRevB.45.13244>.
- [71] A.I. Liechtenstein, M.I. Katsnelson, V.P. Antropov, V.A. Gubanov, Local spin density functional approach to the theory of exchange interactions in ferromagnetic metals and alloys, *J. Magn. Magn. Mater.* 67 (1) (1987) 65–74, [http://dx.doi.org/10.1016/0304-8853\(87\)90721-9](http://dx.doi.org/10.1016/0304-8853(87)90721-9).
- [72] X. Wang, D.-s. Wang, R. Wu, A.J. Freeman, Validity of the force theorem for magnetocrystalline anisotropy, *J. Magn. Magn. Mater.* 159 (3) (1996) 337–341, [http://dx.doi.org/10.1016/0304-8853\(95\)00936-1](http://dx.doi.org/10.1016/0304-8853(95)00936-1).
- [73] R.S. Mulliken, Electronic population analysis on LCAO–MO molecular wave functions. I, *J. Chem. Phys.* 23 (10) (1955) 1833–1840, <http://dx.doi.org/10.1063/1.1740588>.
- [74] K. Momma, F. Izumi, VESTA : A three-dimensional visualization system for electronic and structural analysis, *J. Appl. Crystallogr.* 41 (3) (2008) 653–658, <http://dx.doi.org/10.1107/S0021889808012016>.
- [75] A. Dannenberg, M.E. Gruner, A. Hucht, P. Entel, Surface energies of stoichiometric FePt and CoPt alloys and their implications for nanoparticle morphologies, *Phys. Rev. B* 80 (24) (2009) 245438, <http://dx.doi.org/10.1103/PhysRevB.80.245438>.
- [76] L. Szunyogh, B. Újfalussy, C. Blaas, U. Pustogowa, C. Sommers, P. Weinberger, Oscillatory behavior of the magnetic anisotropy energy in Cu(100)/Co<sub>n</sub> multilayer systems, *Phys. Rev. B* 56 (21) (1997) 14036–14044, <http://dx.doi.org/10.1103/PhysRevB.56.14036>.
- [77] H. Zhang, M. Richter, K. Koepernik, I. Opahle, F. Tasnádi, H. Eschrig, Electric-field control of surface magnetic anisotropy: A density functional approach, *New J. Phys.* 11 (4) (2009) 043007, <http://dx.doi.org/10.1088/1367-2630/11/4/043007>.
- [78] M. Blanco-Rey, P. Perna, A. Gudín, J.M. Diez, A. Anadón, P. Olleros-Rodríguez, L. De Melo Costa, M. Valdiviares, P. Gargiani, A. Guedeja-Marron, M. Cabero, M. Varela, C. García-Fernández, M.M. Otrokov, J. Camarero, R. Miranda, A. Arnaú, J.I. Cerdá, Large perpendicular magnetic anisotropy in nanometer-thick epitaxial graphene/Co/heavy metal heterostructures for spin–orbitronics devices, *ACS Appl. Nano Mater.* 4 (5) (2021) 4398–4408, <http://dx.doi.org/10.1021/acsnm.0c03364>.

- [79] P.-H. Chang, W. Fang, T. Ozaki, K.D. Belashchenko, Voltage-controlled magnetic anisotropy in antiferromagnetic MgO-capped MnPt films, *Phys. Rev. Mater.* 5 (5) (2021) 054406, <http://dx.doi.org/10.1103/PhysRevMaterials.5.054406>.
- [80] M. Cinal, Magnetic anisotropy and orbital magnetic moment in Co films and Co/X bilayers (X=Pt and Pd), *Phys. Rev. B* 105 (10) (2022) 104403, <http://dx.doi.org/10.1103/PhysRevB.105.104403>.
- [81] M. Przybylski, M. Dąbrowski, U. Bauer, M. Cinal, J. Kirschner, Oscillatory magnetic anisotropy due to quantum well states in thin ferromagnetic films (Invited), *J. Appl. Phys.* 111 (7) (2012) 07C102, <http://dx.doi.org/10.1063/1.3670498>.
- [82] P. Bruno, Tight-binding approach to the orbital magnetic moment and magnetocrystalline anisotropy of transition-metal monolayers, *Phys. Rev. B* 39 (1) (1989) 865, <http://dx.doi.org/10.1103/PhysRevB.39.865>.
- [83] L. Ke, Intersublattice magnetocrystalline anisotropy using a realistic tight-binding method based on maximally localized Wannier functions, *Phys. Rev. B* 99 (5) (2019) 054418, <http://dx.doi.org/10.1103/PhysRevB.99.054418>.
- [84] A. Kovacs, H. Ozelt, J. Fischbacher, T. Schrefl, A. Kaidatzis, R. Salikhov, M. Farle, G. Giannopoulos, D. Niarchos, Micromagnetic simulations for coercivity improvement through nano-structuring of rare-earth free  $L1_0$ -FeNi magnets, *IEEE Trans. Magn.* 53 (11) (2017) 1–5, <http://dx.doi.org/10.1109/TMAG.2017.2701418>.
- [85] R. Skomski, J. Coey, Magnetic anisotropy — How much is enough for a permanent magnet? *Scr. Mater.* 112 (2016) 3–8, <http://dx.doi.org/10.1016/j.scriptamat.2015.09.021>.



Contents lists available at ScienceDirect

Journal of Magnetism and Magnetic Materials

journal homepage: [www.elsevier.com/locate/jmmm](http://www.elsevier.com/locate/jmmm)

## Research article

## First-principles study of the magnetic anisotropy of ultrathin B-, C-, and N-doped FeCo films

Joanna Marciniak, Mirosław Werwiński, Justyna Rychły-Gruszecka \*

Institute of Molecular Physics, Polish Academy of Sciences, M. Smoluchowskiego 17, 60-179 Poznań, Poland



## ARTICLE INFO

## Keywords:

Fe and its alloys  
Magnetic anisotropy  
Magnetic properties of thin films, surfaces, and interfaces  
Permanent magnets  
Computational physics  
Density functional theory

## ABSTRACT

Iron-based layered systems are of great interest because of their ability to tune effective material parameters such as magnetic anisotropy energy (MAE). The influence of the crystallographic structure of Fe, its thickness, and the presence of other layers above and below the Fe layer on magnetic parameters, such as the MAE of the studied system, is an intriguing and important topic from an application point of view. Here, we present a density functional theory (DFT) study of the magnetic anisotropy of nine-monolayer Fe, FeCo, and FeCo films with B, C, and N dopants placed in octahedral interstitial positions. The theoretical study is based on calculations using the full-potential local-orbital code FPLO and the generalized gradient approximation. The chemical disorder in the FeCo layers was modeled using the virtual crystal approximation. The structures of the layers were subjected to optimization of the geometry of the interlayer spacings and the neighborhood of the dopant sites. We determined the local magnetic moments and the excess charge at each layer position. We also identified the influence of dopant atoms on the magnetic properties of FeCo layers, such as magnetization and magnetic anisotropy.

## 1. Introduction

Permanent magnets are essential in many consumer and industrial products that convert energy. Rare earth magnets, particularly those based on neodymium and samarium, typically produce the highest energy product. Of the various permanent magnets reported to date, NdFeB has the highest magnetic efficiency. Recently, there has been growing concern about the volatility of the rare earth market, which manifested itself in the so-called rare earth crisis of 2011 [1]. Over the past decade, the rapidly rising and volatile prices of rare earth metals have prompted intensive research efforts worldwide to develop alternative materials for permanent magnets, especially those with very low or zero rare earth content. FeCo has the highest saturation magnetization of all transition metals and their alloys. Still, due to its cubic crystal structure (bcc), it has an extremely low magnetic anisotropy, making it a typical soft magnetic material, which has long been unsuitable for permanent magnets. Burkert et al. [2] performed first-principles calculations using a virtual crystal approximation to theoretically predict that FeCo with a tetragonal crystal structure (bct) would exhibit a giant magnetocrystalline anisotropy constant of up to  $10^7 \text{ J m}^{-3}$ . In a FeCo alloy with lattice parameter ratio  $c/a \approx 1.2$  indication of high tetragonal deformation, the magnetic anisotropy energy (MAE) was predicted to reach  $0.7\text{--}0.8 \text{ meV atom}^{-1}$ . However, the experimental growth of Fe-Co alloys with such high tetragonal

distortion is challenging because their natural structure is bcc (up to about 70% Co concentration). Subsequent theoretical studies have corrected the theoretical MAE to values very close to the experimental ones, using a more realistic treatment of the chemical disorder present in Fe-Co alloys [3,4]. To solve the problem of tetragonal deformation, tiny interstitial atoms (B, C, N, etc.) placed on the  $c$ -axis of FeCo can stretch the unit cell and stabilize the bct structure. As for FeCo, there are studies on adding interstitial elements B [5–7], C [8–10], and N [11–13].

In the race to miniaturize electronic devices, modern science has reached the ultimate level of monoatomic layers. The limit for magnetic tunnel junctions with perpendicular magnetic anisotropy is about twenty atomic monolayers [14,15]. Layered systems are particularly interesting for their ability to tune effective material parameters such as MAE. Among such systems, iron-based layered systems are of considerable interest [16–19]. An intriguing and important topic from the point of view of applications is the influence of the crystallographic structure of Fe, its thickness, and the presence of other layers above and below the Fe layer on magnetic parameters such as the MAE of the studied system.

Here, we present a theoretical study of the magnetic anisotropy of FeCo thin films with B, C, and N dopants located in octahedral interstitial positions. The theoretical study is based on calculations using

\* Corresponding author.

E-mail address: [justyna.rychly-gruszecka@ifmpan.poznan.pl](mailto:justyna.rychly-gruszecka@ifmpan.poznan.pl) (J. Rychły-Gruszecka).<https://doi.org/10.1016/j.jmmm.2023.171563>

Received 23 July 2023; Received in revised form 7 October 2023; Accepted 22 November 2023

Available online 23 November 2023

0304-8853/© 2023 The Authors. Published by Elsevier B.V. This is an open access article under the CC BY license (<http://creativecommons.org/licenses/by/4.0/>).

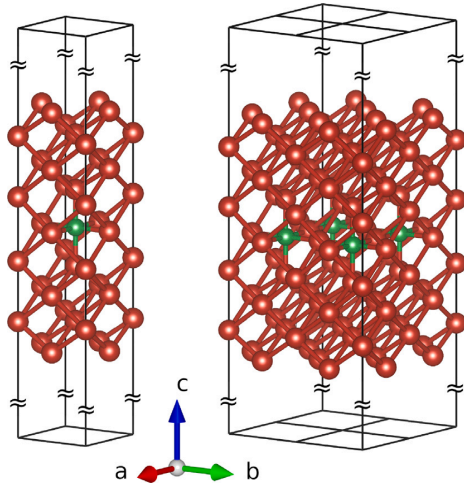


**Fig. 1.** A unit cell of a 9-atomic monolayer thick  $\text{Fe}_{0.7}\text{Co}_{0.3}$  thin film, with the dopant (B or C or N) located in an octahedral interstitial position. A single computational cell is shown on the left, and a multiplied  $2 \times 2$  cell on the right. The unit cell is obtained after geometry optimization. The red spheres represent the  $\text{Fe}_{0.7}\text{Co}_{0.3}$  virtual atoms, while the green sphere represents the dopant atoms. A surrounding vacuum (52 Å) was applied in the computational cells to obtain non-interacting thin films. To improve the visibility of the film's atoms, the height of the vacuum used has been significantly reduced in the figures.

the full-potential local-orbital electronic structure code (FPLO) and the generalized gradient approximation. The chemical disorder in FeCo layers is modeled using the virtual crystal approximation (VCA). The layer structures are subjected to geometry optimization of the interlayer distances and the vicinity region of the dopant sites. We determine the local magnetic moments and excess charge at each atomic position. We identified the dopant atoms' effect on the FeCo films' magnetic properties, such as magnetization and magnetic anisotropy.

## 2. Calculations' details

In this study, we examined the structural and magnetic properties of ultrathin (9 atomic monolayers thick) films of  $\text{Fe}_{0.7}\text{Co}_{0.3}$  alloys with a dopant B, C, or N atoms located in octahedral interstitial position, see Fig. 1, using density functional theory (DFT) calculations. To compare the effect of the dopant, placed in the octahedral gap, on the obtained magnetic properties of the structures, we also performed calculations of thin films of pure iron-cobalt alloy with a given concentration (70% Fe and 30% Co) and a thin film of iron without doping. Altogether, calculations of five different structures were performed.

The structures were prepared in cells with symmetry  $P4/mmm$ , where the lattice parameter equals  $a = 4.0$  Å. In the computational cells, to remove the bulk periodicity in the indicated direction and to model the thin film, a vacuum of 52 Å was added, giving a height of the computational cell equal to 64 Å. In the presented calculations, the VCA approach was used, as implemented in FPLO 18.00-52 code, to simulate a disordered 30% Co alloy. Wyckoff's positions were optimized in each considered system using a scalar-relativistic approach with spin polarization. Atomic positions in [001] were treated by forces optimization on atoms, with convergence criterion set as  $10^{-3}$  eV Å<sup>-1</sup>.

A mesh of  $k$ -points was set as  $65 \times 65 \times 5$ , and the convergence criteria were used  $10^{-8}$  Ha and  $10^{-7}$  for energy and charge density, respectively. The integration over the Brillouin zone was performed using the tetrahedron method. The DFT calculations were performed using the full-potential local-orbital approach implemented in the FPLO 18.00-52 code [20]. Using the Perdew–Burke–Ernzerhof

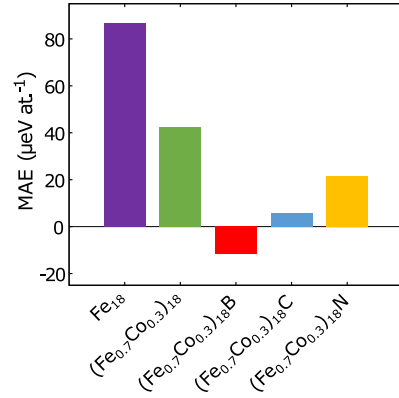


**Fig. 2.** Magnetic anisotropy energy (MAE) calculated for 9 atomic monolayer thick films. From left to right: pure Fe (shown as a purple bar); pure  $\text{Fe}_{0.7}\text{Co}_{0.3}$  alloy (shown as a green bar);  $\text{Fe}_{0.7}\text{Co}_{0.3}$  with a B dopant atom (shown as a red bar);  $\text{Fe}_{0.7}\text{Co}_{0.3}$  with a C dopant atom (shown as a blue bar);  $\text{Fe}_{0.7}\text{Co}_{0.3}$  with a N dopant atom (shown as a yellow bar). The dopant atoms are in the octahedral interstitial position. The DFT calculations were performed with the full-potential local-orbital (FPLO-18) code [20]. The exchange–correlation functional in the Perdew–Burke–Ernzerhof (PBE) parametrization was used [21].

(PBE) exchange–correlation potential [21], scalar-relativistic calculations were performed, followed by single iteration of full-relativistic calculations. MAE was determined by the formula:

$$\text{MAE} = E(\theta = 0^\circ) - E(\theta = 90^\circ), \quad (1)$$

where  $\theta$  is the angle between the magnetization direction and the  $c$  axis. Crystal structures were visualized using the VESTA program [22].

## 3. Results and discussion

We started the calculations for the considered structures by optimizing the  $z$  positions of all atomic sites with a fixed value of the lattice parameter  $a$ . The total thicknesses of the Fe-Co thin films and the distances of the nearest and second-nearest atomic monolayers to the central layer were collected in Table 1. As we can see, the film's total thickness increases due to doping. The lattice stretching in the  $z$  direction is caused by the dopant atom located in the octahedral hole.

Subsequently, we calculated the magnetic anisotropy energy of FeCo thin films (9 atoms thick) with B, C, and N dopants in octahedral interstitial position in the center of the layer. For comparison, we have calculated a pure thin film of an iron-cobalt alloy of a given concentration and a thin film of iron. The MAE for the above structures are shown in Fig. 2. For the structures of a given thickness, we can see that pure Fe layers have the strongest tendency to be magnetized perpendicular to the surface; in the case of the  $\text{Fe}_{0.7}\text{Co}_{0.3}$  alloy, the MAE decreases almost by half, while for the thin films doped with N, C, and B elements the MAE becomes smaller and smaller. In the case of the  $\text{Fe}_{0.7}\text{Co}_{0.3}$  with a B dopant atom, the MAE changes sign, which shows the change in the tendency of this structure and its preference to be magnetized in-plane (and not out-of-plane as was the case for the other systems). While in-plane anisotropy resulting from B doping appears uncommon in comparison to other cases, it is frequently obtained in FeCoB thin films through experimental means [23]. Based on earlier experimental work, the orientation of magnetization in FeCoB films can be altered through various technological methods, including post-deposition annealing in a magnetic field or application of mechanical stress [23]. The direction of magnetization is influenced by various factors, such as the concentration of individual elements, the type and thickness of the substrate and overlay, and the thickness of the magnetic film.

**Table 1**

Total thicknesses of the 9-atomic monolayer thick  $\text{Fe}_{0.7}\text{Co}_{0.3}$  and  $\text{Fe}_{0.7}\text{Co}_{0.3}\text{-X}$  thin films after interlayer spacing optimization, together with distances between the central atomic monolayer and the first and second-nearest monolayer. The double values for the atoms of the first nearest monolayer are due to the presence of dopant atoms in the central layer (see Fig. 1). The  $a$  lattice parameter of the computational unit cell was set at  $4.00 \text{ \AA}$  ( $\sqrt{2} \times 2.83 \text{ \AA}$ ).

	$(\text{Fe}_{0.7}\text{Co}_{0.3})_{18}$	$(\text{Fe}_{0.7}\text{Co}_{0.3})_{18}\text{B}$	$(\text{Fe}_{0.7}\text{Co}_{0.3})_{18}\text{C}$	$(\text{Fe}_{0.7}\text{Co}_{0.3})_{18}\text{N}$
total thickness ( $\text{\AA}$ )	11.27	11.81	11.74	11.75
1st layer ( $\text{\AA}$ )	1.42	1.58/1.86	1.59/1.80	1.60/1.80
2nd layer ( $\text{\AA}$ )	2.83	3.09	3.06	3.07

**Table 2**

Averaged spin ( $m_s$ ) and orbital ( $m_l$ ) magnetic moments, together with magnetocrystalline anisotropy energies (MAE) of 9-monolayer thick films of Fe,  $\text{Fe}_{0.7}\text{Co}_{0.3}$ , and  $\text{Fe}_{0.7}\text{Co}_{0.3}\text{X}$  models, where X = B, C, N. The obtained results were compared with literature values for similar systems.

System	Form	Method	Reference	$m_s$ ( $\mu_B \text{ at}^{-1}$ )	$m_l$ ( $\mu_B \text{ at}^{-1}$ )	MAE ( $\mu\text{eV at}^{-1}$ )	MAE ( $\text{MJ m}^{-3}$ )
Fe	9-monolayers		this work	2.41	0.058	87	1.38
Fe	bulk		[15]	2.16	0.043	0	0
$\text{Fe}_{0.7}\text{Co}_{0.3}$	9-monolayers	VCA	this work	2.38	0.080	43	0.68
$\text{Fe}_{0.7}\text{Co}_{0.3}$	bulk	VCA/CPA	[9]	2.42/2.43	–	54/27	–
$(\text{Fe}_{0.7}\text{Co}_{0.3})_{18}\text{B}$	9-monolayers	VCA	this work	2.18	0.076	–13	–0.18
$(\text{Fe}_{0.65}\text{Co}_{0.35})_{24}\text{B}$	bulk	CPA	[5]	2.16	0.064	23	0.31
$\text{Fe}_{67}\text{Co}_{18}\text{B}_{15}$	>100 nm film	expt.	[7]	$\sim 1.7$	–	$\sim 0$	$\sim 0$
$(\text{Fe}_{0.38}\text{Co}_{0.62})_{0.98}\text{B}_{0.02}$	20 nm films	expt.	[5]	$1.9 \pm 0.2$	–	–	$0.4 \pm 0.2$
$(\text{Fe}_{0.7}\text{Co}_{0.3})_{18}\text{C}$	9-monolayers	VCA	this work	2.16	0.075	6	0.09
$(\text{Fe}_{0.7}\text{Co}_{0.3})_{18}\text{C}$	bulk	VCA/CPA	[9]	1.88/1.85	–	77/81	1.10/–
$(\text{Fe}_{0.69}\text{Co}_{0.31})_{16}\text{C}$	bulk	supercells	[10]	2.35	–	65	0.95
$(\text{Fe}_{0.4}\text{Co}_{0.6})_{0.98}\text{C}_{0.02}$	5 nm films	expt.	[8]	2.0	–	–	$0.80 \pm 0.15$
$(\text{Fe}_{0.7}\text{Co}_{0.3})_{18}\text{N}$	9-monolayers	VCA	this work	2.19	0.076	22	0.33
$(\text{Fe}_{0.75}\text{Co}_{0.25})_{16}\text{N}_2$	bulk	supercells	[13]	1.96	–	–	1.5
$(\text{Fe}_{0.5}\text{Co}_{0.5})_{89}\text{V}_9\text{N}_2$	20 nm film	expt.	[11]	–	–	–	1.24

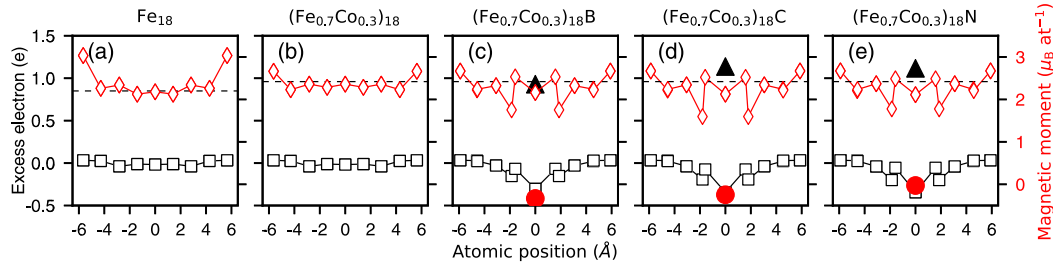


**Fig. 3.** Excess charge (charge transfer) at each atomic position in the calculated thin films presented as black empty squares and big black full triangles for dopant atoms. Local spin magnetic moments at each atomic position in the calculated thin films presented as red empty diamonds and big red full circles for dopant atoms. Considered 9-atomic monolayer thick films of (a) pure Fe; (b) pure  $\text{Fe}_{0.7}\text{Co}_{0.3}$  alloy; (c)  $\text{Fe}_{0.7}\text{Co}_{0.3}$  with a B dopant atom; (d)  $\text{Fe}_{0.7}\text{Co}_{0.3}$  with a C dopant atom; (e)  $\text{Fe}_{0.7}\text{Co}_{0.3}$  with a N dopant atom. The dopant atoms in (c-e) are in the octahedral interstitial position. The thin dashed line has been used to indicate the values of the spin magnetic moment for (a) bulk Fe ( $m_s = 2.2 \mu_B \text{ at}^{-1}$ ), and for (b-e) bulk  $\text{Fe}_{0.7}\text{Co}_{0.3}$  ( $m_s = 2.42 \mu_B \text{ at}^{-1}$ ). Calculations were performed with the PBE exchange-correlation potential [21] in scalar-relativistic formalism using the FPLO18 code [20].

We have also conducted a detailed study of the charge and the spin magnetic moment for all the systems under study and present the results in Fig. 3. We first plotted (for comparison) the charge transfer at each atom of pure Fe and pure  $\text{Fe}_{0.7}\text{Co}_{0.3}$  alloy through the thickness of their layers using black empty squares connected by a black line (see Fig. 3(a) and (b), respectively). Only negligibly small charge oscillations can be observed for these single-component layers, appearing due to the presence of surfaces. By introducing a dopant into the octahedral gap located in the center of a thin FeCo alloy layer, we can observe the transfer of a negative charge to the dopant atom at the expense of the alloy atoms in its vicinity (see Fig. 3(c-e) for dopants with B, C, and N, respectively, where the additional charge on the dopant has been visualized with a full black triangle).

We then plotted, using red empty diamonds connected by a red line, the local spin magnetic moments at each atomic position in the calculated thin films (see Fig. 3). It can be observed that the introduction of surfaces into the structure of pure magnetic layers without

dopants increases the spin magnetic moment near their surface. This is particularly evident for a thin layer of pure Fe (see Fig. 3(a)), a slightly less pronounced increase in the magnetic moment is obtained for a thin layer of  $\text{Fe}_{0.7}\text{Co}_{0.3}$  alloy (see Fig. 3(b)). For comparison, the thin dashed line has been used to indicate the values of the spin magnetic moment for bulk Fe ( $m_s = 2.2 \mu_B \text{ at}^{-1}$ , marked in Fig. 3(a)) and for bulk  $\text{Fe}_{0.7}\text{Co}_{0.3}$  ( $m_s = 2.42 \mu_B \text{ at}^{-1}$ , marked in Fig. 3(b-e)). By introducing the dopant into the octahedral gap in the center of the  $\text{Fe}_{0.7}\text{Co}_{0.3}$  alloy thin film, we can observe a varying spin magnetic moment on the alloy atoms near the dopant. The dopant atom acquires a small negative spin magnetic moment (see Fig. 3(c-e) for dopants with B, C, and N, respectively, where the spin magnetic moment on the dopant has been visualized with a large red solid circle). Averaged values of magnetic moments at Fe/Co position and magnetic moments from literature are summarized in Table 2. The values of spin and orbital magnetic moments on the dopants obtained in the calculations are summarized in Table 3. As can be seen, our results are comparable



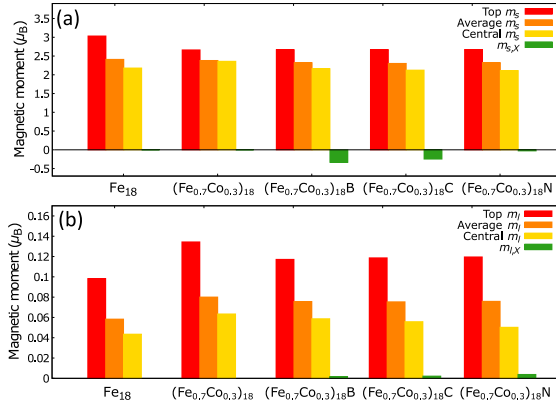


**Fig. 4.** The calculated (a) spin and (b) orbital magnetic moment for all considered 9-atom layers (from left to right: pure Fe; pure  $\text{Fe}_{0.7}\text{Co}_{0.3}$  alloy;  $\text{Fe}_{0.7}\text{Co}_{0.3}$  with B-, C-, or N-atoms located in the octahedral interstitial position, respectively). The red, yellow, and orange bars represent the (a) spin and (b) orbital magnetic moment calculated on the outer, central, average atom (Fe in the case of pure Fe thin film or  $\text{Fe}_{0.7}\text{Co}_{0.3}$  for the rest of the structures), respectively; the green bar represents the (a) spin and (b) orbital magnetic moment on the dopant atom. The DFT calculations were performed with the full-potential local-orbital (FPLO-18) code [20]. The exchange-correlation functional in the Perdew–Burke–Ernzerhof (PBE) parametrization was used [21].

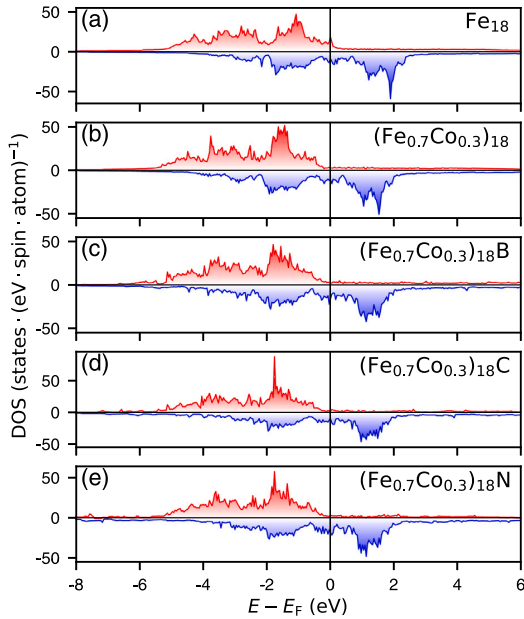


**Fig. 5.** The calculated total density of states (DOS) for the considered 9-atom thick layers of: (a) pure Fe; (b) pure  $\text{Fe}_{0.7}\text{Co}_{0.3}$  alloy; (c)  $\text{Fe}_{0.7}\text{Co}_{0.3}$  with a B dopant atom; (d)  $\text{Fe}_{0.7}\text{Co}_{0.3}$  with a C dopant atom; (e)  $\text{Fe}_{0.7}\text{Co}_{0.3}$  with a N dopant atom. The dopant atoms in (c–e) are in the octahedral interstitial position. The DFT calculations were performed with the full-potential local-orbital (FPLO-18) code [20]. The exchange-correlation functional in the Perdew–Burke–Ernzerhof (PBE) parametrization was used [21].

to those obtained in experiments on thin films and calculations for solids.

To make the spin magnetic moment results easier to read, we have presented the obtained results in the form of a bar chart, where the averaged spin magnetic moment is shown with an orange bar, the spin

**Table 3**

Spin and orbital magnetic moments (in  $\mu_B$ ) on X = B, C, and N in researched systems. The DFT calculations were performed with the full-potential local-orbital (FPLO-18) code [20]. The exchange-correlation functional in the Perdew–Burke–Ernzerhof (PBE) parametrization was used [21].

System	$m_{(s,x)}$	$m_{(l,x)}$
$(\text{Fe}_{0.7}\text{Co}_{0.3})_{18}\text{B}$	−0.33	0.002
$(\text{Fe}_{0.7}\text{Co}_{0.3})_{18}\text{C}$	−0.25	0.002
$(\text{Fe}_{0.7}\text{Co}_{0.3})_{18}\text{N}$	−0.03	0.004

magnetic moment for the central (outer) atom is shown with a yellow (red) bar, and the spin magnetic moment for the dopant atom is shown with a green bar (see Fig. 4(a)). Similarly, we presented the results for the orbital magnetic moment (see Fig. 4(b)).

At the end, we present the calculation of the total density of states to show what happens after doping  $(\text{Fe}_{0.7}\text{Co}_{0.3})_{18}$  thin films with B, C or N, see Fig. 5. First, in Fig. 5(a), we show the total DOS for the pure Fe thin film with the comparison to the pure  $(\text{Fe}_{0.7}\text{Co}_{0.3})_{18}$  thin film shown in Fig. 5(b). Compared to pure Fe,  $(\text{Fe}_{0.7}\text{Co}_{0.3})_{18}$  has 0.3 more electrons per transition metal atom than pure Fe, causing the Fermi level to shift slightly to the right for the  $(\text{Fe}_{0.7}\text{Co}_{0.3})_{18}$  alloy. Doping the  $(\text{Fe}_{0.7}\text{Co}_{0.3})_{18}$  alloy layer with B, C, or N atoms (see Fig. 5(c–e)) results in a small additional contribution of *p*-group electrons, which causes a further shift of the Fermi level to the right. This shift is slight because there is one dopant atom for every 18 atoms of 4s and 3d band atoms in the  $(\text{Fe}_{0.7}\text{Co}_{0.3})_{18}$  alloy thin film. It can be seen that the dopants form a bond with the alloy, as we do not observe sharp peaks in the total DOS curve.

Finally, we would like to comment on the selected limitations of the discussed models resulting from the choice of the size of the system and the usage of virtual crystal approximation. The thickness of the 9-monolayers was chosen slightly above the experimentally observed structural transition of ultrathin Fe films from a structure with strong tetragonal deformation ( $c/a > 1.4$ ) below the critical thickness to a bcc-like structure above it [24]. At the same time, we did not choose a higher thickness to not increase the number of non-equilibrium atoms in the model and thus the time required for calculations. Since we did not consider a range of film thicknesses (e.g., from 1 to 20 atomic monolayers), the value of our results for a single unique thickness is limited. For example, in line with our other research on ultra-thin films [25,26] the variation in MAE with thickness is not monotonic and can change significantly with a change in thickness by as little as one or two monolayers. Hence, the most significant conclusion regarding the MAE of the examined layers is the tendency of MAE to increase with the increase in the atomic number of the dopant. On the other hand, the calculated magnetic moments on the film's surface, around the dopant, and on it depend not so much on the film thickness.

The prepared models also have a specific location of the dopant in relation to the other atoms - it is part of the central layer of the system, creating a very regular distribution of the dopant in it, see Fig. 1. This assumption was dictated by the need to limit the unit cell size, counted in the number of non-equivalent atoms, to a value enabling MAE calculations. Unfortunately, placing dopant atoms in a single monolayer primarily results in overestimating the increase of film thickness due to doping. However, as experiments on FeCo thin films with B and C dopants have shown, the magnitude of the tetragonal deformation in our models is relatively consistent with the measurements [5,8].

Another approximation used in the presented study is the virtual crystal approximation (VCA), which we applied to model Fe/Co alloying. We decided to use it even though it is known for overestimating the value of the MAE for bulk materials. In the case of modeling layered systems containing interstitial defects, which by breaking the symmetry leads to a significant increase in the number of non-equivalent atoms in the system and thus to a significant increase in computational time,

the use of the VCA allows both to optimize the system geometry and to reduce the computational time by at least an order of magnitude, relative to alternative methods of (1) averaging over multiple supercells or (2) the coherent potential approximation (CPA), the latter usually happens in combination with the atomic sphere approximation (ASA), leading to unreliable MAE results.

Comparing the obtained MAE values with the results from the literature for calculations for bulk systems (see Table 2), we notice that the obtained values differ significantly. However, these differences may primarily result from the fact that calculations of the layered system are performed, where size effects come into play. Even calculations provided using the VCA method in the bulk system resulted in much higher values. Comparison with the results of experiments on thin-film systems allows us to confirm the similarity of orders of magnitude.

#### 4. Summary and conclusions

We have conducted a theoretical study of the magnetic anisotropy of ultrathin (9 atomic monolayers thick) FeCo films with B, C, and N dopants located in octahedral interstitial position in the center of the layer. The layer structures were subjected to geometry optimization of the interlayer distances and the vicinity region of the dopant sites. This allowed us to get different distances between different layers according to the placement above/below the dopant atom or next to this place and in the different depths of the film thickness. We determined the local magnetic moments and excess charge at each position in the films and identified the dopant atoms' effect on the FeCo films' magnetic properties, such as magnetization, total DOS, and magnetic anisotropy.

Contrary to the results for bulk systems, our results indicate that doping FeCo with B, C, and N atoms in the octahedral position in 9-atomic-monolayer thick FeCo films can significantly reduce the MAE, even changing its sign to negative in the case of B-doped FeCo thin films. The results of this investigation may have important implications for further research on magnetic thin films for spintronic applications.

#### Declaration of competing interest

The authors declare that they have no known competing financial interests or personal relationships that could have appeared to influence the work reported in this paper.

#### Data availability

Data will be made available on request.

#### Acknowledgments

We acknowledge the financial support of the National Science Centre Poland under the decision DEC-2018/30/E/ST3/00267. We thank Paweł Leśniak and Daniel Depcik for compiling the scientific software and administration of the computing cluster at the Institute of Molecular Physics, Polish Academy of Sciences.

#### References

- [1] J. Coey, Permanent magnets: Plugging the gap, *Scr. Mater.* 67 (6) (2012) 524–529, <http://dx.doi.org/10.1016/j.scriptamat.2012.04.036>.
- [2] T. Burkert, L. Nordström, O. Eriksson, O. Heinonen, Giant magnetic anisotropy in tetragonal FeCo alloys, *Phys. Rev. Lett.* 93 (2) (2004) 027203, <http://dx.doi.org/10.1103/PhysRevLett.93.027203>.
- [3] C. Neise, S. Schönecker, M. Richter, K. Koepnick, H. Eschrig, The effect of chemical disorder on the magnetic anisotropy of strained Fe–Co films, *Phys. Status Solidi b* 248 (10) (2011) 2398–2403, <http://dx.doi.org/10.1002/pssb.201147100>.
- [4] I. Turek, J. Kudrnovský, K. Carva, Magnetic anisotropy energy of disordered tetragonal Fe–Co systems from ab initio alloy theory, *Phys. Rev. B* 86 (17) (2012) 174430, <http://dx.doi.org/10.1103/PhysRevB.86.174430>.
- [5] L. Reichel, L. Schultz, D. Pohl, S. Oswald, S. Fähler, M. Werwiński, A. Edström, E.K. Delczeg-Czirjak, J. Ruzs, From soft to hard magnetic Fe–Co–B by spontaneous strain: a combined first principles and thin film study, *J. Phys.: Condens. Matter* 27 (47) (2015) 476002, <http://dx.doi.org/10.1088/0953-8984/27/47/476002>.
- [6] W. Coene, F. Hakkens, R. Coehoorn, D. De Mooij, C. De Waard, J. Fidler, R. Grössinger, Magnetocrystalline anisotropy of Fe<sub>3</sub>B, Fe<sub>2</sub>B and Fe<sub>1.4</sub>Co<sub>0.6</sub>B as studied by Lorentz electron microscopy, singular point detection and magnetization measurements, *J. Magn. Magn. Mater.* 96 (1–3) (1991) 189–196, [http://dx.doi.org/10.1016/0304-8853\(91\)90627-M](http://dx.doi.org/10.1016/0304-8853(91)90627-M).
- [7] L. Chen, T. Klemmer, K. Ellis, R. Van Dover, S. Jin, Soft-magnetic properties of Fe–Co–B thin films for ultra-high-frequency applications, *J. Appl. Phys.* 87 (9) (2000) 5858–5860, <http://dx.doi.org/10.1063/1.372546>.
- [8] L. Reichel, L. Schultz, S. Fähler, Lattice relaxation studies in strained epitaxial Fe–Co–C films, *J. Appl. Phys.* 117 (17) (2015) 17C712, <http://dx.doi.org/10.1063/1.4908031>.
- [9] E.K. Delczeg-Czirjak, A. Edström, M. Werwiński, J. Ruzs, N.V. Skorodumova, L. Vitos, O. Eriksson, Stabilization of the tetragonal distortion of Fe<sub>3</sub>Co<sub>1-x</sub> alloys by C impurities: A potential new permanent magnet, *Phys. Rev. B* 89 (2014) 144403, <http://dx.doi.org/10.1103/PhysRevB.89.144403>.
- [10] W. Marciniak, M. Werwiński, Structural and magnetic properties of Fe–Co–C alloys with tetragonal deformation: a first-principle study, *Phys. Rev. B* (2023).
- [11] T. Hasegawa, T. Niibori, Y. Takemasa, M. Oikawa, Stabilisation of tetragonal FeCo structure with high magnetic anisotropy by the addition of V and N elements, *Sci. Rep.* 9 (1) (2019) 5248, <http://dx.doi.org/10.1038/s41598-019-41825-7>.
- [12] T. Hasegawa, Challenges toward development of rear-earth free FeCo based permanent magnet, *Electron. Commun. Jpn.* 104 (2) (2021) e12307, <http://dx.doi.org/10.1002/ecj.12307>.
- [13] X. Zhao, C.-Z. Wang, Y. Yao, K.-M. Ho, Large magnetic anisotropy predicted for rare-earth-free Fe<sub>16-x</sub>Co<sub>x</sub>N<sub>2</sub> alloys, *Phys. Rev. B* 94 (22) (2016) 224424, <http://dx.doi.org/10.1103/PhysRevB.94.224424>.
- [14] K. Watanabe, B. Jinnai, S. Fukami, H. Sato, H. Ohno, Shape anisotropy revisited in single-digit nanometer magnetic tunnel junctions, *Nature Commun.* 9 (1) (2018) 663, <http://dx.doi.org/10.1038/s41467-018-03003-7>.
- [15] J. Snarski-Adamski, J. Rychly, M. Werwiński, Magnetic properties of 3d, 4d, and 5d transition-metal atomic monolayers in Fe/TM/Fe sandwiches: Systematic first-principles study, *J. Magn. Magn. Mater.* 546 (2022) 168828, <http://dx.doi.org/10.1016/j.jmmm.2021.168828>.
- [16] A. Perumal, Y. Takahashi, T. Seki, K. Hono, Particulate structure of L1<sub>0</sub> ordered ultrathin FePt films for perpendicular recording, *Appl. Phys. Lett.* 92 (13) (2008) 132508, <http://dx.doi.org/10.1063/1.2830708>.
- [17] K. Hammar, Y. Labaye, L. Messad, A. Ziane, Theoretical estimation of surface magnetic anisotropy on L1<sub>0</sub>-FePt thin films: Case of perfect and defect Surfaces, *Surf. Sci.* 717 (2022) 121999, <http://dx.doi.org/10.1016/j.susc.2021.121999>.
- [18] Y. Miura, S. Ozaki, Y. Kuwahara, M. Tsujikawa, K. Abe, M. Shirai, The origin of perpendicular magneto-crystalline anisotropy in L1<sub>0</sub>-FeNi under tetragonal distortion, *J. Phys.: Condens. Matter* 25 (10) (2013) 106005, <http://dx.doi.org/10.1088/0953-8984/25/10/106005>.
- [19] K. Ito, M. Hayashida, H. Masuda, T. Nishio, S. Goto, H. Kura, T. Koganezawa, M. Mizuguchi, Y. Shimada, T.J. Konno, H. Yanagihara, K. Takanashi, Epitaxial L1<sub>0</sub>-FeNi films with high degree of order and large uniaxial magnetic anisotropy fabricated by denitriding FeNiN films, *Appl. Phys. Lett.* 116 (24) (2020) 242404, <http://dx.doi.org/10.1063/5.0011875>.
- [20] K. Koepnick, H. Eschrig, Full-potential nonorthogonal local-orbital minimum-basis band-structure scheme, *Phys. Rev. B* 59 (3) (1999) 1743–1757, <http://dx.doi.org/10.1103/PhysRevB.59.1743>.
- [21] J.P. Perdew, K. Burke, M. Ernzerhof, Generalized gradient approximation made simple, *Phys. Rev. Lett.* 77 (18) (1996) 3865–3868, <http://dx.doi.org/10.1103/PhysRevLett.77.3865>.
- [22] K. Momma, F. Izumi, VESTA : A three-dimensional visualization system for electronic and structural analysis, *J. Appl. Crystallogr.* 41 (3) (2008) 653–658, <http://dx.doi.org/10.1107/S0021889808012016>.
- [23] L. Kippen, H. Fulara, M. Raju, S. Chaudhary, In-plane magnetic anisotropy and coercive field dependence upon thickness of CoFeB, *J. Magn. Magn. Mater.* 324 (19) (2012) 3118–3121, <http://dx.doi.org/10.1016/j.jmmm.2012.05.012>.
- [24] B.R. Cuenya, M. Doi, S. Löbus, R. Courths, W. Keune, Observation of the fcc-to-bcc Bain transformation in epitaxial Fe ultrathin films on Cu<sub>2</sub>Au (001), *Surf. Sci.* 493 (1–3) (2001) 338–360, [http://dx.doi.org/10.1016/S0039-6028\(01\)01239-0](http://dx.doi.org/10.1016/S0039-6028(01)01239-0).
- [25] J. Marciniak, M. Werwiński, L1<sub>0</sub> FePt thin films with tilted and in-plane magnetic anisotropy: first-principles study, *Phys. Rev. B* (2023).
- [26] J. Meixner, J. Rychly-Gruszecka, M. Werwiński, Magnetic properties and structural phase transition in ultrathin fcc Fe(111) and bccFe (111) films: first-principles study, 2023, <http://dx.doi.org/10.48550/arXiv.2307.11167>, arXiv preprint arXiv:2307.11167.

## Articles included in the dissertation

- <sup>I</sup>J. Marciniak and M. Werwiński, “L1<sub>0</sub> FePt thin films with tilted and in-plane magnetic anisotropy: a first-principles study”, *Phys. Rev. B* **108**, 214406 (2023).
- <sup>II</sup>J. Marciniak and M. Werwiński, “Magnetic anisotropy of L1<sub>0</sub> FeNi (001), (010), and (111) ultrathin films: a first-principles study”, *J. Magn. Magn. Mater.* **609**, 172455 (2024).
- <sup>III</sup>J. Marciniak, M. Werwiński, and J. Rychły-Gruszecka, “First-principles study of the magnetic anisotropy of ultrathin B-, C-, and N-doped FeCo films”, *J. Magn. Magn. Mater.* **589**, 171563 (2023).

## Bibliography

- <sup>1</sup>R. F. L. Evans, R. W. Chantrell, U. Nowak, A. Lyberatos, and H.-J. Richter, “Thermally induced error: Density limit for magnetic data storage”, *Appl. Phys. Lett.* **100**, 102402 (2012).
- <sup>2</sup>M. H. Kryder, E. C. Gage, T. W. McDaniel, W. A. Challener, R. E. Rottmayer, G. Ju, Y.-T. Hsia, and M. F. Erden, “Heat Assisted Magnetic Recording”, *Proc. IEEE* **96**, 1810–1835 (2008).
- <sup>3</sup>*Exos Mozaic 3+ | Seagate Polska*, Seagate.com, (Sept. 19, 2024) <https://www.seagate.com/pl/pl/products/enterprise-drives/exos-x/x-mozaic/> (visited on 09/19/2024).
- <sup>4</sup>M. Albrecht, G. Hu, I. L. Guhr, T. C. Ulbrich, J. Boneberg, P. Leiderer, and G. Schatz, “Magnetic Multilayers on Nanospheres”, *Nat. Mater.* **4**, 203–206 (2005).
- <sup>5</sup>J. M. D. Coey, *Magnetism and magnetic materials* (Cambridge University Press, Cambridge, 2010), 614 pp.
- <sup>6</sup>J. Marciniak, W. Marciniak, and M. Werwiński, “DFT calculation of intrinsic properties of magnetically hard phase L1<sub>0</sub> FePt”, *J. Magn. Magn. Mater.* **556**, 169347 (2022).
- <sup>7</sup>R. Skomski, A. Kashyap, and J. Zhou, “Atomic and micromagnetic aspects of L1<sub>0</sub> magnetism”, *Scr. Mater.* **53**, 389–394 (2005).
- <sup>8</sup>D. E. Laughlin, K. Srinivasan, M. Tanase, and L. Wang, “Crystallographic aspects of L1<sub>0</sub> magnetic materials”, *Scr. Mater.* **53**, 383–388 (2005).
- <sup>9</sup>R. Skomski, “Phase formation in L1<sub>0</sub> magnets”, *J. Appl. Phys.* **101**, 09N517 (2007).
- <sup>10</sup>A. Dannenberg, M. E. Gruner, A. Hucht, and P. Entel, “Surface energies of stoichiometric FePt and CoPt alloys and their implications for nanoparticle morphologies”, *Phys. Rev. B* **80**, 245438 (2009).
- <sup>11</sup>T. Burkert, L. Nordström, O. Eriksson, and O. Heinonen, “Giant Magnetic Anisotropy in Tetragonal FeCo Alloys”, *Phys. Rev. Lett.* **93**, 027203 (2004).
- <sup>12</sup>D. Kim and J. Hong, “Origin of thickness dependent spin reorientation transition of B2 type FeCo alloy films”, *J. Appl. Phys.* **114**, 213911 (2013).



- <sup>13</sup>L. Reichel, G. Giannopoulos, S. Kauffmann-Weiss, M. Hoffmann, D. Pohl, A. Edström, S. Oswald, D. Niarchos, J. Rusz, L. Schultz, and S. Fähler, “Increased magnetocrystalline anisotropy in epitaxial Fe-Co-C thin films with spontaneous strain”, *J. Appl. Phys.* **116**, 213901 (2014).
- <sup>14</sup>I. Turek, J. Kudrnovský, and K. Carva, “Magnetic anisotropy energy of disordered tetragonal Fe-Co systems from ab initio alloy theory”, *Phys. Rev. B* **86**, 174430 (2012).
- <sup>15</sup>W. Marciniak and M. Werwiński, “Structural and magnetic properties of Fe-Co-C alloys with tetragonal deformation: A first-principles study”, *Phys. Rev. B* **108**, 214433 (2023).
- <sup>16</sup>W. Marciniak, J. Marciniak, J. Á. Castellanos-Reyes, and M. Werwiński, *Giant magnetocrystalline anisotropy energy in Fe-Co alloy under uniaxial compression: first-principles prediction*, (Sept. 17, 2024) <http://arxiv.org/abs/2409.11388> (visited on 09/27/2024), pre-published.
- <sup>17</sup>G. R. Liu and S. S. Quek, *The Finite Element Method: A Practical Course* (Butterworth-Heinemann, Aug. 7, 2013), 457 pp.
- <sup>18</sup>J. Dirrenberger, S. Forest, and D. Jeulin, “Effective elastic properties of auxetic microstructures: anisotropy and structural applications”, *Int. J. Mech. Mater. Des.* **9**, 21–33 (2013).
- <sup>19</sup>G. Parisi, P. Zilio, and F. Romanato, “Complex Bloch-modes calculation of plasmonic crystal slabs by means of finite elements method”, *Opt. Express*, OE **20**, 16690–16703 (2012).
- <sup>20</sup>W. Zeng and G. R. Liu, “Smoothed Finite Element Methods (S-FEM): An Overview and Recent Developments”, *Arch. Comput. Methods Eng.* **25**, 397–435 (2018).
- <sup>21</sup>S. Y. Joshi and S. A. Deshmukh, “A review of advancements in coarse-grained molecular dynamics simulations”, *Mol. Simul.* **47**, 786–803 (2021).
- <sup>22</sup>M. J. Abraham, T. Murtola, R. Schulz, S. Páll, J. C. Smith, B. Hess, and E. Lindahl, “GROMACS: High performance molecular simulations through multi-level parallelism from laptops to supercomputers”, *SoftwareX* **1–2**, 19–25 (2015).
- <sup>23</sup>D. Poulikakos, S. Arcidiacono, and S. Maruyama, “Molecular dynamics simulation in nanoscale heat transfer: a review”, *Microscale Thermophys. Eng.* **7**, 181–206 (2003).
- <sup>24</sup>S. A. Hollingsworth and R. O. Dror, “Molecular Dynamics Simulation for All”, *Neuron* **99**, 1129–1143 (2018).
- <sup>25</sup>S. Adam, M. Knapp-Mohammady, J. Yi, and A.-N. Bondar, “Revised CHARMM force field parameters for iron-containing cofactors of photosystem II”, *J. Comput. Chem.* **39**, 7–20 (2018).
- <sup>26</sup>J. Wang, R. M. Wolf, J. W. Caldwell, P. A. Kollman, and D. A. Case, “Development and testing of a general amber force field”, *J. Comput. Chem.* **25**, 1157–1174 (2004).
- <sup>27</sup>P. Wen, G. Tao, D. E. Spearot, and S. R. Phillpot, “Molecular dynamics simulation of the shock response of materials: A tutorial”, *J. Appl. Phys.* **131**, 051101 (2022).
- <sup>28</sup>W. Hergert and R. M. Geilhufe, *Group Theory in Solid State Physics and Photonics: Problem Solving with Mathematica* (John Wiley & Sons, Aug. 20, 2018), 387 pp.

- <sup>29</sup>J. Kostal, “Chapter four - computational chemistry in predictive toxicology: status quo et quo vadis?”, *Advances in Molecular Toxicology* **10**, edited by J. C. Fishbein and J. M. Heilman, 139–186 (2016).
- <sup>30</sup>E. S. Kryachko and E. V. Ludeña, “Density functional theory: Foundations reviewed”, *Phys. Rep.* **544**, 123–239 (2014).
- <sup>31</sup>J. Sólyom, *Fundamentals of the Physics of Solids: Volume 3 - Normal, Broken-Symmetry, and Correlated Systems*, Vol. 3 (Springer Science & Business Media, Dec. 9, 2010), 764 pp.
- <sup>32</sup>P. Hohenberg and W. Kohn, “Inhomogeneous Electron Gas”, *Phys. Rev.* **136**, B864–B871 (1964).
- <sup>33</sup>G. R. Schleder, A. C. M. Padilha, C. M. Acosta, M. Costa, and A. Fazzio, “From DFT to machine learning: recent approaches to materials science—a review”, *J. Phys. Mater.* **2**, 032001 (2019).
- <sup>34</sup>H. Eschrig, M. Richter, and I. Opahle, “Chapter 12 - Relativistic Solid State Calculations”, in *Theoretical and Computational Chemistry*, Vol. 14, edited by P. Schwerdtfeger, Relativistic Electronic Structure Theory (Elsevier, Jan. 1, 2004), pp. 723–776.
- <sup>35</sup>J. Hafner, C. Wolverton, and G. Ceder, “Toward Computational Materials Design: The Impact of Density Functional Theory on Materials Research”, *MRS Bull.* **31**, 659–668 (2006).
- <sup>36</sup>P. Morgante and R. Peverati, “The devil in the details: A tutorial review on some undervalued aspects of density functional theory calculations”, *Int. J. Quantum Chem.* **120**, e26332 (2020).
- <sup>37</sup>J. P. Perdew, K. Burke, and M. Ernzerhof, “Generalized Gradient Approximation Made Simple”, *Phys. Rev. Lett.* **77**, 3865–3868 (1996).
- <sup>38</sup>H. Zhang, M. Richter, K. Koepnik, I. Opahle, F. Tasnádi, and H. Eschrig, “Electric-Field Control of Surface Magnetic Anisotropy: A Density Functional Approach”, *New J. Phys.* **11**, 043007 (2009).
- <sup>39</sup>M. Blanco-Rey, P. Perna, A. Gudin, J. M. Diez, A. Anadón, P. Olleros-Rodríguez, L. De Melo Costa, M. Valvidares, P. Gargiani, A. Guedeja-Marron, M. Cabero, M. Varela, C. García-Fernández, M. M. Otrokov, J. Camarero, R. Miranda, A. Arnau, and J. I. Cerdá, “Large Perpendicular Magnetic Anisotropy in Nanometer-Thick Epitaxial Graphene/Co/Heavy Metal Heterostructures for Spin–Orbitronics Devices”, *ACS Appl. Nano Mater.* **4**, 4398–4408 (2021).
- <sup>40</sup>M. Werwiński and W. Marciniak, “*Ab Initio* study of magnetocrystalline anisotropy, magnetostriction, and Fermi surface of L1<sub>0</sub> FeNi (tetrataenite)”, *J. Phys. Appl. Phys.* **50**, 495008 (2017).